TÉCNICO LISBOA

Volatility Models in Option Pricing

Miguel Ângelo Maia Ribeiro

Thesis to obtain the Master of Science Degree in

Engineering Physics

Supervisors: Prof. Cláudia Rita Ribeiro Coelho Nunes Philippart
Prof. Rui Manuel Agostinho Dilão

Examination Committee

Chairperson: Prof. Full Name
Supervisor: Prof. Full Name 1 (or 2)
Member of the Committee: Prof. Full Name 3

Month Year

To my parents and sister

Acknowledgments

A few words about the university, financial support, research advisor, dissertation readers, faculty or other professors, lab mates, other friends and family...

Resumo

Inserir o resumo em Português aqui com o máximo de 250 palavras e acompanhado de 4 a 6 palavras-chave...

Palavras-chave: palavra-chave1, palavra-chave2,...

Abstract

Insert your abstract here with a maximum of 250 words, followed by 4 to 6 keywords...

Keywords: keyword1, keyword2,...

Contents

List of Tables

List of Figures

Nomenclature

Greek symbols

σ	Stock price volatility.
ν	Stock price variance.
θ	Model parameter set.

Roman symbols

S	Stock price.
r	Risk-free interest rate.
K	Option strike price.
T	Option maturity date.
V	Option price.
C	Call option price.
P	Put option price.

Subscripts

$Euro$	European type option.
$Amer$	American type option.
$Barr$	Barrier type option.
$call$	Call type option.
put	Put type option.
mkt	Market data.
mdl	Model result.
imp,i	Implied (related to volatility).

Glossary

Risk-free interest rate	The risk-free interest rate is the interest an investor would receive from any risk-free investment.
Volatility	Volatility is a measure of the future stock price movement's uncertainty.

Chapter 1

Introduction

1.1 Mathematical Finance

Mathematical finance, also known as quantitative finance, is a field of applied mathematics focused on the modeling of financial instruments. It is rather difficult to overestimate its importance since it is heavily used by investors and investment banks in everyday transactions. In recent decades, this field suffered a complete paradigm shift, following developments in computer science and new theoretical results that enabled investors to better understand the mechanics of financial markets.

With the colossal sums traded daily in financial markets around the world, mathematical finance has become increasingly important and many resources are invested in the research and development of new and better theories and algorithms.

1.2 Derivatives

Derivatives are currently one of the subjects most studied by financial mathematicians. In finance, a *derivative* is simply a contract whose value depends on other simpler financial instruments, known as *underlying assets*, such as stock prices or interest rates. They can virtually take any form desirable, so long as there are two parties interested in signing it and all government regulations are met.

The importance of derivatives has grown greatly in recent years. In fact, as of June 2017, derivatives were responsible for over $542 trillion worth of trades, in the Over-the-Counter (OTC) market alone [Bank for International Settlements], as can be seen in Figure 1.1 (the OTC market refers to all deals signed outside of exchanges). This growth peaked in 2008 but stalled after the global financial crisis due to new government regulations, implemented because of the role of derivatives in market crashes [Financial Times, 2016]. It is easy to see that mishandling derivatives can have disastrous consequences. However, when handled appropriately, derivatives prove to be very powerful tools to investors, as we will see shortly.

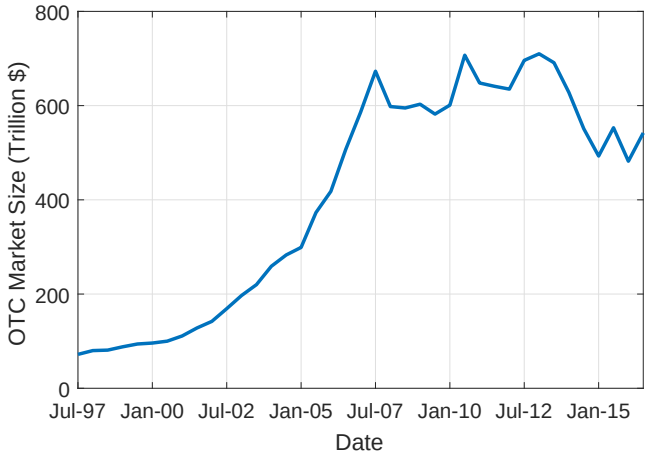

Figure 1.1: Size of OTC derivatives market since July 1997.

1.3 Options

Of all classes of derivatives, in this master thesis we will focus particularly on the most traded type [Hull, 2012]: *options*.

As the name implies, an *option* contract grants its buyer the *option* to buy (in the case of a *call* type option) or sell (for *put* options) its underlying asset at a future date, known as the *maturity*, for a fixed price, known as the *strike price*. In other words, when signing an option, buyers choose a price at which they want to buy/sell (call/put) some asset and a future date to do this transaction. When this date arrives, if the transaction is favorable to the buyers, they exercise their right to execute it.

The description above pertains only to *European* options. In this thesis, this type of contracts will be used for model calibration and validation. Other option types will also be considered, however. We shall approach *American* options, contracts that enable their buyers to exercise their right to buy/sell the underlying asset at any point in time *until* the maturity date. Other less common types, commonly known as *Exotic* options, will also be studied in the following sections, with focus on one of the most common types, known as *Barrier* options.

It's important to emphasize the fact that an option grants its buyer the *right* to do something. If *exercising* the option would lead to losses, the buyer can simply decide to let the maturity date pass, allowing the option to expire without further costs. This is indeed the most attractive characteristic of options.

1.3.1 Why Options are Important

Options are very useful tools to all types of investors. In simple terms, there exist two types of investors in the market: hedgers and speculators.

To hedgers (i.e. investors that want to limit their exposure to risk), options provide safety by fixing a minimum future price on their underlying assets - e.g. if hedgers want to protect themselves against a potential future price crash affecting one of their assets, they can buy put type options on that asset.

With these, even if the asset's value does crash, their losses will always be contained because they can exercise the options and sell the asset at the option's higher strike price.

Options are also very useful to speculators (i.e. investors that try to predict future market movements). The lower price of options when compared to their underlying assets grants this type of investors great leveraging capabilities and, with them, access to much higher profits if their predictions prove right. The opposite is also true and a wrong prediction can equally lead to much greater losses.

Due to all their advantages, and unlike some other types of derivatives, options have a price. Finding the ideal price for an option is a fundamental concern to investors, because knowing their appropriate value can give them a chance to take advantage of under or overpriced options. Finding this price can be very difficult for some option types, however, and though a lot of research has been done towards this goal, a great deal more is still required.

Chapter 2

Background

2.1 Option Types

Before completely focusing on the mechanics of options, what influences their prices and how we can try to predict their behavior, we should begin by clearly defining the main option types, their characteristics, as well as their payoff functions. Not only will we approach the two main types of options - European and American - but we will also shortly introduce other less common types, commonly referred to as Exotic options, focusing particularly on Barrier options.

2.1.1 European Options

European options are the most traded type of option in the OTC market [Investopedia, b]. They are not only extremely useful to investors, but also very simple to study and comparatively easy to price. For all these reasons, they have been the subject of much research and are deeply understood. Furthermore, because of their high availability, they are very useful in model calibration and validation.

As stated before, call and put European options enable their buyers to respectively buy and sell the underlying asset *at the maturity* for the fixed strike price.

To understand the payoff function of such contracts, we'll use an example. In the case of a European call option, if at the maturity the market price of its underlying asset is greater than the strike, investors can exercise the option and buy the asset for the fixed lower strike price. They can then immediately go to the market and sell the asset for its higher value. Thus, in this case, the payoff of the option would be the difference between the asset's price and the option's strike price. On the other hand, if at the maturity the price of the asset decreases past the strike, the investor should let the option expire, since the asset is available in the market for a lower price. In this case, the payoff would be zero. The same reasoning can be made for European put type options, such that the payoff function of both option types can then be deduced as

$$\begin{aligned} \text{Payoff}_{Euro,\ call}(K,T) &= \max\left(S(T)-K,0\right); \\ \text{Payoff}_{Euro,\ put}(K,T) &= \max\left(K-S(T),0\right), \end{aligned} \tag{2.1}$$

where K is the option's strike price and $S(T)$ is the asset's price, $S(t)$, at the maturity, T. These functions are represented in Figure 2.1.

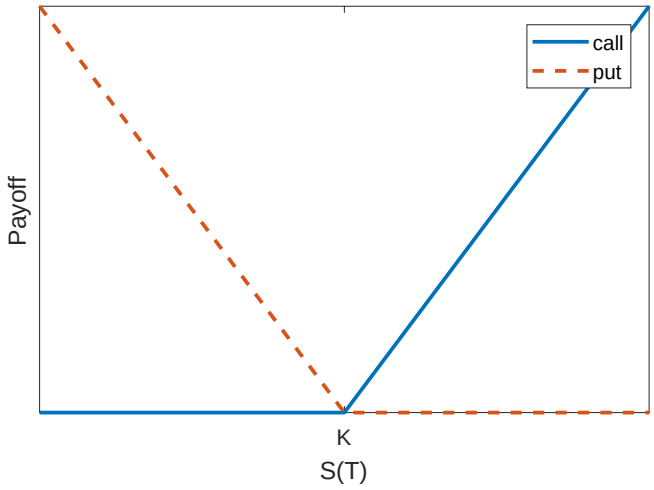

Figure 2.1: Payoff functions of European *call* and *put options*.

2.1.2 American Options

American options are more complex than European and thus harder to price. While European options dominate the OTC market, their American counterparts are the most traded type of option in exchanges [Investopedia, a]. Because of their great importance, many models have been developed to find the prices of these options [Longstaff and Schwartz, 2001].

American options grant the right to buy/sell (call/put) the underlying asset at any point in time *until the maturity date*. Following the logic used in the previous example to find the payoff functions of European calls and puts, we can deduce their American counterparts as

$$\begin{aligned} \text{Payoff}_{Amer,\ call}(K, t^*) &= \max\left(S(t^*) - K, 0\right); \\ \text{Payoff}_{Amer,\ put}(K, t^*) &= \max\left(K - S(t^*), 0\right), \end{aligned} \tag{2.2}$$

where we now define t^* (with $0 \leq t^* \leq T$) as the exercise date.

It should be obvious that the price of American options will always be greater than or equal to the prices of equivalent European options. The reason behind this is the fact that with European contracts our exercising decision is restricted to a single day, whereas with American options we have that same day as well as several others to make this choice.

2.1.3 Exotic Options

While European and American options are, by far, the most traded types, *Exotic options* should not be neglected. Not only does there exist a great number of Exotic option types, but these are also highly

customizable, making this type of derivatives ideal for unconventional investment strategies. Due to their high complexity, these options are only traded in the OTC market, and not in exchanges [Investopedia, c]. We will explore one of the most common types of Exotic options - *Barrier* options - though many others exist.

Barrier Options

A *Barrier option* behaves similarly to a European option with the difference that it only becomes active (or becomes worthless) if the value of its underlying asset reaches a particular value, called the *barrier level*, B, at any point in time until the option's maturity.

There are four main types of Barrier option:

- *up-and-out*: the asset's price starts below the barrier (i.e. $S(0) < B$). If it increases past this threshold, the option becomes *worthless*;
- *down-and-out*: the asset's price starts above the barrier (i.e. $S(0) > B$). If it decreases past this threshold, the option becomes *worthless*;
- *up-and-in*: the asset's price starts below the barrier (i.e. $S(0) < B$). *Only if* it increases past this threshold does the option become *active*;
- *down-and-in*: the asset's price starts above the barrier (i.e. $S(0) > B$). *Only if* it decreases past this threshold does the option become *active*.

Because all of the previously described Barrier option types are handled similarly, we can easily adapt the models from one type to another. Thus, for simplicity, we will henceforth assume that all Barrier options are of the up-and-in type.

We now deduce the payoff function of this type of Exotic contract. Using the up-and-in Barrier option type as an example, if the asset price, $S(t)$, remains below the barrier level B throughout the whole option duration, even if at the maturity the asset's value is higher than the strike price, the option's payoff would nonetheless be zero. On the contrary, if this threshold was surpassed at any point during this period, the option's payoff would be similar to that of its European equivalent. The payoff function of this type of option is therefore given by

$$\begin{aligned}
\text{Payoff}_{Barr,\ call}(K,T) &= \begin{cases} \max\left(S(T)-K,0\right), & \text{if } \exists\, t<T\,:\,S(t)>B \\ 0, & \text{otherwise} \end{cases}; \\
\text{Payoff}_{Barr,\ put}(K,T) &= \begin{cases} \max\left(K-S(T),0\right), & \text{if } \exists\, t<T\,:\,S(t)>B \\ 0, & \text{otherwise} \end{cases}.
\end{aligned} \tag{2.3}$$

Before simulating Barrier options and studying their behavior, we can deduce the effect of the barrier level B on the overall price of the option. For an up-and-in Barrier option, if the barrier level is too high, the price of the option will be very low. This is due to the fact that the likelihood of a stock price increasing

enough to surpass such a high barrier level, activating the option, is very low. On the other hand, if the barrier level is very close to S_0, the probability of the stock price reaching this threshold is approximately 1. Thus, the price of such an option would be very similar to that of its European equivalent. With these two examples, we can conclude that the higher the barrier level, the lower the Barrier option price.

Though Exotic options are used by banks and investors everyday, we will mainly focus on European options: not only are these the most common type of option traded, as we mentioned before, but data is also readily available for many different maturities and strike prices, making European options ideal for model calibration and validation, which will be the main goal of this thesis. Barrier options will nonetheless be implemented and studied, though no benchmark will be used to verify the models' validity in this case.

2.2 Option Prices and Payoffs

It is important to emphasize the difference between an option's payoff and its profit for investors. Because options grant the right to buy/sell some asset, no investors would exercise an option if this action was disadvantageous to them (i.e. negative payoff value, which is very unlikely to occur [Wilmott, 2013]). Thus, the payoff of an option is always positive (it can also, obviously, be zero). This might sound like an arbitrage possibility (i.e. the chance of making profit without risk), but in reality options have a price that investors have to pay in order to acquire them. This means that even if the option's payoff is positive, if this value is lower than the price an investor paid to buy the option, that investor will actually lose money. The profit of an option is thus the difference between its payoff and its price, which can be negative. With this concept in mind, we can price options by setting their expected profit to be the same as a risk-neutral investment, (e.g. bank deposit). The price of an option can thus be deduced as it's expected future payoff, discounted back to the present

$$\text{Price}(K, t^*) = e^{-rt^*}\mathbb{E}\left[\text{Payoff}(K, t^*)\right], \tag{2.4}$$

where t^* denotes the time at which the option is exercised and r corresponds to the risk-free interest rate, which we will approach in section 2.3. In particular, with eqs.(2.1) in mind, the price functions of European call and put options is clearly given by

$$\begin{aligned} C(K,T)_{Euro} &= e^{-rT}\mathbb{E}\left[\max\left(S(T)-K,0\right)\right] = e^{-rT}\mathbb{E}\left[\left(S(T)-K\right)\mathbb{1}_{\{S(T)>K\}}\right]; \\ P(K,T)_{Euro} &= e^{-rT}\mathbb{E}\left[\max\left(K-S(T),0\right)\right] = e^{-rT}\mathbb{E}\left[\left(K-S(T)\right)\mathbb{1}_{\{S(T)<K\}}\right], \end{aligned} \tag{2.5}$$

with $C(K,T)$ and $P(K,T)$ being the values (i.e. prices) of European call and put options, respectively, and $\mathbb{E}[\cdot]$, $\mathbb{1}_{\{\cdot\}}$ corresponding to the expected value and indicator functions, respectively.

When selling or buying options, investment banks add some premium to this zero-profit price, to account for the risk taken. Though this premium is important to define, it is besides the scope of this work and will not be considered here.

2.3 Black-Scholes Formulae

Due to their high importance, options have been studied in great detail in the past. Probably the most important result in this field came from Fischer Black, Myron Scholes and Robert Merton, who developed a mathematical model to price European options - the famous Black-Scholes (BS) model [Black and Scholes, 1973] - still in use in present days [Wilmott, 2006].

This model states that the price of an European (call or put) option follows the partial differential equation (PDE)

$$\boxed{\frac{\partial V}{\partial t} + \frac{1}{2}\sigma^2 S^2 \frac{\partial^2 V}{\partial S^2} + rS\frac{\partial V}{\partial S} - rV = 0,} \tag{2.6}$$

where V is the price of the option, S is the price of the underlying (risky) asset, r is the risk-free interest rate and σ is the stock price volatility. The underlying asset is commonly referred to as *stock*, so these terms will be used interchangeably in the following sections.

Proof Itô's Lemma can be applied to our option price V, which depends on the (stochastic) stock price S and time t, so that we obtain

$$dV = \frac{\partial V}{\partial t}dt + \frac{\partial V}{\partial S}dS + \frac{1}{2}\frac{\partial^2 V}{\partial S^2}(dS)^2. \tag{2.7}$$

We now assume that the stock price S follows a geometric Brownian Motion,

$$dS(t) = rS(t)dt + \sigma S(t)dW(t), \tag{2.8}$$

where $\{W(t),\ t > 0\}$ is a Brownian motion process.

It can be shown that $(dW)^2 = dt$, $(dt)^2 = 0$ and $(dt).(dW) = 0$. With these properties in mind, we can substitute eq.(2.8) into eq.(2.7), giving

$$\begin{aligned} dV =& \frac{\partial V}{\partial t}dt + \frac{\partial V}{\partial S}\left(rSdt + \sigma S dW\right) + \frac{1}{2}\left(rSdt + \sigma S dW\right)^2 \frac{\partial^2 V}{\partial S^2} \\ =& \left(rS\frac{\partial V}{\partial S} + \frac{\partial V}{\partial t} + \frac{1}{2}\sigma^2 S^2 \frac{\partial^2 V}{\partial S^2}\right)dt + \sigma S\frac{\partial V}{\partial S}dW. \end{aligned} \tag{2.9}$$

We now construct a portfolio where we sell *one* option and buy an amount $\partial V/\partial S$ of stocks. The value of such a portfolio would be

$$\Pi = -V + \frac{\partial V}{\partial S}S. \tag{2.10}$$

From this equation we can easily derive the change of the portfolio's value, $d\Pi$, in the time interval dt as

$$\begin{aligned} d\Pi &= -dV + \frac{\partial V}{\partial S}dS \\ &= \left(\frac{\partial V}{\partial t} + \frac{1}{2}\sigma^2 S^2 \frac{\partial^2 V}{\partial S^2}\right)dt. \end{aligned} \tag{2.11}$$

Because the portfolio's value doesn't change with the Brownian motion $\{W(t),\ t > 0\}$, it follows that

it must be *riskless*. To avoid any arbitrage possibilities (i.e. making profit without risk, which is very unlikely to happen), the value of this portfolio must be the same as any risk-free asset. The value of a portfolio with such an asset would change with time as

$$d\Pi = r\Pi dt. \tag{2.12}$$

Substituting eqs.(2.10) and(2.11) into eq.(2.12) gives

$$\frac{\partial V}{\partial t} + \frac{1}{2}\sigma^2 S^2 \frac{\partial^2 V}{\partial S^2} + rS\frac{\partial V}{\partial S} - rV = 0. \tag{2.13}$$

□

The risk-free interest rate, r, is the interest an investor would receive from any risk-free investment (e.g. treasury bills). No investor should ever invest in risky products whose expected return is lower than this interest (e.g. the lottery), since there's the alternative of obtaining a higher (expected) payoff without the disadvantage of taking risks. In general, this rate changes slightly with time and is unknown. Black *et al.*, in their original model (eq.(2.6)), assumed that this rate is a known function of time. Some authors have suggested solutions to deal with this shortcoming, providing stochastic models to replicate the behavior of interest rates [Heath et al., 1992], but because option prices do not significantly depend on this value [Wilmott, 2006], in the remainder of this thesis we shall set this rate to some constant.

As for the stock price volatility, σ, since we will explore it to great extent in chapter 3, suffice it to say for now that it is a measure of the future stock price movement's uncertainty.

Some companies decide to grant their shareholders a part of the profits generated, known as *dividends*. This action decreases the company's total assets, which decreases the value of stocks, changing option prices. Because this occurrence is based on human behavior, it is extremely hard to model. Furthermore, Black *et al.* assumed in their models that no dividends were paid throughout the option's duration. For both these reasons, we will set dividend payment to zero in all our models.

One other important assumption of the BS model is that stock prices follow a stochastic process, known as Geometric Brownian Motion, defined as

$$dS(t) = rS(t)dt + \sigma S(t)dW(t), \tag{2.14}$$

with $\{W(t),\ t > 0\}$ defining a one-dimensional Brownian motion and where we define $S_0 = S(0)$ as the stock price at time $t = 0$. An example of such processes is represented in Figure 2.2.

Many other diffusion processes exist, and this choice made by Black *et al.* might seem a bit arbitrary, but there is actually a reason behind it. Changes in the stock price are geometric and not arithmetic. If an asset of price 1.000×10^3 € changed by 9 €, we would barely take notice. If another asset of price 1.0×10^1 € changed by 9 €, the drop would be quite surprising, even though the change was the same in both assets. This seems to indicate that changes in the stock price depend on the stock price itself and justifies the choice made by Black *et al.* to model stock prices using a Geometric Brownian Motion process.

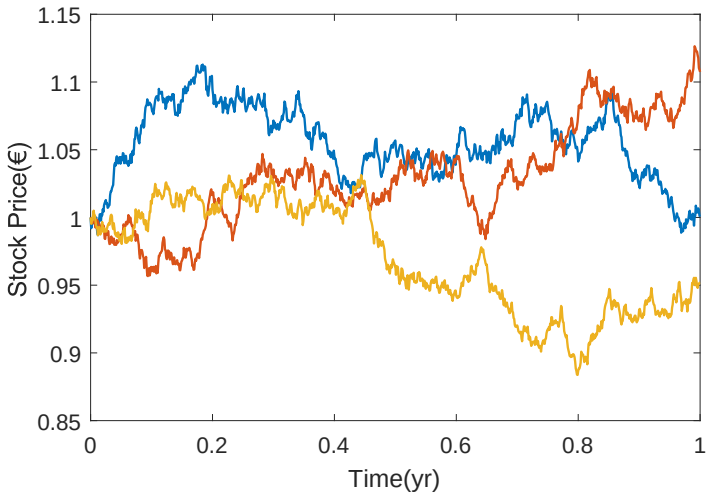

Figure 2.2: Example of three Geometric Brownian Motion processes with maturity $T = 1\,\text{yr}$, interest rate $r = 1 \times 10^{-2}\,\text{yr}^{-1}$, volatility $\sigma = 1 \times 10^{-1}\,\text{yr}^{-1/2}$ and initial stock price $S_0 = 1\,€$.

With this result, pricing options is fairly straightforward - we simply need to solve the PDE in eq.(2.6) as we would for the diffusion equation's initial value problem [Dilão et al., 2009]. The results published originally by Black *et al.* state that, at time t, call and put options can be valued as

$$\begin{aligned} C &= N(d_1)S_0 - N(d_2)Ke^{-rT}; \\ P &= -N(-d_1)S_0 + N(-d_2)Ke^{-rT}, \end{aligned} \tag{2.15}$$

where $N(\cdot)$ is the cumulative distribution function of the standard normal distribution and where d_1, d_2 are given by

$$\begin{aligned} d_1 &= \frac{1}{\sigma\sqrt{T}}\left[\log\left(\frac{S_0}{K}\right) + \left(r + \frac{\sigma^2}{2}\right)T\right]; \\ d_2 &= d_1 - \sigma\sqrt{T}. \end{aligned} \tag{2.16}$$

This is a very important result that can be used to precisely price European options, so long as all the parameters are exactly known and remain constant throughout the option's duration. Both assumptions are never true for any real market option, though.

From eq.(2.15) we can also derive the relationship between the call and put prices, C and P, known as the *put-call parity*, given by

$$C = S_0 - Ke^{-rT} + P. \tag{2.17}$$

Because of this duality, we can always easily obtain the prices of put options from the prices of call options with the same underlying asset, maturity and strike. For this reason, some of the results presented in later sections only apply to call options, though we can just as easily find their put option equivalent.

Finally, we can obtain a lower bound for the prices of European call and put options. Using some

non-arbitrage arguments it can be shown that

$$\begin{aligned} C &\geq \max\left[S_0 - Ke^{-rT}, 0\right]; \\ P &\geq \max\left[Ke^{-rT} - S_0, 0\right]. \end{aligned} \tag{2.18}$$

Proof Consider two portfolios, A and B, with the following composition:

Portfolio A: one European call option plus an amount Ke^{-rT} in cash

Portfolio B: one stock

With portfolio A, we invest the cash at the risk-free rate so that, at maturity, it reaches K. At the maturity, if $S_T > K$, we use the cash to exercise the option, buying the stock, and sell it immediately after for S_T. If $S_T < K$, the option expires worthless, and we are left with the cash K. Thus, the payoff of this portfolio is $\max[S_T, K]$. On the other hand, the payoff of portfolio B at the maturity is S_T, which is always equal to or smaller than that of portfolio A (i.e. portfolio A is always worth more than B). We can thus conclude that

$$C + Ke^{-rT} \geq S_0. \tag{2.19}$$

We also note that the payoff of an option is always positive, so that its value is always greater than 0. Joining these two conclusions, we obtain the result presented in eq.(2.18). □

As we did for European call and put options, we can equally derive the theoretical prices of Barrier options, changing the boundary condition to incorporate the barrier level [Taleb, 1997]. The resulting *up-and-in call* Barrier option price is given by

$$C_{Barr} = S_0\left(N(d_3) + b\left(N(d_4) - N(d_5)\right)\right) - Ke^{-rT}\left(N(d_6) + a\left(N(d_7) - N(d_8)\right)\right), \tag{2.20}$$

where we define the variables a, b and d_3 through d_8 as

$$a = \left(\frac{B}{S_0}\right)^{-1+\frac{2r}{\sigma^2}}, \tag{2.21}$$

$$b = \left(\frac{B}{S_0}\right)^{1+\frac{2r}{\sigma^2}}, \tag{2.22}$$

$$d_3 = \frac{1}{\sigma\sqrt{T}}\left[\log\left(\frac{S_0}{B}\right) + \left(r + \frac{\sigma^2}{2}\right)T\right], \tag{2.23}$$

$$d_4 = \frac{1}{\sigma\sqrt{T}}\left[\log\left(\frac{S_0}{B}\right) - \left(r + \frac{\sigma^2}{2}\right)T\right], \tag{2.24}$$

$$d_5 = \frac{1}{\sigma\sqrt{T}}\left[\log\left(\frac{S_0K}{B^2}\right) - \left(r + \frac{\sigma^2}{2}\right)T\right], \tag{2.25}$$

$$d_6 = \frac{1}{\sigma\sqrt{T}}\left[\log\left(\frac{S_0}{B}\right) + \left(r - \frac{\sigma^2}{2}\right)T\right], \tag{2.26}$$

$$d_7 = \frac{1}{\sigma\sqrt{T}}\left[\log\left(\frac{S_0}{B}\right) - \left(r - \frac{\sigma^2}{2}\right)T\right], \tag{2.27}$$

$$d_8 = \frac{1}{\sigma\sqrt{T}}\left[\log\left(\frac{S_0 K}{B^2}\right) - \left(r - \frac{\sigma^2}{2}\right)T\right], \tag{2.28}$$

where B defines the barrier level, at which the option becomes activated.

Chapter 3

Volatility

As mentioned, volatility is a measure of the uncertainty of future stock price movements. In other words, a higher volatility will lead to greater future fluctuations in the stock price, whereas a stock with lower volatility is more stable. This phenomenon is exemplified in Figure 3.1, where we can see the greater fluctuations of the high-volatility process (red) compared to the much smaller variations of the low-volatility process (orange), using the same driving Brownian motion.

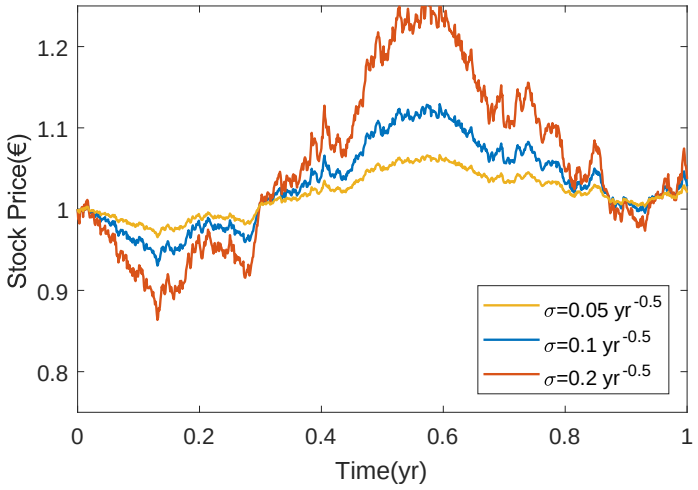

Figure 3.1: Example of three identical GBM processes with maturity $T = 1\,\text{yr}$, interest rate $r = 1 \times 10^{-2}\,\text{yr}^{-1}$ and initial stock price $S_0 = 1\,€$. The volatilities are $\sigma = 5 \times 10^{-2}\,\text{yr}^{-1/2}$, $\sigma = 1 \times 10^{-1}\,\text{yr}^{-1/2}$ and $\sigma = 2 \times 10^{-1}\,\text{yr}^{-1/2}$ for the orange, blue and red plot lines represented, respectively. To emphasize this effect, the underlying Brownian Motion $\{W(t),\, t > 0\}$ used to generate all three paths was the same.

Of all the parameters in the BS formula (eq.(2.6)), volatility is the only one we can't easily measure from market data. Furthermore, unlike the interest rate, volatility has a great impact on the behavior of stock prices and, consequently, on the price of options [Wilmott, 2006]. These two factors make volatility one of the most important subjects in all of mathematical finance and thus the focus of much research.

Usually, volatility can be estimated empirically from the standard deviation of the historical rate of log-

returns [Hull, 2012]. We begin by measuring the stock price at fixed time intervals (e.g. daily, monthly), such that S_i corresponds to the stock price at the end of the ith interval. We define the log-return rate, u_i, as

$$u_i = \log\left(\frac{S_i}{S_{i-1}}\right). \tag{3.1}$$

We can then calculate the standard deviation, s, of this rate as

$$s = \sqrt{\frac{1}{n-1}\sum_{i=1}^{n}(u_i - \overline{u})^2}, \tag{3.2}$$

assuming we have $n+1$ observations and denoting $\overline{u}$ as the average value of the log-return rates. The volatility (measured yearly) can be *estimated* with

$$\hat{\sigma} = \frac{s}{\sqrt{\tau}}, \tag{3.3}$$

where τ defines the time interval length measured in years. As an example, if we only have monthly data for the S_i prices, the time interval would obviously be one month, which, measured in years is equal to $1/12$, which corresponds to τ. The volatility can also be measured in other time periods: we can define a monthly or a daily volatility, instead of a yearly volatility as we defined before, but these are less common and will therefore not be used.

We are now able to estimate the volatility of any given asset at the present moment. With this result, we could assume that the volatilities remain constant over time and use today's volatility to price options with maturities in the future. The clear problem with this approach is that, when observing market data, we can see that volatilities change over time, so that even if we had the exact value of this parameter in the present, it can, and will, change in the future. If we try to price options assuming a constant volatility, our options will become mispriced, causing potential losses. Our goal is therefore to model the volatility of any given stock price, and, with this model, predict its future behavior, using this knowledge to better price options. We begin by introducing the concept of implied volatility, crucial to fully grasping the concepts used later. Afterwards, we will introduce four models to replicate market volatility: one with local volatility (Dupire's formula) and three with stochastic volatility (Heston and Static/Dynamic SABR).

We should note that other very common models exist. The GARCH model (Generalized Autoregressive Conditional Heteroskedasticity) along with all its many variations (EGARCH, NGARCH, ...) is particularly popular among econometricians. However, this model is mostly used to forecast volatility, and performs poorly when used to price derivatives [Chourdakis, 2008]. Because pricing is our objective, GARCH will not be covered in this work. We will also study the constant volatility model, as used by Black *et al.*, as a benchmark for the quality of our models.

3.1 Implied Volatility

Implied volatility can be described as the value of stock price volatility that, when input into the BS pricer in eq.(2.15), outputs a value equal to the market price of a given option. In other words, it would be the stock price volatility that the seller/buyer of the option used when pricing it (assuming the BS model was used).

Because eq.(2.15) is not invertible w.r.t. σ, we need to use some numerical procedure (e.g. Newton's method) to find the value of implied volatility that matches the market and model prices, i.e. we must find, numerically, the solution to the equation

$$C(\sigma_{imp}) = C_{\text{mkt}}, \tag{3.4}$$

where $C(\sigma_{imp})$ corresponds to the result of eq.(2.15) using σ_{imp} as (implied) volatility and C_{mkt} to the price of the option observed in the market.

Solving eq.(3.4) to find the implied volatility of different option market prices, we find the relationship depicted in Figure 3.2, for three different strike prices.

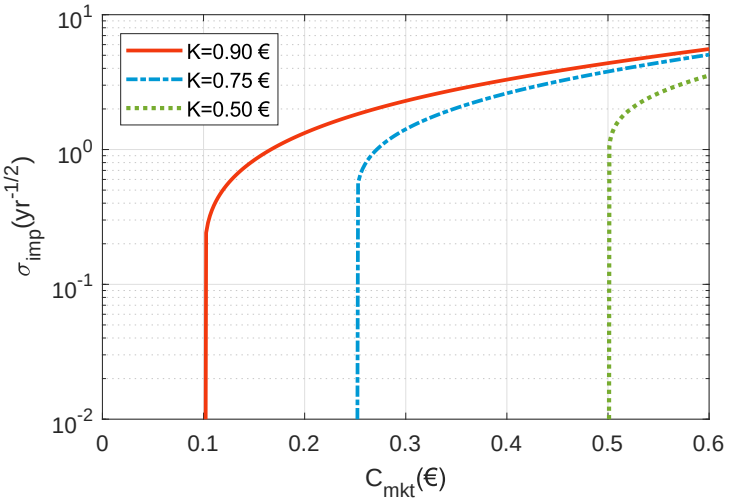

Figure 3.2: Relationship between the implied volatility and the market price of a call option. The parameters used were $T = 21$ days, interest rate $r = 1 \times 10^{-2}\,\text{yr}^{-1}$ and initial stock price $S_0 = 1\,€$. The strike prices are $K = 9 \times 10^{-1}\,€$, $K = 7.5 \times 10^{-1}\,€$ and $K = 5 \times 10^{-1}\,€$ for the red full line, the blue dot-dashed line and the green dot-dashed line, respectively.

We can see that the implied volatility goes to zero extremely fast when we approach the lower bound of the call option's price, $S_0 - Ke^{-rT}$ (from eq.(2.18)) - the lower bounds for the option prices with strikes $K = 9 \times 10^{-1}\,€$, $K = 7.5 \times 10^{-1}\,€$ and $K = 5 \times 10^{-1}\,€$ are, respectively, $C = 1.007 \times 10^{-1}\,€$, $C = 2.506 \times 10^{-1}\,€$ and $C = 5.004 \times 10^{-1}\,€$). We can thus conclude that the implied volatility is extremely sensitive to the option's market price when this price approaches its lower bound. We can also observe

that this property is more pronounced for lower strikes. This observation will become very important in later sections.

From Figure 3.2 we can also observe that the relation between implied volatility and market option price is a monotonous increasing function. This means that we can obtain the implied volatility of an option from its price and vice versa (i.e. the relationship is bijective). This duality is so fundamental that investors often disclose options by providing their implied volatility instead of their price [Wilmott, 2013], as is indeed the case for the data we will use later to calibrate the models. To understand why option price is an increasing monotonous function w.r.t. the volatility we note that volatility is very desirable to investors when dealing with options. A high volatility means that there is an increased probability that the stock price will increase or decrease very significantly. In the case of a call option, if the stock price increases considerably, the investor earns a large amount of money. If the price decreases considerably, the investor may let the option expire. Thus we see that a higher volatility provides a greater change of potentially very high profits with a limited potential downfall. We thus conclude that a higher volatility increases the value of an option.

One important property of implied volatility is that, in the real-world, it depends on the strike price and the maturity. This should not occur in the "Black-Scholes world". Because the volatility is a property of the stock, if investors really used the the BS model to price their options, two options with the same underlying stock should have the same implied volatility, regardless of their strike prices or maturities (i.e. the same stock can't have two different volatilities at the same time). However, when observing real market data, this is in fact what is observed.

The implied volatilities' dependence on the strike price can take one of two forms, known as *smile* and *skew*. An implied volatility smile presents higher volatilities for options with strikes farther from the current stock price (i.e. the shape of a smile). A skew, on the other hand, only presents higher volatilities in one of these directions (i.e. only for strikes either greater or smaller than the current stock price). Both phenomena are represented in Figure 3.3.

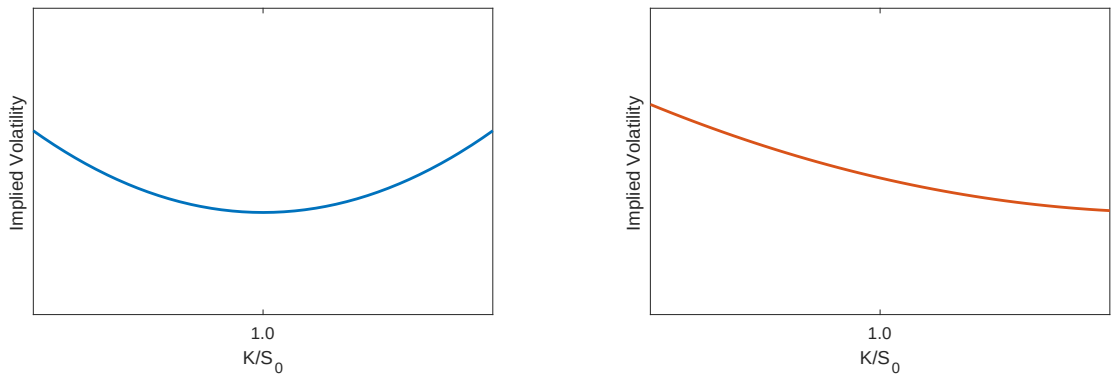

(a) Smile (b) Skew

Figure 3.3: Representation of the implied volatility smile (left) and skew (right) functions.

Because of their higher implied volatility, we can conclude that, if we observe a smile in the data,

options with strikes different from the current stock price are *overpriced*. The reason behind this odd market behavior is related to the simple demand-supply rule [Wilmott, 2006]. On the one hand, some investors are risk-averse and want to hedge their losses in case of a big market movement (as explained in subsection 1.3.1). They don't mind paying a higher price for an option if this means they would be relatively safe from potentially devastating price changes. For this reason, the demand of call options with lower strikes increases, driving their prices and, consequently, their implied volatility up. On the other hand, other investors are risk-seekers and want to take advantage of possible sudden price movements, buying the stocks after the possible price increase for the lower strike prices. They don't mind paying higher prices for the chance of earning high profits and this drives the prices of high strike call options and, consequently, their implied volatility up. This fear-greed duality gives rise to the observed volatility smile. In the case of the volatility skew, only one of the two phenomena described occurs.

The presence of a smile in the data instead of a skew, and vice-versa, is determined by the type of product serving as underlying asset - Forex market options usually exhibit volatility smiles whereas index and commodities options usually show a volatility skew or a skewed smile [Wilmott, 2006].

The dependence of the implied volatility on the maturity date is more complex, but in general it decreases with the maturity.

It can also be shown that the implied volatility is the same for calls and puts [Hull, 2012], though the causes of the volatility smile/skew for put options are the opposite of the ones described before for calls.

Though the implied volatility is usually defined for European options, we can just as easily adapt this term for Barrier options. We again have to solve eq.(3.4), but now using the (Barrier) implied volatility, $\sigma_{imp,Barr}$, to generate the theoretical Barrier option price, $C(\sigma_{imp,Barr})$. This result will be used later when we study barrier options.

3.2 Local Volatility

In their original work, Black *et al.* assumed that volatility is constant throughout the whole option duration. From market data, it can be clearly seen that this is not the case [S&P Dow Jones Indices]. There may be times when new information reaches the market (e.g. the results of an election) and trading increases, driving volatility up. It is equally true that shortly before this information is known, trading may stall due to expectancy, and volatilities go down.

The constant volatility BS model is therefore clearly incapable of completely grasping real-world trading. We should use a model where volatility is dynamic, measuring the uncertainty on the stock price movement at any point in time. However, as we saw in section 3.1, the market's view of volatility also depends on the stock price itself. The volatility should therefore be a function of both time and stock price: $\sigma(S(t), t)$. We call this model *local volatility* and the geometric Brownian motion from eq.(2.14) is transformed into the new diffusion process

$$dS(t) = rS(t)dt + \sigma(S(t), t)S(t)dW(t), \tag{3.5}$$

where $\sigma(S(t),t)$ is a function of $S(t)$ and t, with certain properties, which we omit as they are only used to ensure the strong solution of this SDE (i.e. $\sigma(S(t),t)$ is "well behaved").

This local volatility model implies that we have a nonlinear *deterministic* volatility surface, $\sigma(S(t),t)$, which can be thought of as the market's expectation of future volatility at time t if the stock price is $S(t)$ at that time.

Because we can't directly measure the local volatility of a stock from market data, we need some models to estimate it. One of the most used of these is known as Dupire's formula, which we explain in the following subsection.

3.2.1 Dupire's model

One of the most famous results in the modelling of the local volatility function was obtained by Dupire [Dupire, 1994]. In his article, this author derives a theoretical formula for $\sigma(S(t),t)$, given by

$$\sigma(S(t),t) = \sqrt{\frac{\frac{\partial C}{\partial T} + rS\frac{\partial C}{\partial K}}{\frac{1}{2}S^2\frac{\partial^2 C}{\partial K^2}}}, \tag{3.6}$$

where $C = C(K,T)$ is the price of an European call option with strike price K and maturity T. All the derivatives are evaluated at $K = S(t)$ and $T = t$.

Proof

We begin by assuming that the stock price $S(t)$ follows a dynamic transition probability density function $p(S(t),t,S'(t'),t')$. In other words, by integrating this density function we would obtain the probability of the stock price reaching a price S' at a time t' having started at price S at time t.

The present value of a call option, $C(K,T)$, can be deduced as its expected future payoff, discounted backwards in time, which results in

$$\begin{aligned} C(K,T) = e^{-r(T-t)}\mathbb{E}\left[\max\left(S'-K,0\right)\right] &= e^{-r(T-t)}\int_0^\infty \max\left(S'-K,0\right)p(S,t,S',T)dS' \\ &= e^{-r(T-t)}\int_K^\infty (S'-K)p(S,t,S',T)dS', \end{aligned} \tag{3.7}$$

where S' denotes the stock price at maturity.

Taking the first derivative of this result with respect to the strike price K, we obtain

$$\frac{\partial C}{\partial K} = -e^{-r(T-t)}\int_K^\infty p(S,t,S',T)dS'. \tag{3.8}$$

The second derivative results in

$$\frac{\partial^2 C}{\partial K^2} = e^{-r(T-t)}p(S,t,K,T), \tag{3.9}$$

assuming $p(S,t,\infty,T) = 0$.

We now make a brief digression to derive the Fokker-Planck equation (following the procedure shown in Wilmott [Wilmott, 2006]), which we require for the next steps. This equation is widely used in stochastic

calculus, and is applicable to stochastic processes in general. To make its proof simpler, we make a simplification assuming that the stochastic process is a stock price following a trinomial model: at each time step δt, the stock price can only increase or decrease by an amount δS, with probabilities ϕ^+ and ϕ^-, respectively, or remain the same, with probability $(1 - \phi^+ - \phi^-)$. The resulting equation still works, however, for any general stochastic process.

Assuming the trinomial model, the expected value of the change is given by

$$\phi^+ \delta S + (1 - \phi^+ - \phi^-).0 + \phi^-(-\delta S) = (\phi^+ - \phi^-)\delta S, \tag{3.10}$$

and its variance is approximately given by

$$(\delta S)^2(\phi^+ + \phi^- - (\phi^+ - \phi^-)^2) \approx (\phi^+ + \phi^-)(\delta S)^2 \tag{3.11}$$

where we take only the first order terms. The expected value of the change of a GBM can be thought of as its drift term (i.e. $rS\delta t$), and the variance is its stochastic term squared (i.e. $(\sigma S dW)^2 = \sigma^2 S^2 \delta t$), so that we have

$$\begin{aligned} rS\delta t &= (\phi^+ - \phi^-)\delta S; \\ \sigma^2 S^2 \delta t &= (\phi^+ + \phi^-)(\delta S)^2, \end{aligned} \tag{3.12}$$

from which we can derive the probabilities ϕ^+ and ϕ^- as

$$\begin{aligned} \phi^+(S,t) &= \frac{1}{2}\frac{\delta t}{\delta S^2}(rS\delta S + \sigma^2 S^2); \\ \phi^-(S,t) &= \frac{1}{2}\frac{\delta t}{\delta S^2}(-rS\delta S + \sigma^2 S^2). \end{aligned} \tag{3.13}$$

We can now move backwards and derive the probability of reaching the price S' at time t' having started at the previous time $t' - \delta t$ with some (unknown) price S, which could be either $S' + \delta S$, $S' - \delta S$ or S' (assuming a trinomial movement). Applying the same logic as before, the probability of reaching S' at time t', having started at S at time t, is the same as the probability of being at $S' - \delta S$ at time $t' - \delta t$ and moving up, plus the probability of being at $S' + \delta S$ at time $t' - \delta t$ and moving down plus the probability of being at S' at time $t' - \delta t$ and remaining at the same value. We can thus derive the transition probability density, $p(S, t, S', t')$ as

$$\begin{aligned} p(S,t,S',t') =& \phi^-(S' + \delta S, t' - \delta t)p(S,t,S' + \delta S, t' - \delta t) \\ &+ (1 - \phi^+(S', t' - \delta t) - \phi^-(S', t' - \delta t))p(S,t,S',t' - \delta t) \\ &+ \phi^+(S' - \delta S, t' - \delta t)p(S,t,S' - \delta S, t' - \delta t) \end{aligned} \tag{3.14}$$

If we expand each term on its Taylor series around point (S', t'), we get

$$\begin{aligned} p(S,t,S',t') = \phi^-(S'+\delta S, t'-\delta t)\left(p(S,t,S',t') + \delta S\frac{\partial p}{\partial S'} + \frac{1}{2}(\delta S)^2\frac{\partial^2 p}{\partial S^2} - \delta t\frac{\partial p}{\partial t'}\right) \\ + (1-\phi^+(S',t'-\delta t) - \phi^-(S',t'-\delta t))\left(p(S,t,S',t') - \delta t\frac{\partial p}{\partial t'}\right) \\ + \phi^+(S'-\delta S, t'-\delta t)\left(p(S,t,S',t') - \delta S\frac{\partial p}{\partial S'} + \frac{1}{2}(\delta S)^2\frac{\partial^2 p}{\partial S^2} - \delta t\frac{\partial p}{\partial t'}\right), \end{aligned} \tag{3.15}$$

from which, collecting all the terms, we can derive the famous Fokker-Planck equation [Wilmott, 2006] (with rather sloppy notation) as

$$\frac{\partial p}{\partial T} = \frac{1}{2}\frac{\partial^2(\sigma^2 S'^2 p)}{\partial S'^2} - \frac{\partial(rS'p)}{\partial S'}. \tag{3.16}$$

where we have used $t' = T$.

From eq.(3.7) we can easily obtain the first derivative w.r.t. time

$$\frac{\partial C}{\partial T} = -rC + e^{-r(T-t)}\int_K^\infty (S'-K)\frac{\partial p}{\partial T}dS', \tag{3.17}$$

where, for simplicity, we drop the terms of the transition probability density, p.

Using the Fokker-Planck formula in eq.(3.16), we can transform this relation into

$$\frac{\partial C}{\partial T} = -rC + e^{-r(T-t)}\int_K^\infty (S'-K)\left(\frac{1}{2}\frac{\partial^2(\sigma^2 S'^2 p)}{\partial S'^2} - r\frac{\partial(S'p)}{\partial S'}\right)dS'. \tag{3.18}$$

We now split the terms in the integral to evaluate them independently. We integrate the second term by parts as

$$\begin{aligned} \int_K^\infty (S'-K)\left(-r\frac{\partial(S'p)}{\partial S'}\right)dS' &= -r(S'-K)(S'p)\big|_{S'=K}^\infty + r\int_K^\infty S'pdS' \\ &= r\int_K^\infty (S'-K)pdS' + rK\int_K^\infty pdS' \\ &= e^{r(T-t)}rC - rK\frac{\partial C}{\partial K} \end{aligned} \tag{3.19}$$

where in the first step we assumed that p and its first derivative w.r.t. S go sufficiently fast to zero when S goes to infinity and where in last step we used eqs.(3.7) and(3.8).

Turning now to the first term of the integral, we integrate twice by parts as

$$\begin{aligned} \int_K^\infty (S'-K)\left(\frac{1}{2}\frac{\partial^2(\sigma^2 S'^2 p)}{\partial S'^2}\right)dS' &= \frac{1}{2}(S'-K)\frac{\partial(\sigma^2 S'^2 p)}{\partial S'}\bigg|_{S'=K}^\infty - \frac{1}{2}\int_K^\infty \left(\frac{\partial(\sigma^2 S'^2 p)}{\partial S'}\right)dS' \\ &= -\frac{1}{2}\sigma^2 S'^2 p\big|_{S'=K}^\infty = \frac{1}{2}\sigma^2(K,T)K^2 p(S,t,K,T) \\ &= \frac{1}{2}e^{r(T-t)}\sigma^2(K,T)K^2\frac{\partial^2 C}{\partial K^2}, \end{aligned} \tag{3.20}$$

where in the last step we used eq.(3.9) and again assumed that p goes to zero sufficiently fast.

Collecting all the terms, we obtain

$$\frac{\partial C}{\partial T} = \frac{1}{2}\sigma^2(K,T)K^2\frac{\partial^2 C}{\partial K^2} - rK\frac{\partial C}{\partial K}. \tag{3.21}$$

from which, by rearranging all the terms and applying the variable change $\sigma(K,T) \implies \sigma(S,t)$, we get

$$\sigma(S(t),t) = \sqrt{\frac{\frac{\partial C}{\partial T} + rS\frac{\partial C}{\partial K}}{\frac{1}{2}S^2\frac{\partial^2 C}{\partial K^2}}}. \tag{3.22}$$

assuming all the derivatives are evaluated at $K = S(t)$ and $T = t$.

□

As can be seen, we need to differentiate the option prices with respect to their strikes and maturities. To achieve this, we need first to gather, from the market, a large number of prices for options with different maturities and strikes. We then implement some interpolation on these values to obtain an option price surface (with K and T as variables). Finally, we calculate the gradients of this interpolated surface and input them into eq.(3.6) to obtain the local volatility surface. We can then sample from this surface to obtain the local volatility for any stock price $S(t)$ at any time t.

A major problem can be pointed out in eq.(3.6). For options far in or far out of the money (i.e. with strikes much greater or much smaller that S_0), it can be shown that the option price depends almost linearly on the strike. This means that the second derivative of the price w.r.t. the strike is extremely small in these regions. Because this value is in the denominator of eq.(3.6), the local volatility will explode in such cases, which is unrealistic.

One possible solution to this problem is to relate our local volatility with the implied volatility surface instead of the option price's [Wilmott, 2013]. The relation obtained is

$$\boxed{\sigma(S(t),t) = \sqrt{\frac{\sigma_{imp}^2 + 2t\sigma_{imp}\frac{\partial \sigma_{imp}}{\partial T} + 2r(S(t))t\sigma_{imp}\frac{\partial \sigma_{imp}}{\partial K}}{\left(1 + (S(t))d_1\sqrt{t}\frac{\partial \sigma_{imp}}{\partial K}\right)^2 + (S(t))^2 t\sigma_{imp}\left(\frac{\partial^2 \sigma_{imp}}{\partial K^2} - d_1\left(\frac{\partial \sigma_{imp}}{\partial K}\right)^2\sqrt{t}\right)}},} \tag{3.23}$$

where d_1 is given by

$$d_1 = \frac{\log(S_0/S(t)) + \left(r + \frac{1}{2}\sigma_{imp}^2\right)t}{\sigma_{imp}\sqrt{t}}, \tag{3.24}$$

with S_0 being the stock price at $t = 0$. We define $\sigma_{imp} = \sigma_{imp}(K,T)$ as the implied volatilities of options with maturity T, and strike K. Furthermore, σ_{imp} and all its derivatives are evaluated at $K = S(t)$ and $T = t$. This formula can be obtained from eq.(3.6) by applying the transformation from call prices to implied volatilities.

We now need to generate the implied volatility surface in order to obtain the gradients needed in eq.(3.23) to generate the local volatility. Again, this surface can be obtained by interpolating between market data for several implied volatilities. The problem with this approach is that we only have access to market data for a very limited set of implied volatilities. This problem is therefore very much ill-posed

(i.e. a small change in the input generates a very different output) and the resulting local volatility surface might look unrealistic [Wilmott, 2013]. Furthermore, this procedure is heavily dependent on the interpolation/extrapolation method chosen, which is problematic.

As an advantage, we note that because we are directly using the market data, the implied volatility surface is nonparametric and therefore no fitting procedure is required. To ease the problem of ill-posedness, we could heuristically choose some functions to model this surface, fitting their parameters to better replicate the market data, and finally replacing these functions in eq.(3.23), as done by Dewynne [Dewynne et al., 1998]. However, this solution depends heavily on the functions chosen and will not be considered.

Three other problems can be identified in Dupire's local volatility model. First, it can be shown that the local volatility surface changes with time [Wilmott, 2013]. This means that the whole interpolation procedure must be done regularly in order for the model to work properly. Secondly, some authors have pointed out that the volatility smile obtained from Dupire's local-volatility model doesn't follow real market dynamics [Hagan et al., 2002]: it can be shown that when the price of the stock either increases or decreases, the volatility smile predicted by Dupire's model shifts in the opposite direction. The minimum of the volatility smile would therefore be offset and no longer correspond to the local stock price (i.e. the spot price). The volatility smile dynamics obtained from the local-volatility model would thus be actually worse than if we assumed a constant volatility. Finally, the gradients used in eq.(3.23) have to be generated numerically. This numerical differentiation is very unstable, especially when done on our rough interpolated surface, which might lead to errors in the local volatility obtained.

Despite its problems, Dupire's formula is still very much used by practitioners and performs surprisingly well, as we will see in chapter 5.

3.3 Stochastic Volatility

As stated before, the volatility is not constant, is not observable and is very unpredictable, despite our attempts to model it. This seems to indicate that volatility is itself also a stochastic process. Some research has been done into this hypothesis, and many models have been developed to replicate real-world volatilities with this assumption.

We assume that the stock price follows the diffusion process

$$dS(t) = rS(t)dt + \sigma(S(t), t)S(t)dW_1(t), \tag{3.25}$$

and we further hypothesize that the volatility follows

$$d\sigma(S(t), t) = p(S(t), \sigma(S(t), t), t)dt + q(S(t), \sigma(S(t), t), t)dW_2(t), \tag{3.26}$$

where $p(S(t), \sigma(S(t), t), t)$ and $q(S(t), \sigma(S(t), t), t)$ are functions of the stock price $S(t)$, time t and of the volatility $\sigma(S(t), t)$ itself. We also assume that W_1 and W_2 are two Brownian motion processes with a

correlation $\rho(t)$, i.e.

$$dW_1(t)dW_2(t) = \rho(t)dt, \quad \forall t > 0, \tag{3.27}$$

which is usually assumed constant, $\rho(t) = \rho$. This correlation coefficient can be explained by the relationship between prices and volatilities [Chourdakis, 2008]. Historically, we can see that high volatility periods usually occur when the market is under stress due to low returns (i.e. stock prices decrease). On the other hand, whenever the market stabilizes and returns increase, the volatility goes down. These factors seem to indicate the existence of a negative correlation between stock prices and volatilities. Thus, to fully grasp market behavior, this correlation must be taken into account.

Choosing the appropriate functions $p(S(t), \sigma(S(t), t), t)$ and $q(S(t), \sigma(S(t), t), t)$ is very important since the whole evolution of the stock price depends on them. All stochastic volatility models present a different version of these functions, and each may be more adequate for some types of assets. Furthermore, these functions have some parameters that we have to calibrate in order to best fit our model to market data, as we will see later.

Many stochastic volatility models exist, such as Hull-White [Hull and White, 1987] and Stein-Stein [Stein and Stein, 1991]. However, the *Heston* model is by far the most popular of these [Chourdakis, 2008]. Another model, known as *SABR*, is also widely used by practitioners, especially in the interest rate derivative markets (i.e. derivatives whose underlying asset is an interest rate). For these reasons, both these models will be studied in this work.

3.3.1 Heston Model

The *Heston model* was developed in 1993 by Steven Heston [Heston, 1993] and it states that stock prices satisfy the relations

$$\boxed{dS(t) = rS(t)dt + \sqrt{\nu(t)}S(t)dW_1(t),} \tag{3.28}$$

$$\boxed{d\nu(t) = \kappa(\overline{\nu} - \nu(t))dt + \eta\sqrt{\nu(t)}dW_2(t),} \tag{3.29}$$

with $\nu(t)$ corresponding to the stock price variance (i.e. the square of the volatility, $\nu(t) = (\sigma(t))^2$) and where $W_1(t)$ and $W_2(t)$ have a constant correlation ρ. We furthermore define ν_0 as the initial variance (i.e. variance at time $t = 0$). The original model used a drift parameter μ instead of the risk-free measure drift r presented here, but a measure transformation, using Gisarnov's theorem, can be easily implemented [Rouah, 2013].

The parameters κ, $\overline{\nu}$ and η are, respectively, the *mean-reversion rate* (i.e. how fast the variance converges to its mean value), the *long-term variance* (i.e. the mean value of variance) and the *volatility of the variance* (i.e. how erratic is the variance process).

One of the reasons why the Heston model is so popular is the fact that there exists a closed-form solution for the prices of European options priced under this model. This closed form solution is given

by

$$\begin{aligned} C_H(K,T;\theta) &= e^{-rT}\mathbb{E}\left[(S(T)-K)\,\mathbb{1}_{\{S(T)>K\}} \mid \theta\right] \\ &= e^{-rT}\left(\mathbb{E}\left[S(T)\mathbb{1}_{\{S(T)>K\}} \mid \theta\right] - K\mathbb{E}\left[\mathbb{1}_{\{S(T)>K\}} \mid \theta\right]\right) \\ &= S_0 P_1(K,T;\theta) - e^{-rT}K P_0(K,T;\theta), \end{aligned} \tag{3.30}$$

where $C_H(K,T;\theta)$ corresponds to the theoretical European call option price, with strike K and maturity T, under the Heston model, assuming a parameter set $\theta = \{\kappa, \overline{\nu}, \eta, \nu_0, \rho\}$. The variables $P_1(K,T;\theta)$ and $P_2(K,T;\theta)$ are given by

$$P_1(K,T;\theta) = \frac{1}{2} + \frac{1}{\pi}\int_0^\infty \mathrm{Re}\left(\frac{e^{-iu\log K}}{iuS_0e^{rT}}\phi(u-i,T;\theta)\right)du, \tag{3.31}$$

$$P_0(K,T;\theta) = \frac{1}{2} + \frac{1}{\pi}\int_0^\infty \mathrm{Re}\left(\frac{e^{-iu\log K}}{iu}\phi(u,T;\theta)\right)du, \tag{3.32}$$

where i is the imaginary unit and $\phi(u,t;\theta)$ is the characteristic function of the logarithm of the stock price process (the characteristic function of a random variable is the Fourier transform of the probability density function of that variable).

It is crucial to define the appropriate characteristic function $\phi(u,t;\theta)$ in order to evaluate the integrals in eqs.(3.31) and(3.32) and, with them, find the option price with eq.(3.30). In his original article, Heston proposed a solution to this very characteristic function [Heston, 1993]. However, some posterior authors demonstrated that, for large maturities, some discontinuities appeared for the proposed solution [Kahl and Jäckel]. One possible alternative, proposed by Schoutens [Schoutens et al.], avoids this shortcoming and is given by

$$\phi(u,t;\theta) = \exp\left\{iu\left(\log S_0 + rt\right) + \frac{\kappa\overline{\nu}}{\eta^2}\left[(\xi-\alpha)\,t - 2\log\left(\frac{1-ge^{-\alpha t}}{1-g}\right)\right] + \frac{\nu_0}{\eta^2}\left(\xi-\alpha\right)\frac{1-e^{-\alpha t}}{1-ge^{-\alpha t}}\right\}, \tag{3.33}$$

where we define

$$\xi = \kappa - \eta\rho iu, \tag{3.34}$$

$$\alpha = \sqrt{\xi^2 + \eta^2(u^2+iu)}, \tag{3.35}$$

$$g = \frac{\xi-\alpha}{\xi+\alpha}. \tag{3.36}$$

Proof We will follow the derivation presented in Gatheral [Gatheral, 2006] with slight changes of variables, for consistency.

We begin by defining Itô's Lemma for a function V (such as the price of an option) dependent on the behavior of two diffusion processes X and Y (such as the stock price and variance processes, but also applicable to two different stock price processes), which is given by

$$dV = \frac{\partial V}{\partial t}dt + \frac{\partial V}{\partial X}dX + \frac{\partial V}{\partial Y}dY + \frac{1}{2}\sigma_X^2\frac{\partial^2 V}{\partial X^2}dt + \rho\sigma_X\sigma_Y\frac{\partial^2 V}{\partial X\partial Y}dt + \frac{1}{2}\sigma_Y^2\frac{\partial^2 V}{\partial Y^2}dt, \tag{3.37}$$

where we have assumed that the two diffusion processes are defined as

$$\begin{aligned} dX &= \mu_X(X,Y,t)dt + \sigma_X(X,Y,t)dW_X; \\ dY &= \mu_Y(X,Y,t)dt + \sigma_Y(X,Y,t)dW_Y, \end{aligned} \tag{3.38}$$

where W_X and W_Y have a correlation of ρ.

If we apply this lemma (as well as the usual non-arbitrage arguments) to the price of a call option's value, assuming the diffusion processes to be the stock price and variance defined in eqs.(3.28) and (3.29), we arrive at

$$\frac{\partial C}{\partial t} + \frac{1}{2}\nu S^2 \frac{\partial^2 C}{\partial S^2} + \rho\eta\nu S \frac{\partial^2 C}{\partial \nu \partial S} + \frac{1}{2}\eta^2 \nu \frac{\partial^2 C}{\partial \nu^2} + rS\frac{\partial C}{\partial S} - rC + \kappa(\overline{\nu} - \nu)\frac{\partial C}{\partial \nu} = 0. \tag{3.39}$$

We now define the forward price as $F(t) = S(t)e^{r(T-t)}$, and introduce the variables $\tau = T - t$ and $x(t) = \log(F(t)/K)$. We furthermore denote C^* as the future value to expiration of the option price (i.e. $C^* = Ce^{rT}$). The relation in eq.(3.39) reduces to

$$-\frac{\partial C^*}{\partial \tau} + \frac{1}{2}\nu \frac{\partial^2 C^*}{\partial x^2} + \rho\eta\nu \frac{\partial^2 C^*}{\partial x \partial \nu} + \frac{1}{2}\eta^2\nu \frac{\partial^2 C^*}{\partial \nu^2} - \frac{1}{2}\nu\frac{\partial C^*}{\partial x} + \kappa(\overline{\nu} - \nu)\frac{\partial C^*}{\partial \nu} = 0, \tag{3.40}$$

which has a solution of the form [Duffie et al., 2000]

$$C^*(x,\nu,\tau) = Ce^{rT} = \left(S_0 P_1 - e^{-rT} K P_0\right) e^{rT} = K\left[e^x P_1(x,\nu,\tau) - P_0(x,\nu,\tau)\right]. \tag{3.41}$$

Substituting the solution of eq.(3.41) in eq.(3.40) implies that P_0 and P_1 must satisfy

$$-\frac{\partial P_j}{\partial \tau} + \frac{1}{2}\nu\frac{\partial^2 P_j}{\partial x^2} - \left(\frac{1}{2} - j\right)\nu\frac{\partial P_j}{\partial x} + \frac{1}{2}\eta^2\nu\frac{\partial^2 P_j}{\partial \nu^2} + \rho\eta\nu\frac{\partial^2 P_j}{\partial x \partial \nu} + \left(\kappa(\overline{\nu} - \nu) + j\nu\rho\eta\right)\frac{\partial P_j}{\partial \nu} = 0, \tag{3.42}$$

for $j = 0, 1$ and subject to the terminal condition $P_j(x, \nu, \tau = 0) = \mathbb{1}_{\{x>0\}}$.

To solve this problem we use a Fourier transform technique. Defining $\tilde{P}_j$ as the Fourier transform of P_j,

$$\tilde{P}_j(u,\nu,\tau) = \int_{-\infty}^{\infty} e^{-iux} P_j(x,\nu,\tau)dx, \tag{3.43}$$

and substituting this result in eq.(3.42) produces

$$\nu\left\{\omega_j \tilde{P}_j - \beta_j \frac{\partial \tilde{P}_j}{\partial \nu} + \frac{\eta^2}{2}\frac{\partial^2 \tilde{P}_j}{\partial \nu^2}\right\} + \kappa\overline{\nu}\frac{\partial \tilde{P}_j}{\partial \nu} - \frac{\partial \tilde{P}_j}{\partial \tau} = 0, \tag{3.44}$$

with

$$\omega_j = -\frac{u^2}{2} - \frac{iu}{2} + iju, \tag{3.45}$$

$$\beta_j = \kappa - \rho\eta iu - \rho\eta j. \tag{3.46}$$

Heston proposed that $\tilde{P}_j$ is a function of the form

$$\tilde{P}_j(u,\nu,\tau) = \frac{1}{iu}\exp\left\{\zeta_j(u,\tau)\overline{\nu} + \psi_j(u,\tau)\nu\right\}. \tag{3.47}$$

We can therefore derive

$$\frac{\partial \tilde{P}_j}{\partial \tau} = \left\{\overline{\nu}\frac{\partial \zeta_j}{\partial \tau} + \nu\frac{\partial \psi_j}{\partial \tau}\right\}\tilde{P}_j, \tag{3.48}$$

$$\frac{\partial \tilde{P}_j}{\partial \nu} = \psi_j \tilde{P}_j, \tag{3.49}$$

$$\frac{\partial^2 \tilde{P}_j}{\partial \nu^2} = \psi_j^2 \tilde{P}_j. \tag{3.50}$$

Thus, eq.(3.44) is only satisfied if

$$\frac{\partial \zeta_j}{\partial \tau} = \kappa\psi_j, \tag{3.51}$$

$$\frac{\partial \psi_j}{\partial \tau} = \omega_j - \beta_j\psi_j + \frac{\eta^2}{2}\psi_j^2. \tag{3.52}$$

Integrating these solutions with terminal conditions $\zeta_j(u,0) = \psi_j(u,0) = 0$, yields

$$\zeta_j(u,\tau) = \frac{\kappa}{\eta^2}\left[(\beta_j - \gamma_j)\,\tau - 2\log\left(\frac{1 - g_j e^{-\gamma_j \tau}}{1 - g_j}\right)\right], \tag{3.53}$$

$$\psi_j(u,\tau) = \frac{1}{\eta^2}(\beta_j - \gamma_j)\frac{1 - e^{-\gamma_j\tau}}{1 - g_j e^{-\gamma_j\tau}}, \tag{3.54}$$

where we define

$$\gamma_j = \sqrt{\beta_j - 2\omega_j\eta^2}, \tag{3.55}$$

$$g_j = \frac{\beta_j - \gamma_j}{\beta_j + \gamma_j}. \tag{3.56}$$

We finally arrive at the solution for P_j given by

$$P_j(x,\nu,\tau) = \frac{1}{2} + \frac{1}{\pi}\int_0^\infty \mathrm{Re}\left(\frac{\exp\left\{\zeta_j(u,\tau)\overline{\nu} + \psi_j(u,\tau)\nu + iux\right\}}{iu}\right)du. \tag{3.57}$$

A change of variables is possible, as shown by Crisostomo [Crisóstomo, 2015], such that the two different characteristic functions for P_1 and P_0 can be transformed into a single one by defining

$$P_1 = \frac{1}{2} + \frac{1}{\pi}\int_0^\infty \mathrm{Re}\left(\frac{e^{-iu\log K}}{iuS_0 e^{rT}}\phi(u - i, T;\theta)\right)du, \tag{3.58}$$

$$P_0 = \frac{1}{2} + \frac{1}{\pi}\int_0^\infty \mathrm{Re}\left(\frac{e^{-iu\log K}}{iu}\phi(u, T;\theta)\right)du, \tag{3.59}$$

with the characteristic function $\phi(u,T;\theta)$ given by

$$\phi(u,t;\theta) = \exp\left\{iu\left(\log S_0 + rt\right) + \frac{\kappa\overline{\nu}}{\eta^2}\left[(\xi - \alpha)\,t - 2\log\left(\frac{1 - ge^{-\alpha t}}{1 - g}\right)\right] + \frac{\nu_0}{\eta^2}(\xi - \alpha)\frac{1 - e^{-\alpha t}}{1 - ge^{-\alpha t}}\right\}. \tag{3.60}$$

□

The main problem with the characteristic function presented in eq.(3.33) is the fact that it is highly nonlinear. Because we will apply some optimization procedure to minimize the difference between the model and the market option prices (i.e. calibration), the optimizer is very likely become stuck in some local minimum and not find the globally optimal solution. This shortcoming led some authors to propose several modified versions of this function, such as Rollin *et al.* [del Baño Rollin et al., 2010]. Most recently, Cui *et al.* [Cui et al., 2017] presented a characteristic function that not only doesn't have the previously mentioned discontinuities but also solves the nonlinearity problem, given by

$$\phi(u,t;\theta) = \exp\left\{iu\left(\log S_0 + rt\right) - \frac{t\kappa\overline{\nu}\rho iu}{\eta} - \nu_0 A + \frac{2\kappa\overline{\nu}}{\eta^2}D\right\}, \tag{3.61}$$

with A and D given by

$$A = \frac{A_1}{A_2}, \tag{3.62}$$

$$D = \log\alpha + \frac{(\kappa-\alpha)t}{2} - \log\left(\frac{\alpha+\xi}{2} + \frac{\alpha-\xi}{2}e^{-\alpha t}\right), \tag{3.63}$$

where ξ and α are given by eqs.(3.34) and(3.35), respectivelly, and where we introduce the variables A_1, A_2, given by

$$A_1 = (u^2 + iu)\sinh\frac{\alpha t}{2}, \tag{3.64}$$

$$A_2 = \alpha\cosh\frac{\alpha t}{2} + \xi\sinh\frac{\alpha t}{2}. \tag{3.65}$$

With this result we are now able to find the prices of options under the Heston model for a given set of parameters θ. We just need to calibrate the parameters to some market data to be able to model the volatility process.

One last consideration is required for the Heston model. By analyzing eqs.(3.28) and(3.29) we can see that the square root of the variance is used. This shouldn't pose a problem, since the variance of any process is always positive. However, because in our case this variable is itself stochastic, we must guarantee that it doesn't become negative, or else the square root would output imaginary numbers. To ensure this, we can apply Feller's condition [Albrecher et al., 2006] and force the parameters to obey

$$2\kappa\overline{\nu} > \eta^2. \tag{3.66}$$

However, this condition restricts the sample space of our model. One possible alternative is to set the variance to zero every time it becomes negative:

$$\nu = \max\left[\nu^*, 0\right], \tag{3.67}$$

where ν^* corresponds to the unrestricted variance and ν is the new (always positive) variance, ensuring that the square root outputs a real number. Because this alternative allows any value for the parameters, it will be adopted in the implementation of the Heston model.

3.3.2 Static SABR Model

One other very famous model for stochastic volatility was developed by Hagan *et al.* [Hagan et al., 2002] and is known as *SABR* - we will henceforth refer to it by *Static SABR*, to distinguish it from the *Dynamic SABR* model that we will see next. SABR stands for "*stochastic-*$\alpha\beta\rho$" and in this model it is assumed that the option prices and volatilities follow [Vlaming, 2011]

$$\boxed{dS(t) = rS(t)dt + e^{-r(T-t)(1-\beta)}\sigma(t)(S(t))^{\beta}dW_1(t),} \tag{3.68}$$

$$\boxed{d\sigma(t) = \nu\sigma(t)dW_2(t),} \tag{3.69}$$

where we define $\alpha = \sigma(0)$ as the starting volatility and $S_0 = S(0)$ as the starting stock price. Furthermore, as before, the two Brownian motion processes $W_1(t)$ and $W_2(t)$ have a *constant* correlation of ρ.

The parameters β and ν correspond, respectively to the *skewness* (i.e. how the volatility smile moves when the stock price changes) and the *volatility of volatility* (i.e. how erratic is the volatility process).

In the original article, the authors claim that β can be fitted from historical market data, but usually investors choose this value heuristically, depending on the type of assets traded. Typical values used are $\beta = 1$ (stochastic lognormal model), used for foreign exchange options, $\beta = 0$ (stochastic normal model), typical for interest rate options and $\beta = 0.5$ (stochastic CIR model), also common for interest rate options [Hagan et al., 2002]. Because are trying to compare several models, we will make no assumptions on the data used. Therefore, we will leave this parameter free when fitting the model to the market data, assuming no heuristics.

One of the main problems with the static SABR model is the fact that, unlike the Heston model, the stochastic volatility process is not mean-reverting. This shortcoming enables the volatility to evolve unrestrictedly which is problematic - it may become negative, which is clearly absurd, or it may become extremely large, which is troublesome. Labordère [Labordère, 2005] proposed a mean-reverting correction to static SABR, but we will study the original model by Hagan *et al.*, as it is more commonly used. We should still note that while negative volatilities make no sense in the real world, by examining eq.(3.68) we can see that this should pose no problem upon simulations, since this effect would be equivalent to inverting the Brownian motion process (i.e. $dW(t) \implies -dW(t)$), which is obviously allowed.

One of the main reasons why static SABR is so popular is due to its quasi-closed-form solutions that enable us to quickly find the implied volatilities of options priced under this model. With the corrections done by Oblój on Hagan's original formula [Obloj, 2008], it can be shown that these implied volatilities are given by

$$\begin{aligned}\sigma_{SABR}(K,f,T) \approx & \frac{1}{\left[1 + \frac{(1-\beta)^2}{24}\log^2\left(\frac{f}{K}\right) + \frac{(1-\beta)^4}{1920}\log^4\left(\frac{f}{K}\right)\right]} \cdot \left(\frac{\nu \log(f/K)}{x(z)}\right) \\ & \cdot \left\{1 + T\left[\frac{(1-\beta)^2}{24}\frac{\alpha^2}{(Kf)^{1-\beta}} + \frac{1}{4}\frac{\rho\beta\nu\alpha}{(Kf)^{(1-\beta)/2}} + \frac{2-3\rho^2}{24}\nu^2\right]\right\},\end{aligned} \tag{3.70}$$

with z and $x(z)$ defined as

$$z = \frac{\nu\left(f^{1-\beta} - K^{1-\beta}\right)}{\alpha(1-\beta)}, \tag{3.71}$$

$$x(z) = \log\left\{\frac{\sqrt{1-2\rho z+z^2}+z-\rho}{1-\rho}\right\}, \tag{3.72}$$

where we have used $f = S_0 e^{rT}$. The proof of this solution is quite lengthy and will not be replicated here, though it can be found in the original article [Hagan et al., 2002].

For the particular case where $f = K$, evaluating eq.(3.70) produces a $0/0$ indeterminate form. This poses no problem because the closed form solution actually simplifies to [Hagan et al., 2002]

$$\sigma_{SABR}(K, f=K, T) \approx \frac{\alpha}{K^{1-\beta}}.\left\{1 + T\left[\frac{(1-\beta)^2}{24}\frac{\alpha^2}{K^{2(1-\beta)}} + \frac{1}{4}\frac{\rho\beta\nu\alpha}{K^{1-\beta}} + \frac{2-3\rho^2}{24}\nu^2\right]\right\}. \tag{3.73}$$

As for the Heston model, we again need to calibrate the parameters of this model to be able to model the volatility process.

3.3.3 Dynamic SABR Model

One of the main setbacks of the static SABR model is the fact that it should only be calibrated on a set of options with the same maturity. The model behaves badly when we try to fit options with different maturities [Hagan et al., 2002].

To solve this problem, Hagan *et al.* suggested a similar model known as *Dynamic SABR* [Hagan et al., 2002]. It follows the same diffusion processes presented in eqs.(3.68) and(3.69) but with time-dependent parameters $\rho(t)$ and $\nu(t)$,

$$\boxed{dS(t) = rS(t)dt + e^{-r(T-t)(1-\beta)}\sigma(t)(S(t))^{\beta}dW_1(t),} \tag{3.74}$$

$$\boxed{d\sigma(t) = \nu(t)\sigma(t)dW_2(t),} \tag{3.75}$$

with the correlation between $W_1(t)$ and $W_2(t)$ now given by

$$dW_1(t)dW_2(t) = \rho(t)dt, \quad \forall t > 0. \tag{3.76}$$

where $\rho(t)$ is now a function of time.

Hagan *et al.* derived again a quasi-closed-form solution for the implied volatilities of options priced under this model. Osajima later simplified this expression using asymptotic expansion [Osajima, 2007]. The resulting formula is given by

$$\sigma_{DynSABR}(K, f, T) = \frac{1}{\omega}\left(1 + A_1(T)\log\left(\frac{K}{f}\right) + A_2(T)\log^2\left(\frac{K}{f}\right) + B(T)T\right), \tag{3.77}$$

where $f = S_0 e^{rT}$, $\omega = f^{1-\beta}/\alpha$ and where $A_1(T)$, $A_2(T)$ and $B(T)$ are given by

$$A_1(T) = \frac{\beta-1}{2} + \frac{\eta_1(T)\omega}{2}, \tag{3.78}$$

$$A_2(T) = \frac{(1-\beta)^2}{12} + \frac{1-\beta-\eta_1(T)\omega}{4} + \frac{4\nu_1^2(T) + 3(\eta_2^2(T) - 3\eta_1^2(T))}{24}\omega^2, \tag{3.79}$$

$$B(T) = \frac{1}{\omega^2}\left(\frac{(1-\beta)^2}{24} + \frac{\omega\beta\eta_1(T)}{4} + \frac{2\nu_2^2(T) - 3\eta_2^2(T)}{24}\omega^2\right), \tag{3.80}$$

with $\nu_1^2(T)$, $\nu_2^2(T)$, $\eta_1(T)$ and $\eta_2^2(T)$ defined as

$$\nu_1^2(T) = \frac{3}{T^3}\int_0^T (T-t)^2\nu^2(t)dt, \tag{3.81}$$

$$\nu_2^2(T) = \frac{6}{T^3}\int_0^T (T-t)t\nu^2(t)dt, \tag{3.82}$$

$$\eta_1(T) = \frac{2}{T^2}\int_0^T (T-t)\nu(t)\rho(t)dt, \tag{3.83}$$

$$\eta_2^2(T) = \frac{12}{T^4}\int_0^T\int_0^t \left(\int_0^s \nu(u)\rho(u)du\right)^2 dsdt, \tag{3.84}$$

where $\rho(t)$ and $\nu(t)$ are the functions chosen to model the time dependent parameters.

We now need to empirically choose some appropriate functions for $\rho(t)$ and $\nu(t)$. We can choose these functions such that the integrals in eqs.(3.81)-(3.84) are analytically solvable, greatly simplifying the calibration of this model. One possible solution [Fernández et al., 2013] is to define $\rho(t)$ and $\nu(t)$ as

$$\rho(t) = \rho_0 e^{-at}, \tag{3.85}$$

$$\nu(t) = \nu_0 e^{-bt}, \tag{3.86}$$

with $\rho_0 \in [-1, 1]$, $\nu_0 > 0$, $a > 0$ and $b > 0$. In this particular case, $\nu_1^2(T)$, $\nu_2^2(T)$, $\eta_1(T)$ and $\eta_2^2(T)$ can be exactly derived as

$$\nu_1^2(T) = \frac{6\nu_0^2}{(2bT)^3}\left[\left(\frac{(2bT)^2}{2} - 2bT + 1\right) - e^{-2bT}\right], \tag{3.87}$$

$$\nu_2^2(T) = \frac{12\nu_0^2}{(2bT)^3}\left[e^{-2bT}(1+bT) + bT - 1\right], \tag{3.88}$$

$$\eta_1(T) = \frac{2\nu_0\rho_0}{T^2(a+b)^2}\left[(a+b)T + e^{-(a+b)T} - 1\right], \tag{3.89}$$

$$\eta_2^2(T) = \frac{3\nu_0^2\rho_0^2}{T^4(a+b)^4}\left[e^{-2(a+b)T} - 8e^{-(a+b)T} + (7 + 2T(a+b)(-3 + (a+b)T))\right]. \tag{3.90}$$

There exist other more complicated functions for $\rho(t)$ and $\nu(t)$ which, due to their increased complexity, can better fit the data. An example of such functions can be found in Fernandez [Fernández et al., 2013]. The main concern with these functions is that they usually don't have analytically solvable solutions for the integrals in eqs.eqs.(3.81)-(3.84), and need to be computed numerically. For this reason, these will not be considered in the present work.

Chapter 4

Implementation

4.1 Option Pricing

The theoretical models introduced in chapter 3 attempt to replicate the behavior of real-world volatilities. With these predictions, we should be able to better reproduce real option prices than if we assumed a simple constant volatility, as done by Black *et al.*

Currently, the two most used methods to computationally price options are known as *finite differences* [Hull, 2012] and *Monte Carlo* [Glasserman, 2004].

The finite differences method is an extremely fast procedure when used to price either European or American-type options, making it very appealing in these circumstances. However, when applied to other option types whose payoff depends on the stock price path itself (e.g. Asian options, that depend on the average value of all the stock prices until maturity), the algorithm requires some considerable changes that make it very slow, rendering it almost useless. The implementation of both Heston and SABR models (presented before) using finite differences can nonetheless be found in deGraaf [de Graaf].

With the Monte Carlo algorithm, we begin by simulating a very large number of stock price paths (e.g. 100 000 simulations). The option's payoff is then calculated for each of these simulated paths and averaged, providing a fairly good estimate of the option's future payoff. The option's price can be extracted from its expected payoff, using eq.(2.4). This algorithm can be easily adapted to price path-dependent options, making it very attractive in such cases. In the past, simulating all the stock price paths took prohibitively long computation times and this method was often discarded for this reason. However, with the recent advancements in computer hardware and new algorithmic developments, such as GPU implementation, this shortcoming has been, to some extent, mitigated, making the Monte Carlo algorithm quite popular in the present. For these reasons, the Monte Carlo method will be used for the implementation and analysis of the models introduced in chapter 3, so this model will be studied to some extent in the present chapter.

4.1.1 Simulating stock prices

As stated, to implement the Monte Carlo algorithm, one needs to simulate stock price paths. However, by analyzing eq.(2.14), we can see that the stock prices depend on a Brownian motion process which, due to its self-similarity, is not differentiable [Mikosch, 1998]. It follows that stock price paths can never be exactly simulated. Despite this, we can approximate the movement of stock price paths by discretizing the Brownian motion process in time, thus avoiding its self-similarity problem. We now introduce two of the most common discretization procedures.

Euler–Maruyama discretization

One of the simplest and most used discretization methods is known as *Euler–Maruyama discretization*, and can be applied to stochastic differential equations of the type

$$dX(t) = a(X(t))dt + b(X(t))dW(t), \tag{4.1}$$

where $a(X(t))$ and $b(X(t))$ are given functions of $X(t)$ and where $\{W(t),\ t > 0\}$ defines a one-dimensional Brownian motion process. To apply this discretization, we begin by partitioning the time interval $[0, T]$ into N subintervals of width $\Delta t = T/N$ and then iteratively defining

$$X_{n+1} = X_n + a(X_n)\Delta t + b(X_n)\Delta W_n, \quad n = 1, \ldots, N, \tag{4.2}$$

with X_0 equal to some given value and where $\Delta W_n = W_{t+\Delta t} - W_t$. Using the known properties of Brownian motion processes, it can be shown that $\Delta W_n \sim \sqrt{\Delta t} Z(t)$, where $Z(t) \sim N(0, 1)$ defines a normal distributed random variable.

Applying this discretization to the Geometric Brownian motion followed by stock price paths, as seen in eq.(2.14), we arrive at

$$S(t + \Delta t) = S(t) + rS(t)\Delta t + \sigma(S(t), t)S(t)\sqrt{\Delta t} Z. \tag{4.3}$$

Due to its simplicity, the Euler–Maruyama discretization method is the most common in the simulation of stock price paths whenever we have constant or deterministic volatilities.

Milstein Discretization

For stochastic volatility models, such as Heston and SABR, where the volatility itself follows a stochastic process, the Euler–Maruyama discretization may not be sufficiently accurate. In these cases, we can apply the more precise Milstein method [Milstein, 1975], defined as

$$X_{n+1} = X_n + a(X_n)\Delta t + b(X_n)\Delta W_n + \frac{1}{2} b(X_n)b'(X_n)((\Delta W_n)^2 - \Delta t), \tag{4.4}$$

where $b'(X_n)$ denotes the derivative of $b(X_n)$ w.r.t. X_n. Note that when $b'(X_n) = 0$, the Milstein method degenerates to the simpler Euler–Maruyama discretization. This discretization should be applied not only to the stock price process but also to the stochastic volatility.

Applying this discretization to the stock price and variance processes of the Heston model produces

$$S(t+\Delta t) = S(t) + rS(t)\Delta t + S(t)\sqrt{\nu(t)}\sqrt{\Delta t}(Z_1(t)) + \frac{1}{2}\nu(t)S(t)\Delta t((Z_1(t))^2 - 1), \tag{4.5}$$

$$\nu(t+\Delta t) = \nu(t) + \kappa(\overline{\nu} - \nu(t))\Delta t + \eta\sqrt{\nu(t)\Delta t}(Z_2(t)) + \frac{\eta^2}{4}\Delta t((Z_2(t))^2 - 1), \tag{4.6}$$

where Z_1 and Z_2 are two normal random variables with a correlation of ρ.

As for the SABR model, this discretization results in

$$\begin{aligned} S(t+\Delta t) =& S(t) + rS(t)\Delta t + e^{-r(T-t)(1-\beta)}\sigma(t)S^{\beta}(t)\sqrt{\Delta t}(Z_1(t)) + \\ &+ \frac{\beta}{2}e^{-2r(T-t)(1-\beta)}\sigma^2(t)S^{2\beta-1}(t)\Delta t((Z_1(t))^2 - 1), \end{aligned} \tag{4.7}$$

$$\sigma(t+\Delta t) = \sigma(t) + \nu\sigma(t)\sqrt{\Delta t}(Z_2(t)) + \frac{\nu^2}{2}\sigma(t)\Delta t((Z_2(t))^2 - 1). \tag{4.8}$$

For the Dynamic SABR model, the discretization is the same as its Static equivalent, replacing only the variables ν and ρ by the functions $\nu(t)$ and $\rho(t)$, respectively

In all of these models we need to generate two correlated normal variables, $Z_1(t)$ and $Z_2(t)$, say with a correlation of $\rho(t)$. This can be easily achieved with

$$\begin{aligned} &Z_1(t) \sim N(0,1); \\ &Z_2(t) = \rho(t)Z_1(t) + \sqrt{1-(\rho(t))^2}Y(t), \end{aligned} \tag{4.9}$$

where $Y(t) \sim N(0,1)$ is a random variable independent of $Z_1(t)$.

Because it is more precise, the Milstein method will be used in the implementation of the Heston and Static/Dynamic SABR stochastic volatility models. The simpler Euler–Maruyama discretization will be assumed for both constant and Dupire's local volatility.

It is important to note that, the smaller our subintervals Δt are, the better is the approximation done when discretizing the Brownian motion process. However, by decreasing Δt we increase the number of intervals needed and, with it, the number of calculations required to generate a stock price path. This compromise between computation time and precision must be handled appropriately. In Figure 4.1 we can see how the size of the subintervals influences the resemblance of a simulated GBM process to its continuous version.

We should also note that this discretization is more problematic when we try to price Barrier options. As we stated before, a Barrier option becomes activated/void if the stock price reaches a certain barrier level B. When we discretize a continuous stock price process, we ignore any prices that this process might have taken in the time between two time steps. However, it is perfectly possible that during this interval the stock price goes below/above this barrier level, which is not considered in the discretization. A barrier option might have crossed a barrier with a non-discretized Brownian motion process and not

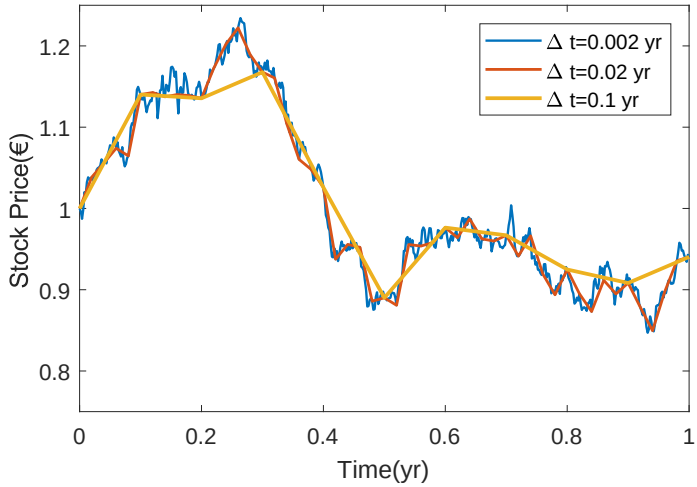

Figure 4.1: Effect of the subinterval size on the GBM discretization with maturity $T = 1\,\text{yr}$, interest rate $r = 1 \times 10^{-2}\,\text{yr}^{-1}$, volatility $\sigma = 1 \times 10^{-1}\,\text{yr}^{-1/2}$ and initial stock price $S_0 = 1\,€$. The subinterval sizes selected were $\Delta t = 2 \times 10^{-3}\,\text{yr}$, $\Delta t = 2 \times 10^{-2}\,\text{yr}$ and $\Delta t = 1 \times 10^{-1}\,\text{yr}$ for the blue, red and orange plot lines, respectively. To emphasize this effect, the underlying Brownian Motion $\{W(t),\ t > 0\}$ used to generate all three paths was the same.

with its discretization. Thus, Barrier options will always be underpriced or overpriced when priced with Monte Carlo. This problem can be mitigated by significantly increasing the number of time steps, reducing their size, though this will increase computation time. Furthermore, reducing the step size merely diminishes the severity of the problem and doesn't actually solve it.

4.1.2 Pricing options from simulations

To price options using the Monte Carlo algorithm, we generate M paths by recursively calculating $\{S_i(t_j),\ \ i = 1, \ldots, M,\ \ t_j = 0, \ldots, T\}$, using either of the discretization methods described before.

When the stock price at the maturity, $S_i(T)$, is obtained for all paths, the option's payoff for each path is calculated using eqs.(2.1)-(2.3). We then average all these results and discount them back to the present, obtaining the option's value

$$\begin{aligned} C(K,T) &= e^{-rT}\frac{1}{M}\sum_{i=1}^{M}\text{Payoff}_{i,call}(K,T); \\ P(K,T) &= e^{-rT}\frac{1}{M}\sum_{i=1}^{M}\text{Payoff}_{i,put}(K,T), \end{aligned} \tag{4.10}$$

where $\text{Payoff}_{i,\cdot}(K,T)$ denotes the payoff function of the chosen option type (e.g. European, Barrier, ...) for the i^{th} path.

Despite its versatility, the Monte Carlo method can lead to an erroneous estimate for the price of options, in particular for options with very high strike prices. To understand this problem, notice that the payoff function of European options is zero for stocks below the strike. If we have a very large strike,

very few of the simulated paths will actually cross the strike at maturity and contribute to the calculation of the option's price (all the other paths will contribute with a payoff of zero). The averaging procedure shown in eq.(4.10) will therefore be performed on an extremely small subset of paths, thus producing a bad estimation for the option price. We could counter this effect by simulating an even larger number of paths, so that we always have a significant number of paths above a given strike that end up contributing to the option's price, though this comes at the cost of increased computation times. Furthermore, on the limit, there will always be a strike high enough that none of the simulated paths reach it, meaning that the option's value for that simulation would be zero. This does not hold in real life, since there is always a positive price for any option, even for extremely high strikes. This problem is further aggravated for Barrier options, since only the paths that are above the strike price at maturity *and* have crossed the barrier level contribute to the option price. This further reduces the number of paths considered and is quite problematic for high barrier levels.

4.2 Surface Interpolation (Dupire)

To apply Dupire's local volatility model, as shown in eq.(3.23), we need to generate the implied volatility surface from the market data. Because we only have data for a finite set of maturities and strikes, the implied volatility surface must be obtained by some form of interpolation and extrapolation. From this interpolated surface we must also calculate the gradients needed for the local volatility formula.

One possible interpolation method is known as *Delaunay triangulation* [Amidror, 2002]. In short, assuming a 2-dimensional data set, this interpolation algorithm generates a triangulation between points P_1, P_2 and P_3 if the circumscribed circle of these points contains no other points P_j inside. A scheme of this interpolation method is shown in Figure 4.2.

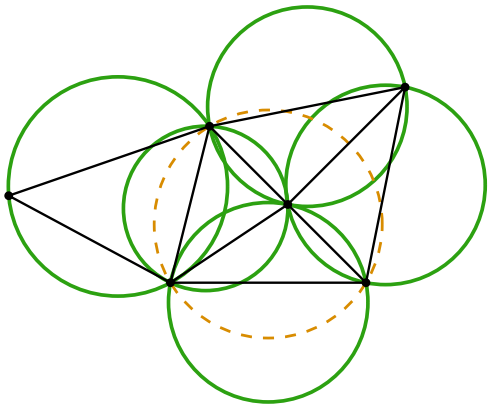

Figure 4.2: Example of a Delaunay triangulation, where we connect the points for which the circumscribed circles (green) don't contain any other points inside. A circle for which this property does not hold (orange dashed) is also represented, though no triangulation is possible in this case.
Source: `https://www.ti.inf.ethz.ch/ew/Lehre/CG13/lecture/Chapter%206.pdf`

We can easily adapt this algorithm to 3-dimensions (as is the case of our data), using spheres instead of circles. The resulting interpolated surface will simply be a set of merged triangles, with the data points serving as a vertices. Though this is usually a good approximation, it will produce wrong results when

calculating the derivatives used in the local volatility formula (e.g. calculating the second derivative on the triangular planes of the interpolation results in zero). If we used the first version of Dupire's formula, shown in eq.(3.6), where we use the second derivative in the denominator, the resulting local volatility surface would become highly unrealistic. However, since we will use the formula in eq.(3.23), which is not so sensitive to this value, no significant problems are expected.

The function *scatteredInterpolant*, implemented in MATLAB, applies this Delaunay triangulation to a set of scattered data, and will therefore be used in the implied volatility surface generation.

From the interpolated surface obtained, we need to calculate the gradients. These have to be obtained numerically, as we do not have an analytical formula for the surface. To obtain them we use the formulas

$$\frac{\partial \sigma_{imp}}{\partial K} = \frac{\sigma_{imp}(K + \Delta K, T) - \sigma_{imp}(K - \Delta K, T)}{2\Delta K} \tag{4.11}$$

$$\frac{\partial^2 \sigma_{imp}}{\partial K^2} = \frac{\sigma_{imp}(K + \Delta K, T) + \sigma_{imp}(K - \Delta K, T) - 2\sigma_{imp}(K, T)}{(\Delta K)^2} \tag{4.12}$$

$$\frac{\partial \sigma_{imp}}{\partial T} = \frac{\sigma_{imp}(K, T + \Delta T) - \sigma_{imp}(K, T)}{\Delta T} \tag{4.13}$$

where ΔK and ΔT are some (small) intervals for the strike and maturity, respectively. Note that the derivative of the implied volatility w.r.t. maturity is different from the derivative w.r.t. strike. This is due to the fact that negative maturities make no mathematical sense. If we used the same formula as for the derivative w.r.t. the strikes, the case of $T = 0$ would require $\sigma_{imp}(\cdot, T - \Delta T < 0)$, which makes no sense. We thus use the forward derivative in this case. As for the strikes, since there is no mathematical restriction for negative values (though they make no sense in financial terms), we are allowed to use both $\sigma_{imp}(K \pm \Delta K, \cdot)$.

4.3 Model Calibration (Heston and SABR)

Both SABR and Heston stochastic volatility models contain parameters that need to be calibrated in order to appropriately replicate market option prices.

Calibrating the models' parameters means finding the optimal values for these parameters such that the difference between the prices of real market options and options priced under the models' assumptions is minimized. However, because we are modeling volatilities, one possibly better calibration procedure would be to use the difference between the implied volatilities of market options and options priced under each model. This difference should be measured with a cost function, such as the least-squares error, given by

$$\boxed{\mathrm{Cost}(\theta) = \sum_{i=1}^{n} \sum_{j=1}^{m} w_{i,j} \left(\sigma_{imp,\mathrm{mkt}}(T_i, K_j) - \sigma_{imp,\mathrm{mdl}}(T_i, K_j; \theta) \right)^2,} \tag{4.14}$$

where we denote θ as the model's parameter set, w_i corresponds to some weight function and where $\sigma_{imp,\mathrm{mkt}}(\cdot)$ and $\sigma_{imp,\mathrm{mdl}}(\cdot)$ correspond to the real-market and the model's implied volatilities, respectively,

for maturities $\{T_i,\ i = 1, \ldots, n\}$ and strikes $\{K_j,\ j = 1, \ldots, m\}$. This will be the cost function used in the calibration of all models.

The weight function $w_{i,j}$ should be chosen such that higher weights are given to options with strikes closer to the current stock price S_0, because these points have a higher influence in the shape of the volatility smile than the others. One example of such a function is

$$w_{i,j} = \left(1 - \left|1 - \frac{K_j}{S_0}\right|\right)^2, \tag{4.15}$$

where we assume strikes are restricted to $K < 2S_0$. This function is represented in Figure 4.3. Many other possible weight functions are also possible. One other possibility is to give a higher weight to the earliest maturities, though this will not be used.

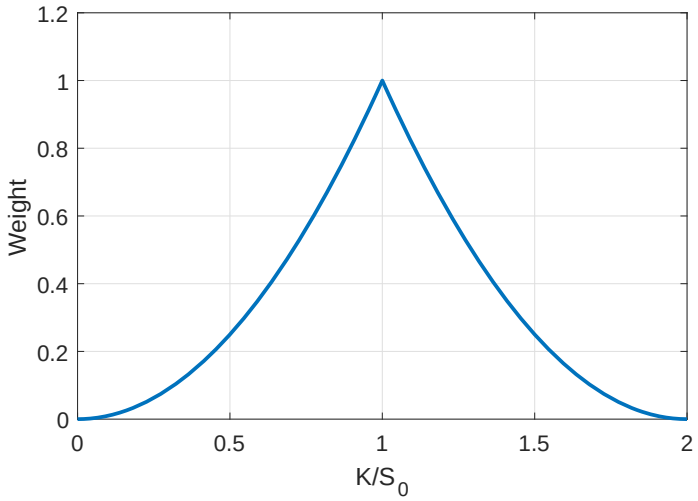

K/S_0	Weight
0.50	0.2500
0.75	0.5625
0.90	0.8100
1.00	1.0000
1.10	0.8100
1.25	0.5625
1.50	0.2500

Figure 4.3: Weight function plot and significant weight values

As we can see, the maximum weight value is given to the point where the strike equals the initial stock price ($K = S_0$) and less weight is given for points farther from this value.

To obtain the value of the cost function for a given set of parameters, we need to calculate $m \times n$ model option prices (see eq.(4.14)). We could achieve this by implementing the Monte Carlo method with the discretization procedures described before. Because we want to calibrate the model's parameters, a large number N of instances of the cost function will have to be executed for our optimization algorithms to converge to an optimal solution. Thus, it can be seen that a very great number of Monte Carlo pricers will have to be executed ($m \times n \times N$). For this reason, even with GPU implementation and advanced hardware, using Monte Carlo to calibrate the model's parameters will become prohibitively slow. We could reduce the computation time by limiting the number of simulated paths, but this would worsen the price estimation obtained, making the optimization procedure much more difficult. Thus, we can conclude that, though the Monte Carlo algorithm is very useful to price options, it is nearly useless in the calibration methods required in both Heston and SABR models.

We must also mention the fact that, while volatility models are commonplace in finance, investors use different models with different parameters to price their options. This means that even if our calibrated model perfectly fits market data at a given time, after a while the prices will change and the calibration will become outdated. Therefore, a frequent recalibration of the parameters is required which demands fast calibration methods to be employed, further dismissing the Monte Carlo calibration.

Fortunately, as mentioned, both Heston and SABR have closed-form solutions, shown in eqs. (3.30), (3.70) and (3.77), that we can use to directly price the options with each model's parameters, without the need to run the slow Monte Carlo pricer. With these closed-form solutions, not only are we able to find the prices and implied volatilities extremely fast, but the result obtained should also be very accurate, with very little to no noise. With both these properties, the optimization algorithms should have no problem in finding optimal solutions for each model's parameters, and doing so very fast.

4.3.1 Optimization Algorithms

There are many optimization algorithms able to find the parameter set that minimizes the cost function shown in eq.(4.14). Our main concern when choosing the best algorithm for this calibration is the nonlinearity of our cost function. This is problematic because several local minima might exist and an unsuitable algorithm may get stuck in these points, causing the globally optimal solution to not be found.

With this issue in mind, we selected a powerful algorithm known as *CMA-ES* [Hansen, 2006] (short for Covariance Matrix Adaptation Evolution Strategy), which we will summarize below. It should be noted that we will only provide a general idea of how this optimizer works. For detailed descriptions, the original source should be consulted.

The optimization algorithm will search the D-dimensional sample space for the optimal solution, θ^*, where D denotes the number of parameters of each model. Each point in this space corresponds to a possible set of parameters, θ.

CMA-ES Optimizer

The CMA-ES optimizer belongs to the class of evolutionary algorithms. These methods are based on the principle of biological evolution: at each iteration (generation), new candidate solutions (individuals) are generated from a given random distribution (mutation) obtained using the data (genes) of the previous solutions (parents). Of these newly generated solutions (individuals), we select the ones where the cost function is minimized (with the best fitness) to generate the candidate solutions of the next iterations (to become the parents of the next generation) and we reject the others.

As for the CMA-ES in particular, the algorithm takes λ samples from a multivariate normal distribution in the D-dimensional sample space, i.e. $\mathbf{x} \sim N(\mathbf{m}, \mathbf{C})$, with density function given by

$$N(\mathbf{x}; \mathbf{m}, \mathbf{C}) = \frac{1}{\sqrt{(2\pi)^D |\det \mathbf{C}|}} \exp\left(-\frac{1}{2}(\mathbf{x}-\mathbf{m})^T \mathbf{C}^{-1} (\mathbf{x}-\mathbf{m})\right), \tag{4.16}$$

where $\mathbf{m}$ and $\mathbf{C}$ correspond to the distribution's mean vector and covariance matrix, respectively. These

λ samples are our candidate solutions.

We classify each of these points according to their fitness (i.e. the cost function's value for a given point). We then select the μ samples with the lowest cost and discard the others. These new points will be the parents of the next generation, i.e. they will be used to generate the new mean and covariance matrix for the normal distribution.

At each iteration, the new mean is produced from a weighted average of the points, with the weights proportional to each point's fitness. The method for the covariance matrix update is rather complex and depends not only on the μ best samples but also on the values of the covariance matrices used in previous iterations. All the basic equations required for the implementation of this optimizer can be found in Appendix B. For a more detailed explanation, as well as other aspects of the algorithm, see Hansen [Hansen, b].

These sampling-classification-adaptation steps are repeated until some stopping criterion is met, such as a fixed number of iterations or an minimum error threshold. When this stopping criterion is verified, the mean vector of the last iteration is assumed as the optimal parameter vector, θ^*.

The number of candidate solutions generated at each step, λ, and the ones that remain after classification, μ, can be chosen arbitrarily, but an adequate heuristic is to choose $\lambda = \lfloor 4 + 3 \log D \rfloor + 1$ and $\mu = \lfloor \lambda/2 \rfloor + 1$.

This optimization procedure is summarized in Algorithm 1.

Algorithm 1: CMA-ES Optimizer

Define mean vector $\mathbf{m} = \theta_0$ `/* Initial guess */`

Define covariance matrix $\mathbf{C} = I$

while *Termination criterion not met* **do**

Sample λ points from multivariate normal distribution $N(\mathbf{x}; \mathbf{m}, \mathbf{C})$

Calculate the cost for all generated points and keep the μ best. Discard the rest

Update the mean vector and covariance matrix (using eqs.(B.5) and (B.9))

end

Optimal parameters: $\theta^* = \mathbf{m}$

The complexity of the covariance matrix updating process makes the CMA-ES a very robust optimization algorithm, enabling it to find the global optimum of highly nonlinear functions [Dilão and Muraro, 2013]. Furthermore, unlike many other optimizers, the CMA-ES is almost non-parametric. It simply requires a starting guess, to generate the starting mean vector, and the algorithm is expected to converge to a global minimum. As for disadvantages, because we have to generate a set of samples at each iteration, if this generation process is slow (such as the Monte Carlo pricer), the convergence may stall significantly, particularly when many parameters are used in the model. Other algorithms may perform faster than CMA-ES, but this optimizer is expected to outperform them in terms of precision.

This optimizer was implemented by Hansen in MATLAB (as well as in other computer languages) as a function named *purecmaes* [Hansen, a] and will be used with only very slight changes, to account for the volatility models used used.

Chapter 5

Results

Having described the implementation of all the models introduced in chapter 3 and the calibration and interpolation methods referenced in chapter 4, in this chapter we study the results of the calibration and compare all the models.

We will calibrate the SABR and Heston models' parameters to a dataset of implied volatilities for European options with different maturities and strike prices. This data was kindly provided by *BNP Paribas* and is shown in Appendix A. As stated, the closed form solutions will be used in this calibration procedure. After the calibration, we are able to produce a function from these closed-form solutions using the models' calibrated parameters. These functions - henceforth named *theoretical functions* - should, in principle, closely fit the implied volatility data.

To validate the SABR and Heston models' closed-form solutions, after finding the optimal parameters with the calibration procedure, we will input them into a Monte Carlo pricer, adapted to each model, and calculate the simulated option prices of each calibrated model. This price will then be converted into an implied volatility (using eq.(3.4)) in order for the simulation to be comparable to the data and the closed form solutions. To better grasp the behavior of the simulations we will repeat them a large number of times, N_{reps}, averaging the results to produce a function - henceforth named *simulated function* - and extracting from them the 95% confidence bands of the simulations - these confidence bands are obtained by sorting the simulated implied volatilities for each strike, extracting both the 97.5% highest and the 2.5% lowest and setting these values to the upper and lower bounds of the confidence bands, so that 95% of all observations are inside them.

As for Dupire's local volatility data, the required Delaunay triangulation introduced in section 4.2 will be performed on the aforementioned data. The resulting interpolation will be used to obtain the local volatility surface, which will be input into a Monte Carlo pricer to generate the option price under this model's assumptions. As done for the Heston and SABR models, we will run this pricer a large number of times, N_{reps}, to obtain the average simulated function and the 95% confidence bands.

In order for the models to be comparable, we need to make sure that the same global parameters are used in all the adjustments and simulations, namely the initial stock price, S_0, the risk-free interest rate, r, the number of pricer repetitions (to be averaged, producing the expected simulated function and

the confidence bands), N_{reps}, and the time step size and the number of paths simulated, Δt and N_{paths}, both used in the Monte Carlo simulations. Their values are shown in Table 5.1.

S_0(€)	r(yr^{-1})	Δt(days)	N_{paths}	N_{reps}
1	0	0.5	100 000	100

Table 5.1: Parameters used throughout all simulations.

The Monte Carlo pricers of each model will then be modified to price Barrier options instead of the European options used in the calibration. These results will be studied with some detail but, due to a lack of data, there is no way to corroborate their validity.

5.1 Constant Volatility Model

To find how well our models perform, we need some reference against which to compare them. One clear possibility is to assume a constant volatility throughout the options' duration, since this is the simplest possible case.

The equation that generates each stock price path is therefore given by

$$dS(t) = rS(t)dt + \sigma S(t)dW(t). \tag{5.1}$$

As we can see in Figure A.1, the implied volatility data is not constant, so we can expect the theoretical implied volatility curve (which, in this case will be a horizontal line) to fit the data very badly.

With this constant volatility model, we can choose to fit the datasets with different maturities independently of one another or together in a single general dataset. In other words, we can do several fits, one for each maturity, or a single one, for all maturities together. The former will be useful when benchmarking the Static SABR model, since for that model the adjustments will also be performed independently (Static SABR performs badly for multiple maturities). The latter will be more appropriate when studying the remaining models - Dupire, Heston and Dynamic SABR - since these fit the whole implied volatility surface (i.e. multiple maturities together). Thus, both versions will be implemented and briefly studied.

5.1.1 Independent Fits

We begin by presenting the results of fitting a constant volatility function to the sets of data with different maturities *independently*.

In Figure 5.1 we show the plots of each fitted implied volatility curve - the *theoretical functions* - along with the provided market data. We also present the results of the Monte Carlo pricer - the *simulated functions* - and the simulations' confidence bands.

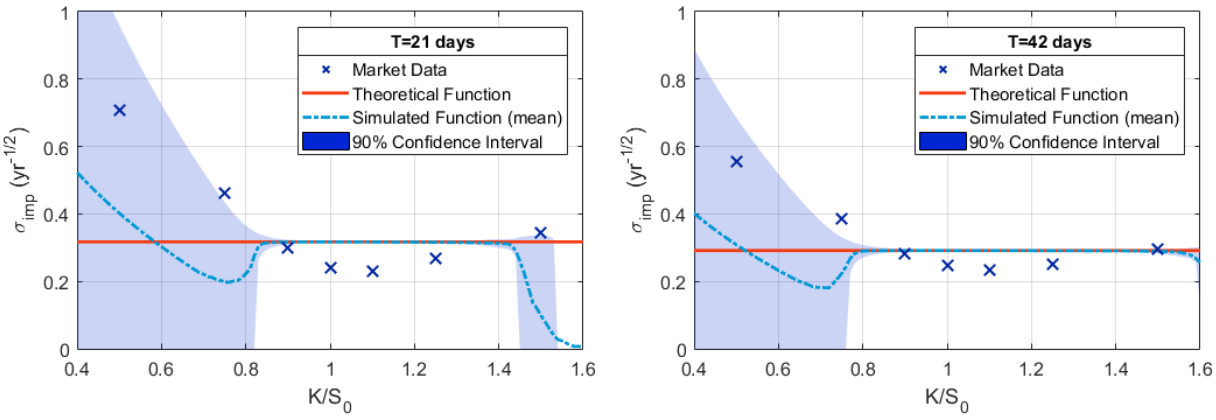

(a) $T = 21$ days

(b) $T = 42$ days

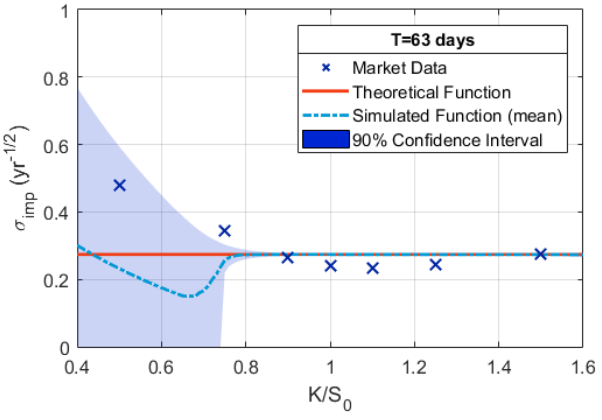

(c) $T = 63$ days

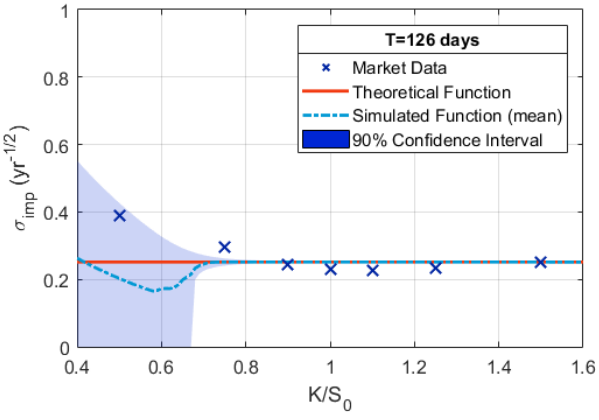

(d) $T = 126$ days

Figure 5.1: Implied volatility functions (red lines) fitted *independently* to the implied volatility data (crosses) for different maturities under constant volatility model, plotted with their respective Monte Carlo simulated functions (light-blue dot-dashed lines) along with their 95% confidence bands (blue region).

The fitted parameter, which, in this case, is only the constant implied volatility, is presented in Table 5.2 for each of the maturities, along with the respective cost function's value (eq.(4.14)).

T (days)	$\sigma_{imp,\mathrm{mdl}}$ (yr$^{-1/2}$)	Cost
21	0.3174	0.0635
42	0.2918	0.0282
63	0.2742	0.0164
126	0.2518	0.0069

Table 5.2: Fitted implied volatilities for each maturity (fitted independently) under constant volatility model.

T(days)	K(€)	$\sigma_{imp,\mathrm{mdl}}$(yr$^{-1/2}$)	$\mathrm{Error}_\sigma(\%)$	C_{mdl}(€)	$\mathrm{Error}_C(\%)$
	0.50		55	5.000×10^{-1}	0
	0.75		31	2.500×10^{-1}	0
	0.90		6	1.054×10^{-1}	1
21	1.00	0.3174	31	3.654×10^{-2}	31
	1.10		37	7.406×10^{-3}	206
	1.25		18	2.501×10^{-4}	368
	1.50		8	1.119×10^{-7}	81
	0.50		47	5.000×10^{-1}	0
	0.75		25	2.503×10^{-1}	1
	0.90		3	1.117×10^{-1}	1
42	1.00	0.2918	19	4.749×10^{-2}	19
	1.10		24	1.500×10^{-2}	76
	1.25		16	1.575×10^{-3}	154
	1.50		2	1.244×10^{-5}	21
	0.50		43	5.000×10^{-1}	0
	0.75		21	2.508×10^{-1}	1
	0.90		3	1.165×10^{-1}	1
63	1.00	0.2742	14	5.465×10^{-2}	14
	1.10		18	2.069×10^{-2}	46
	1.25		12	3.331×10^{-3}	85
	1.50		0	7.437×10^{-5}	3
	0.50		35	5.000×10^{-1}	0
	0.75		15	2.534×10^{-1}	1
	0.90		3	1.288×10^{-1}	1
126	1.00	0.2518	10	7.094×10^{-2}	10
	1.10		11	3.488×10^{-2}	22
	1.25		8	9.977×10^{-3}	32
	1.50		0	8.510×10^{-4}	1

Table 5.3: Comparison between fitted functions (fitted independently) and original data under constant volatility model with the respective relative errors.

By observing the fit results in Table 5.2 we see that the cost function decreases with the maturity. This is indeed what is expected, since the implied volatility surface becomes flatter as maturity increases, as can be seen from the market data (and also as we can see in Figure 5.3). This makes the constant

volatility function a better approximation in such cases, which decreases the cost function's value.

One other property that we can observe is that the constant implied volatility also decreases with maturity. The reason behind this is the simple fact that earlier maturities contain higher implied volatilities (for the strikes far from S_0), which pull the constant volatility function upwards.

We now focus on the simulated results in Figure 5.1. First, we can see that the theoretical functions (full red lines) clearly don't represent the market data. This is indeed what is expected, since the constant volatility model doesn't cover the volatility smiles phenomenon, which we covered before.

Secondly, by comparing the theoretical and simulated functions, we must note that the simulation performs extremely well for strikes near S_0. Notice that the simulated function (dot-dashed blue line) perfectly follows the constant volatility theoretical result (full red line) in this region, and that the confidence bands converge to the simulated function indicating that all simulations produced the same result. This suggests that the simulation is working as expected for this particular region.

Thirdly, we notice that on the earliest maturity (i.e. 21 days), for strikes much larger than S_0 (e.g. $K = 1.5S_0$), the simulated implied volatilities go to zero, even though they should remain constant. The reason behind this has already been discussed in subsection 4.1.2 and relates to the very, very small number of paths that reach such high strikes and end up contributing to the option price (which is then converted to an implied volatility). For the case of strike $K = 1.5S_0$, and maturity $T = 21$ days, the number of paths that reach the strike is indeed approximately 0.25 out of $100\,000$ (i.e. one out of four Monte Carlo simulations of $100\,000$ paths contains a single path that is able to reach such a high strike). This problem is not observed for the remaining maturities for the simple reason that, because they are given more time to evolve, more paths are able to reach these high strikes. To solve this problem we could significantly increase the number of simulations, so that the number of paths that are able to reach these high strikes is enough to produce a good estimate of the option price. The problem with this solution is the very significant increase in the computation time required, which makes it impractical. If we lowered the number of simulated paths from $100\,000$ to any other smaller amount, the problem described before would become even more severe, and the later maturities would eventually also display the problem observed in the earliest maturity.

Finally we must discuss the large confidence bands for strikes much lower than S_0, occurring over all maturities. To explain this we require the information presented in Figure 3.2, relating the implied volatility with the option's market price. We saw that the implied volatility was extremely sensitive to option prices very close to their lower bounds, $S_0 - Ke^{-rT}$. If we now look, for example, at the market price of the option with strike $K = 5 \times 10^{-1}$€ and maturity $T = 21$ days, which is $C = 0.5000$€, and we compare it with its lower bound, $S_0 - Ke^{-rT} = 0.5000$€ (assuming the parameters shown in Table 5.1), we can clearly see that they are the same (with a difference only on the fourth decimal place, which is not shown here). We can then conclude that, in this case, we are in the extremely high sensitivity region of the implied volatility functions shown in Figure 3.2. Even though the Monte Carlo pricer is expected to produce a good estimation of option prices with lower strikes (a very large number of paths contribute to the option price, so a low amount of noise is produced - the opposite of what we described before for high strikes), because there will always be *some* error associated with the simulations, the

pricer is expected to produce some very slighty different results when executed multiple times, which is enough to cause some of the simulated implied volatilities to go to approximately zero or to increase significantly, which explains the large confidence bands. For options with strikes near S_0 and above, the market option price is much farther from its lower bound, so that we are far from the high sensitivity region. Indeed, the lower bound of options with strikes equal to or above S_0 is 0 (assuming interest rate $r = 0$).

These two last problems are not only applicable to the constant volatility model and will also be observed in all the other models.

5.1.2 Dependent Fits

We now present the results obtained from the fit of a constant volatility function to all the implied volatility data, regardless of maturity.

In Figure 5.2 we shown the theoretical and simulated functions as well as the provided market data.

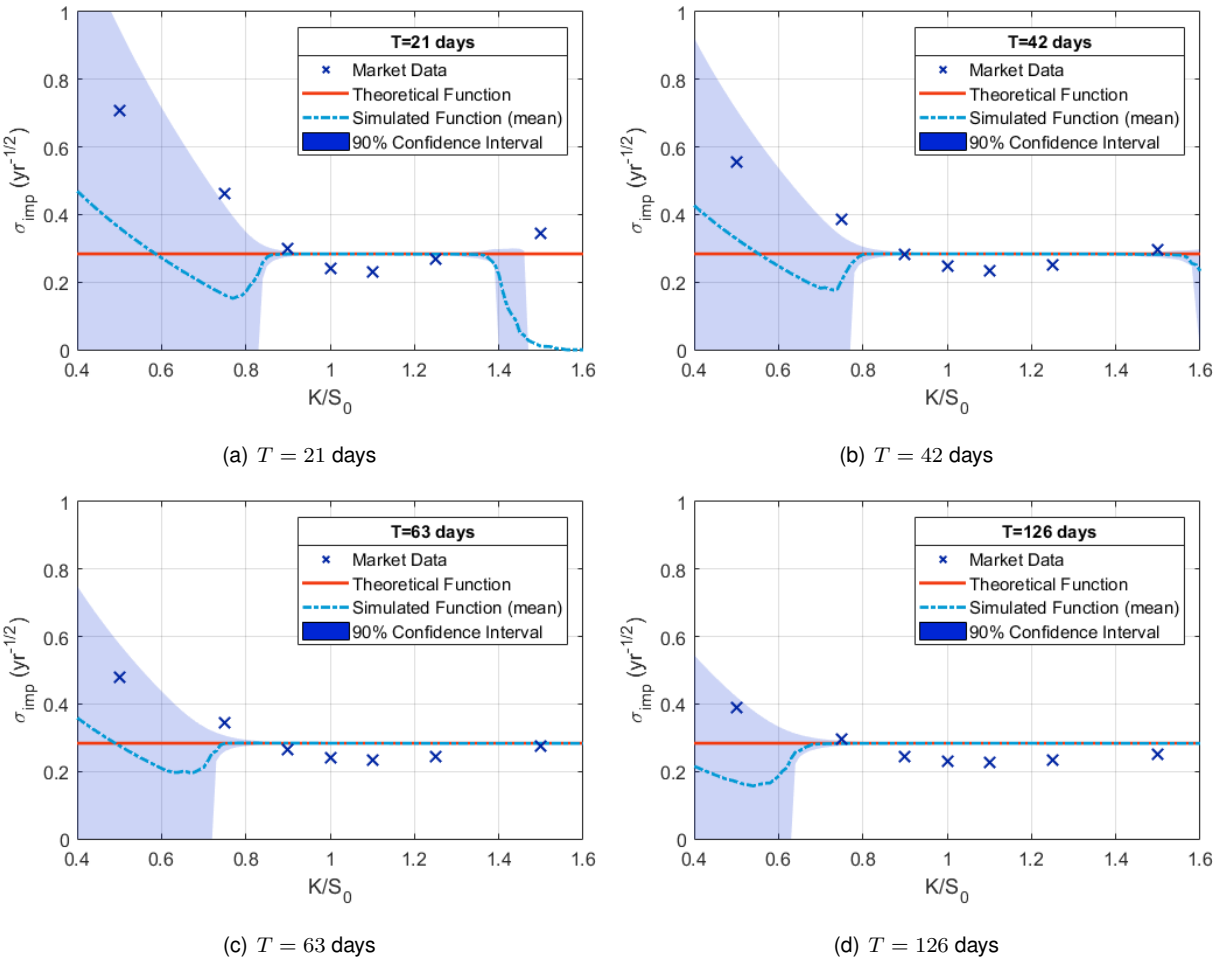

(a) $T = 21$ days

(b) $T = 42$ days

(c) $T = 63$ days

(d) $T = 126$ days

Figure 5.2: Implied volatility functions (red lines) fitted *simultaneously* to the implied volatility data (crosses) for different maturities under constant volatility model, plotted with their respective Monte Carlo simulated functions (light-blue dot-dashed lines) along with their 95% confidence bands (blue region).

The fitted implied volatility is represented in Table 5.4 as well as the cost function's value.

$\sigma_{imp,\mathrm{mdl}}$ (yr$^{-1/2}$)	Cost
0.2838	0.1248

Table 5.4: Fitted implied volatility for all maturities (fitted simultaneously) under constant volatility model.

T(days)	K(€)	$\sigma_{imp,\mathrm{mdl}}$(yr$^{-1/2}$)	$\mathrm{Error}_\sigma(\%)$	C_{mdl}(€)	$\mathrm{Error}_C(\%)$
	0.50		60	5.000×10^{-1}	0
	0.75		39	2.500×10^{-1}	0
	0.90		5	1.036×10^{-1}	1
21	1.00	0.2838	17	3.267×10^{-2}	17
	1.10		23	5.191×10^{-3}	114
	1.25		5	8.977×10^{-5}	68
	1.50		17	7.031×10^{-9}	99
	0.50		49	5.000×10^{-1}	0
	0.75		27	2.502×10^{-1}	1
	0.90		1	1.108×10^{-1}	0
42	1.00	0.2838	15	4.620×10^{-2}	15
	1.10		21	1.402×10^{-2}	64
	1.25		12	1.336×10^{-3}	115
	1.50		4	8.299×10^{-6}	48
	0.50		41	5.000×10^{-1}	0
	0.75		18	2.510×10^{-1}	1
	0.90		7	1.179×10^{-1}	2
63	1.00	0.2838	18	5.656×10^{-2}	18
	1.10		22	2.227×10^{-2}	57
	1.25		16	3.925×10^{-3}	118
	1.50		3	1.087×10^{-4}	42
	0.50		27	5.000×10^{-1}	0
	0.75		4	2.559×10^{-1}	0
	0.90		16	1.361×10^{-1}	7
126	1.00	0.2838	24	7.992×10^{-2}	24
	1.10		25	4.317×10^{-2}	51
	1.25		21	1.499×10^{-2}	98
	1.50		13	1.967×10^{-3}	129

Table 5.5: Comparison between fitted functions (fitted simultaneously) and original data under constant volatility model.

First, when we compare the implied volatility fitted to all the maturities with the results of the independent fits (in Table 5.2) we see that the former is actually the average of the latter. why?

If we now compare their cost function values, we see that the cost of the dependent fit (0.1248), is larger than the sum of the costs of the independent fits $(0.0635 + 0.0282 + 0.0164 + 0.0069 = 0.1150)$. This is indeed expected: when fitting all maturities at once, the optimizer will find the implied volatility that minimizes the cost for all maturities, which will not be the one that minimizes the cost of each single maturity.

As for the plots in Figure 5.2 they look very similar to those in Figure 5.1, so not much more can be added regarding their analysis.

5.2 Dupire Model

The stochastic differential equation for the stock price paths under the local volatility model was hypothesized to be given by

$$dS(t) = rS(t)dt + \sigma(S(t), t)S(t)dW(t), \tag{5.2}$$

where $\sigma(S(t), t)$ can be obtained through Dupire's model, defined in subsection 3.2.1, which is given by

$$\sigma(S(t), t) = \sqrt{\frac{\sigma_{imp}^2 + 2t\sigma_{imp}\frac{\partial \sigma_{imp}}{\partial T} + 2r(S(t))t\sigma_{imp}\frac{\partial \sigma_{imp}}{\partial K}}{\left(1 + (S(t))d_1\sqrt{t}\frac{\partial \sigma_{imp}}{\partial K}\right)^2 + (S(t))^2 t\sigma_{imp}\left(\frac{\partial^2 \sigma_{imp}}{\partial K^2} - d_1\left(\frac{\partial \sigma_{imp}}{\partial K}\right)^2\sqrt{t}\right)}}, \tag{5.3}$$

where d_1 is defined as

$$d_1 = \frac{\log(S_0/S(t)) + \left(r + \frac{1}{2}\sigma_{imp}^2\right)t}{\sigma_{imp}\sqrt{t}}. \tag{5.4}$$

As we mentioned in section 4.2, we must produce the implied volatility surface from the market data using an interpolation algorithm. Applying the Delaunay triangulation defined earlier, we obtain the implied volatility surface, shown in Figure 5.3 along with its contour plot. From this surface we can easily extract (numerically) the gradients required for the local volatility formula.

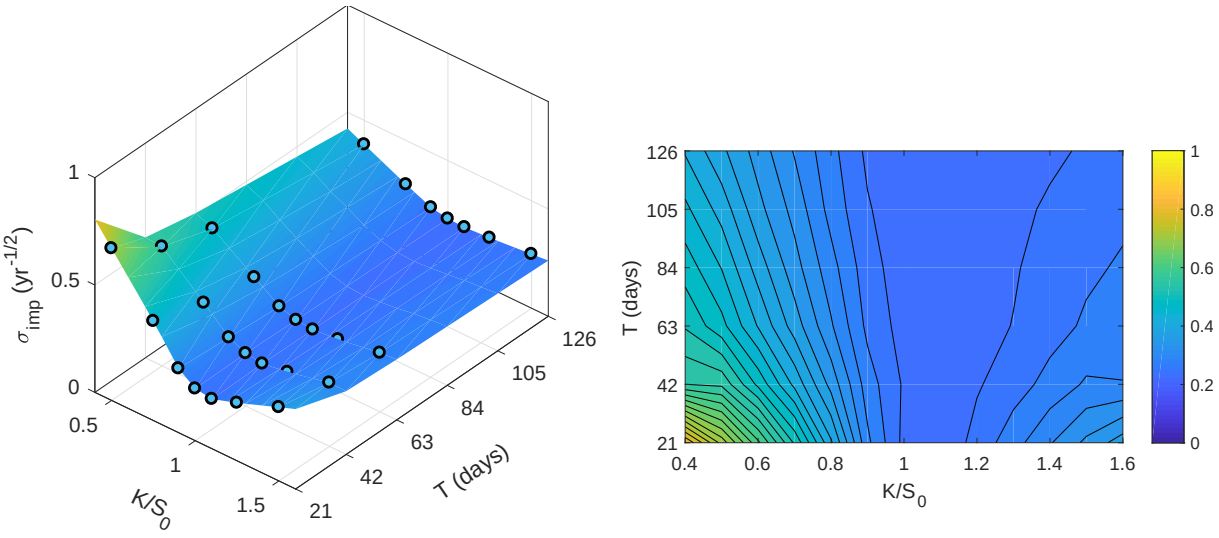

(a) σ_{imp} surface

(b) σ_{imp} contour plot

Figure 5.3: Implied volatility surface (left) and corresponding contour plot (right) of the function interpolated linearly between the original data points (blue circles) using Delaunay triangulation.

Observing this interpolated surface we see that its curvature decreases with maturity - the volatility smile becomes less prominent for later maturities - which can also be observed in the provided data, shown in Appendix A.

We are now be able to generate the *local* volatility surface. To do this, we simply evaluate the interpolated implied volatility surface, as well as all the required gradients, at multiple points K_j, T_i to produce multiple local volatility values $\sigma(K_j, T_i)$ with eq.(5.3). The points should be uniformly spaced in

a grid, with K_{min} and K_{max} being the smallest and largest strikes in the grid, with intervals ΔK between the strikes, and with T_{min} and T_{max} the smallest and largest maturities, with intervals ΔT. The values for these quantities that we used throughout this section are shown in Table 5.6. Interpolating again between these local volatility values we are able to generate the local volatility surface, which we show in Figure 5.4, along with its respective contour plot. We now simply need to make a variable change $\sigma(K,T) \implies \sigma(S,t)$ to be able to simulate stock price paths under this local volatility model, as we explain next.

T_{min}(days)	T_{max}(days)	ΔT(days)	K_{min}(€)	K_{max}(€)	ΔK(€)
21	126	10.5	0.4	1.6	0.05

Table 5.6: Parameters used in the interpolation section of Dupire's model.

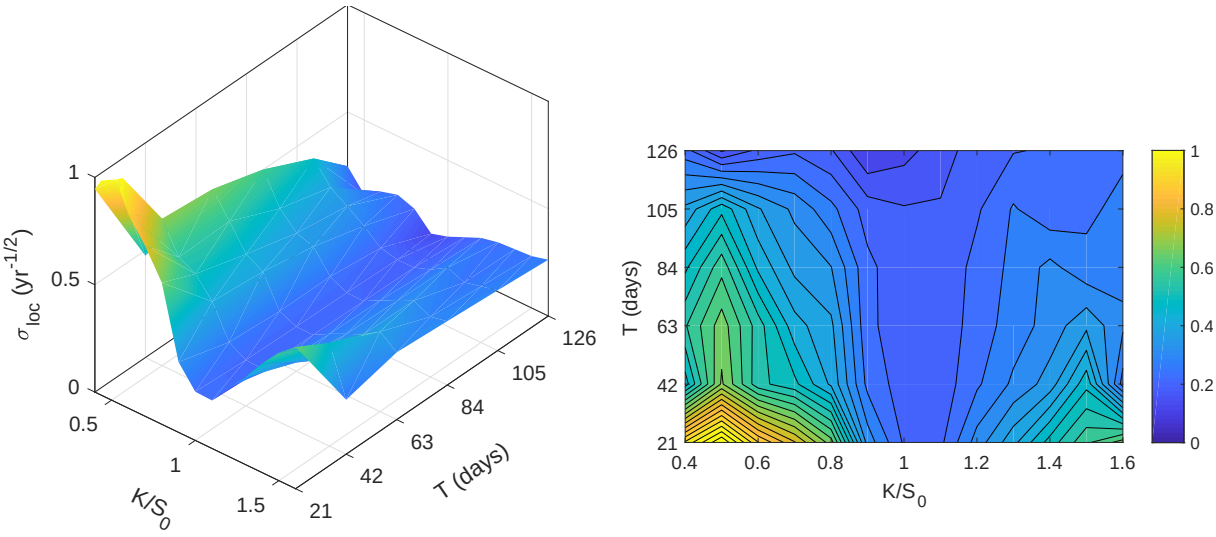

(a) σ_{loc} surface

(b) σ_{loc} contour plot

Figure 5.4: Local volatility surface (left) and corresponding contour plot (right) of the function obtained with Dupire's formula (eq.(3.23)) from the interpolated implied volatility surface in Figure 5.3.

To simulate a stock price path we need to sample the surface at the point (S_i, t_j) when we are at the time step t_j of the simulation with a stock price S_i and assume that value as the local volatility, to be used on the generation of the next stock price value, S_{i+1}. We iterate this procedure for all paths until we reach the maturity. Having obtained all the simulated stock prices at maturity, pricing the option is done as usual.

The results of these simulations are shown in Figure 5.5, along with the confidence bands and the original market data. To prevent volatilities from becoming too high, we implemented a maximum cutoff value of σ_{max}=1.5 $\text{yr}^{-1/2}$, limiting the volatilities sampled from the surface.

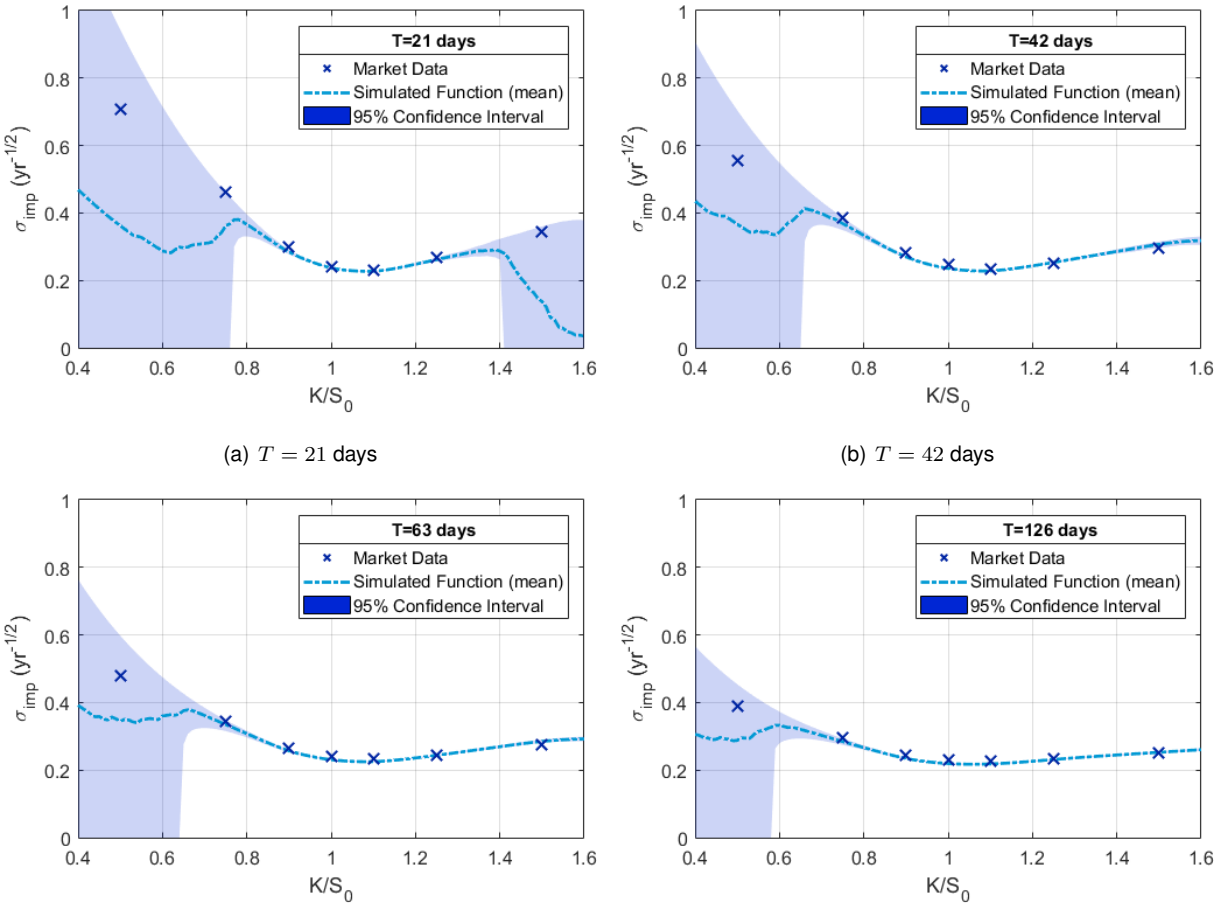

(a) $T = 21$ days

(b) $T = 42$ days

(c) $T = 63$ days

(d) $T = 126$ days

Figure 5.5: Implied volatility functions (light-blue dot-dashed) simulated with Monte Carlo under Dupire's local volatility model with their corresponding 95% confidence interval, plotted against the original market data (crosses).

As before, we now see the very large confidence bands for very low strikes. The cause of this behavior was identified on the constant volatility model (with independent fits). We can also observe the low implied volatilities for high strikes in the earliest maturities, which has also already been discussed.

The great improvement of Dupire's model over the constant volatility model is the presence of the implied volatility smiles in the simulated implied volatilities. Furthermore, these smiles follow the market data almost perfectly for strikes near S_0. We can therefore conclude that the model greatly outperforms the constant volatility model presented earlier, which is unsurprising.

The simulations shown in the plots of Figure 5.5 can be thought of as slices of a simulated implied volatility surface. Ideally, this surface would look exactly like the one shown in Figure 5.3. However, in the regions where the simulations behave badly (large strikes for early maturities and low strikes), we expect there to be a very high amount of noise. This simulated surface is shown in Figure 5.6, along with the simulated functions of the earlier plots (red dashed lines) and the market data (red circles). The respective contour plot is also represented.

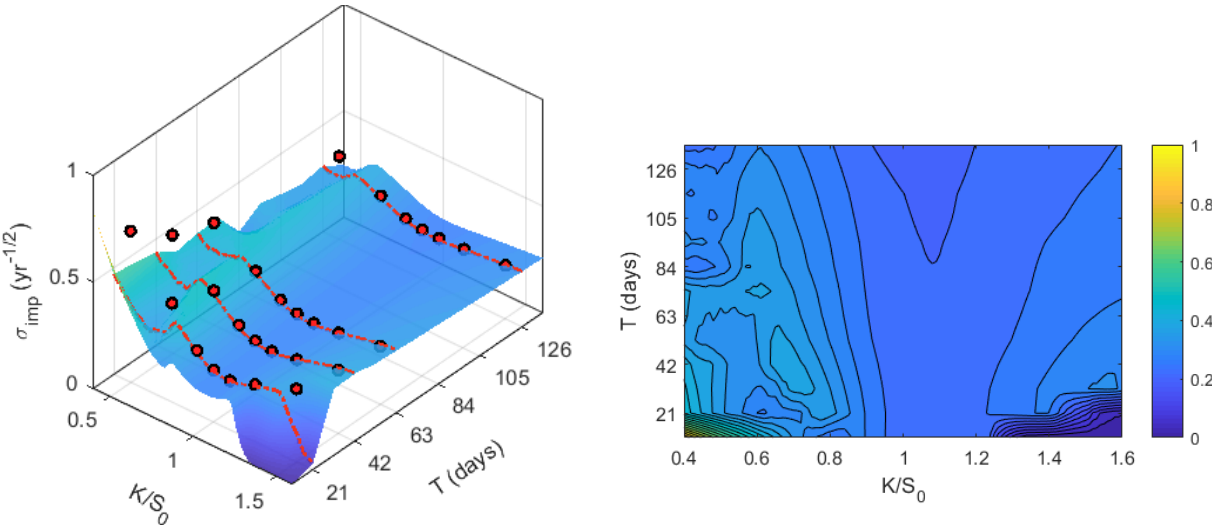

(a) σ_{imp} surface

(b) σ_{imp} contour plot

Figure 5.6: Implied volatility surface (left) and corresponding contour plot (right) simulated with Monte Carlo under Dupire's local volatility model plotted against the original market data (blue circles) and the generated functions shown in Figure 5.5 (red dot-dashed lines).

As expected, the amount of noise is quite overwhelming in the regions where the Monte Carlo pricer performs badly. For the regions where the strike approaches S_0, the picture is quite different and the simulations closely follow the data, as expected.

5.3 Static SABR Model

As we saw before, in the Static SABR model stock prices and volatilities are governed by the stochastic differential equations

$$dS(t) = rS(t)dt + e^{-r(T-t)(1-\beta)}\sigma(t)(S(t))^{\beta}dW_1(t), \tag{5.5}$$

$$d\sigma(t) = \nu\sigma(t)dW_2(t), \tag{5.6}$$

with $\alpha = \sigma(0)$ and where $W_1(t)$ and $W_2(t)$ have a constant correlation of ρ.

The closed-form solution, shown in eq.(3.70), enables us to obtain the theoretical implied volatilities of options priced under this model and will be used in the calibration process.

Before calibrating the model to the market data, we should study the influence of each parameter of this model on the shape of the implied volatility curve, in order to better interpret the results. This influence is represented in Figure 5.7, where we vary one parameter at a time, keeping all the others constant, thus directly observing that parameter's influence.

We should note that the influence of the parameters is more complicated than we show here. On the one hand, their impact depends on the maturity. However, for this effect to become evident, we would have to repeat all the plots in Figure 5.7 for several maturities, which would simply become too cumbersome and is out of the scope of this thesis. On the other hand, the parameters have combined effects on the curve shape. These influences would be quite difficult to represent. Furthermore, they are discussed in the original article by Hagan [Hagan et al., 2002], and will, for these reasons, not be discussed here. That being said, we can still have a general view of each parameter's impact on the curve.

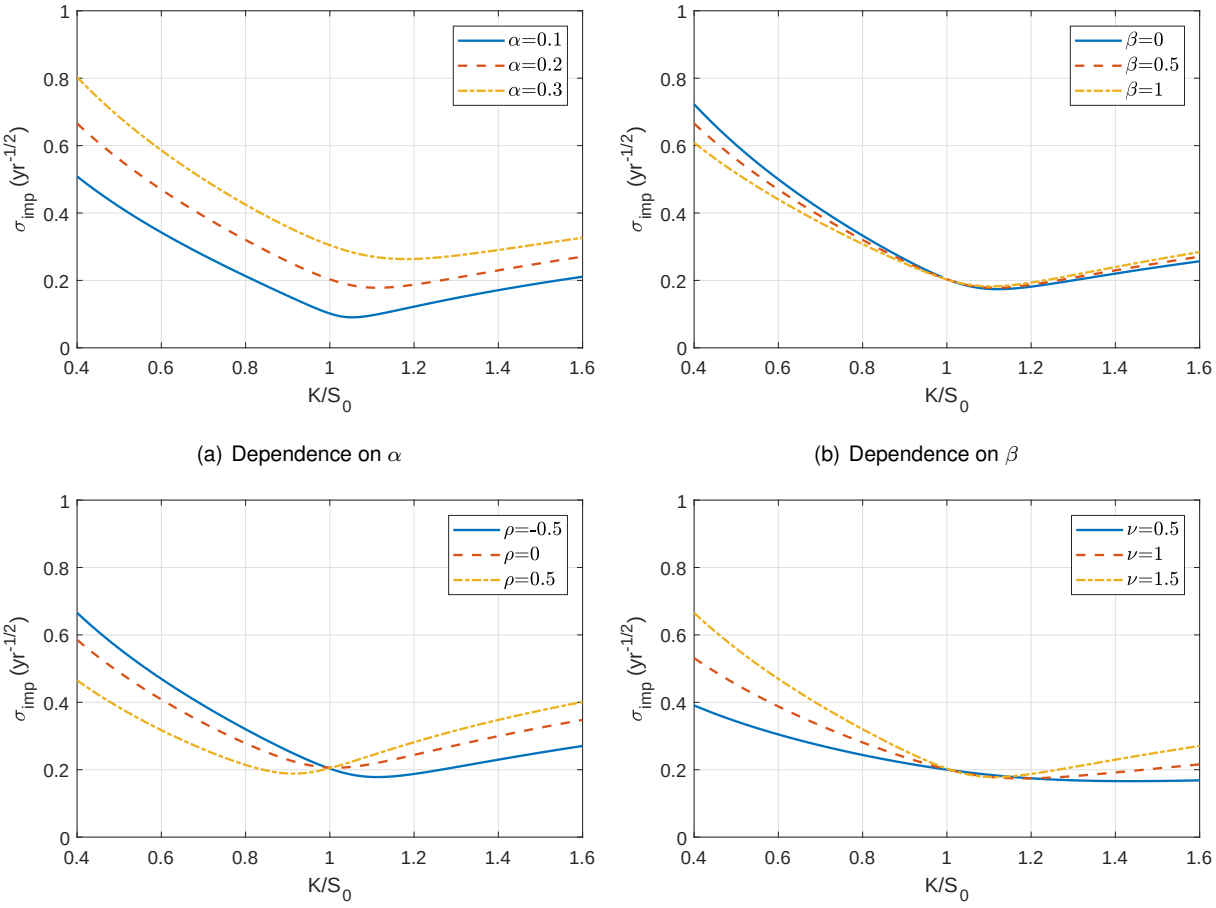

(a) Dependence on α

(b) Dependence on β

(c) Dependence on ρ

(d) Dependence on ν

Figure 5.7: Dependence of the implied volatility curve on each of the Static model SABR parameters. The default parameters used were $S_0 = 1€$, $T = 42$ days and $r = 0$. Furthermore, on all plots, except when the dependence on a parameter is represented, the parameters used were $\alpha = 0.2$, $\beta = 1$, $\rho = -0.5$ and $\nu = 1.5$.

In Figure 5.7(a) we see that the parameter α, which corresponds to the initial value of the volatility process, has quite an impact on the implied volatility curve. We can see that this parameter seems to control the height of the curve. This is indeed expected, because the implied volatility and the stochastic (local) volatility are inherently related. Increasing α is expected to shift the volatility process to higher values, thus increasing the implied volatility.

The influence of the parameter β, which is an exponent in the stock price process, is represented in Figure 5.7(b). The impact of this parameter seems to be almost negligible. Indeed, at a single point in time, the implied volatility curve barely depends on this value, but this parameter becomes very important when time passes and the stock prices change. Hagan *et al.* [Hagan et al., 2002] show that β controls how the curve shifts when the stock prices move: if the stock price increases, the implied volatility curve at that time should shift to the right; for $\beta = 0$, the curve also shifts downwards, whereas for $\beta = 1$ it doesn't. Despite this, because in Static SABR we are only fitting data for a single maturity, this parameter should barely have any influence in the resulting implied volatility function, though it will become quite relevant in the Dynamic SABR model.

In Figure 5.7(c) is represented the effect of the parameter ρ, the correlation between the stock price and the volatility processes. We can see that this parameter impacts the skewness of the implied volatility curve. Because this parameter relates the stock price and volatility, in the case of a negative ρ when the prices increase (decrease), the volatilities decrease (increase), so that options with higher (lower) strikes have lower (higher) associated volatilities. This justifies why we have a lower implied volatility for higher strikes when the correlation is negative. The inverse logic can be applied for the positive ρ curve observed.

Finally, the impact of the parameter ν, the volatility of the volatility process, is shown in Figure 5.7(d). This parameter seems to control the curvature of the implied volatility curve. It should be clear that higher values of ν result in greater changes in the volatility process, enabling, at times, the volatility to become quite large. This allows the stock price process to evolve quite erratically, thus making it easier for stock prices to reach higher values, making high strike options more valuable. This effect pushes their implied volatility upwards. The inverse effect also holds and a low ν will force the stochastic volatility process to become quite limited, preventing the stock prices from changing too much, and restraining them from reaching high strikes, pulling the implied volatility curve downwards.

We now present the results of the calibration as well as the simulations in Figure 5.8.

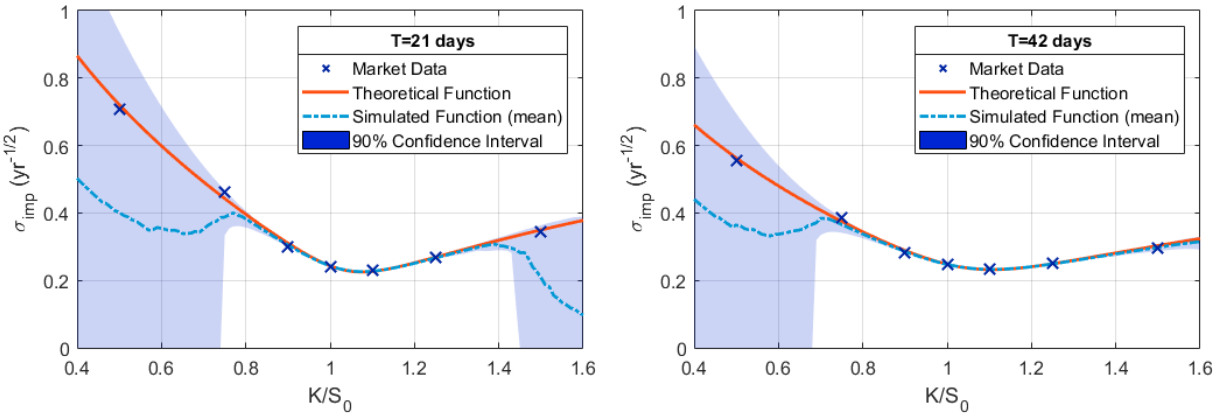

(a) $T = 21$ days

(b) $T = 42$ days

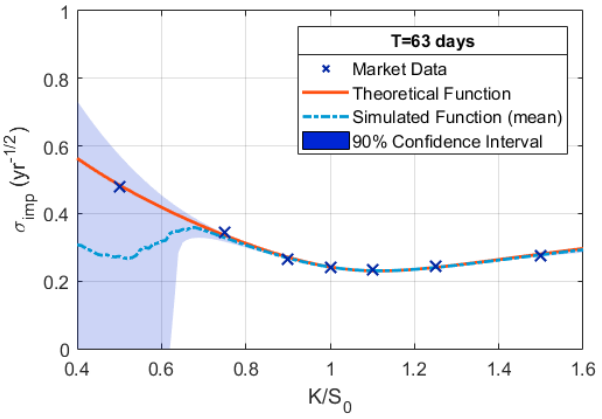

(c) $T = 63$ days

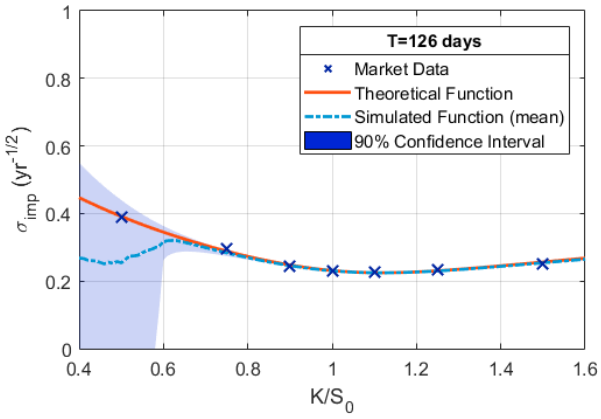

(d) $T = 126$ days

Figure 5.8: Implied volatility functions (red lines) fitted independently to the implied volatility data (crosses) for different maturities under the static SABR model, plotted with their respective Monte Carlo simulated functions (light-blue dot-dashed lines) along with their 95% confidence bands (blue region).

As mentioned before, the Static SABR model is only expected to work for data on options with a single maturity. For this reason, we fitted the model to each maturity independently. The parameters obtained in the calibration for each maturity are shown in Table 5.7.

T(days)	α (yr$^{-1/2}$)	β	ρ	ν	Cost
21	0.2381	0.3766	-0.3760	2.1022	0.0004
42	0.2434	0.7362	-0.3664	1.4451	0.0002
63	0.2375	0.7750	-0.3119	1.1420	0.0001
126	0.2267	0.8771	-0.2383	0.8215	0.0001

Table 5.7: Fitted parameters for each maturity (fitted independently) under static SABR model.

We now analyze the results of this model. Observing the plots in Figure 5.8 we see that the theoretical function (full red line), obtained by the closed form solution of the Static SABR model, fits the data extremely well through the whole range of strikes and for each of the maturities.

Though the model seems to fit almost perfectly to the data, the fits may not be very robust. The reason for this is that we have an extremely small amount of data points (7 for each maturity) for the

comparatively large number of parameters used (4 parameters in total). This will cause our model to overfit the data.

As for the simulated function, we note that it very closely follows the theoretical curve in the regions around S_0, indicating that the Monte Carlo pricer implementation was done correctly. This feature doesn't hold at the high strike region in the first maturity and the low strike regions of all maturities for the same reasons described earlier.

Examining now the calibrated parameters in Table 5.7 we first note that the parameter α doesn't seem to vary too much between maturities, which is expected, since it controls the height of the implied volatility curve and this doesn't seem to change too much in the plots.

The parameter β appears to change wildly between maturities, though this is not surprising since, as we saw, this parameter doesn't significantly affect the shape of the implied volatility function, meaning that different values of β would fit the data equally well.

As for the parameter ρ, we first note that it is always negative, which is expected from reality. It also seems to decrease with time why?.

Finally, the parameter ν also seems to decrease with time. This is no surprise as the curvature of the implied volatility function is expected to decrease with time, with the function becoming increasingly horizontal, as can be seen from the provided data.

If we now compare the cost function values of the Static SABR model in Table 5.7 with the independently fitted results of the constant volatility model in Table 5.2 we clearly see that they improve very significantly. For all maturities, the costs decrease between 99.2 and 99.4% here, which is an extreme improvement. This is no surprise, since the constant volatility model was expected to perform very badly. These costs should be considered carefully, however, due to the overfitting mentioned earlier - for such a low amount of data (compared to the high number of parameters) we can find many possible combinations of parameters that fit the data as well as the parameters found by the optimizer.

T(days)	K(€)	$\sigma_{imp,\mathrm{mdl}}(\mathrm{yr}^{-1/2})$	$\mathrm{Error}_\sigma(\%)$	C_{mdl}(€)	$\mathrm{Error}_C(\%)$
21	0.50	0.7209	2	5.000×10^{-1}	0
	0.75	0.4428	4	2.505×10^{-1}	0
	0.90	0.3105	4	1.050×10^{-1}	1
	1.00	0.2435	0	2.804×10^{-2}	0
	1.10	0.2269	2	2.227×10^{-3}	8
	1.25	0.2692	0	5.183×10^{-5}	3
	1.50	0.3500	2	8.317×10^{-7}	45
42	0.50	0.5631	1	5.001×10^{-1}	0
	0.75	0.3751	3	2.515×10^{-1}	0
	0.90	0.2891	2	1.114×10^{-1}	1
	1.00	0.2481	1	4.039×10^{-2}	1
	1.10	0.2322	1	8.194×10^{-3}	4
	1.25	0.2497	1	5.746×10^{-4}	7
	1.50	0.3033	2	2.120×10^{-5}	34
63	0.50	0.4845	1	5.001×10^{-1}	0
	0.75	0.3357	3	2.526×10^{-1}	0
	0.90	0.2710	2	1.160×10^{-1}	1
	1.00	0.2421	1	4.826×10^{-2}	1
	1.10	0.2305	1	1.384×10^{-2}	3
	1.25	0.2409	1	1.678×10^{-3}	7
	1.50	0.2804	2	9.557×10^{-5}	25
126	0.50	0.3914	1	5.004×10^{-1}	0
	0.75	0.2887	2	2.563×10^{-1}	0
	0.90	0.2479	1	1.279×10^{-1}	1
	1.00	0.2314	1	6.522×10^{-2}	1
	1.10	0.2251	1	2.817×10^{-2}	2
	1.25	0.2309	1	7.177×10^{-3}	5
	1.50	0.2567	2	9.822×10^{-4}	14

Table 5.8: Comparison between fitted results and original data under static SABR model.

5.4 Heston Model

The Heston model is defined as

$$dS(t) = rS(t)dt + \sqrt{\nu(t)}S(t)dW_1(t), \tag{5.7}$$

$$d\nu(t) = \kappa(\overline{\nu} - \nu(t))dt + \eta\sqrt{\nu(t)}dW_2(t), \tag{5.8}$$

where $\nu_0 = \nu(0)$ and with $W_1(t)$ and $W_2(t)$ having a constant correlation of ρ.

With the closed form solution of the Heston model, shown in eq.(3.30), we are able to find the theoretical prices of options priced under this model, which we can easily convert to implied volatilities. These last will be used in the calibration process.

As we did for the Static SABR model, we now study the influence of each parameter of the Heston model on the shape of the implied volatility curve, which is represented in Figure 5.9.

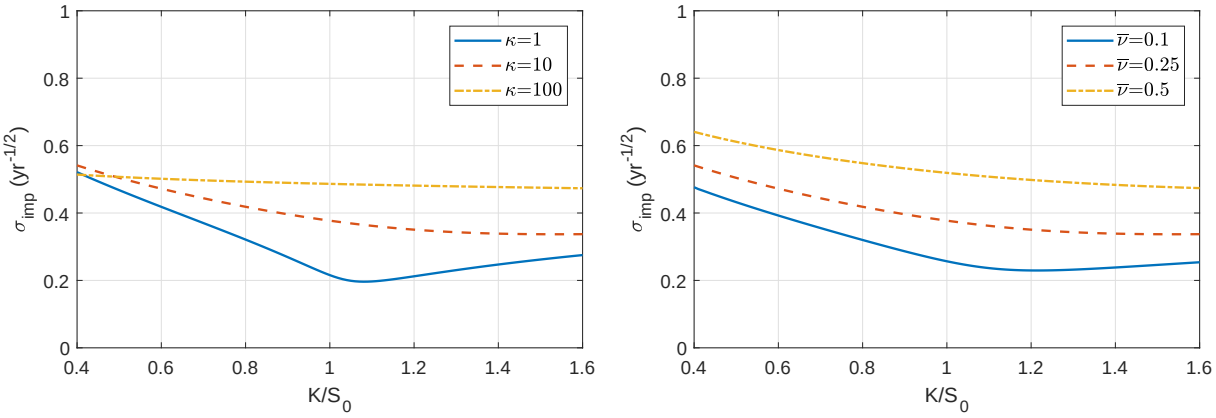

(a) Dependence on κ

(b) Dependence on $\overline{\nu}$

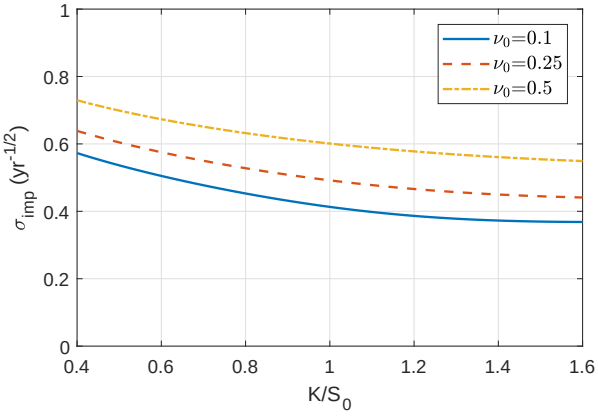

(c) Dependence on ν_0

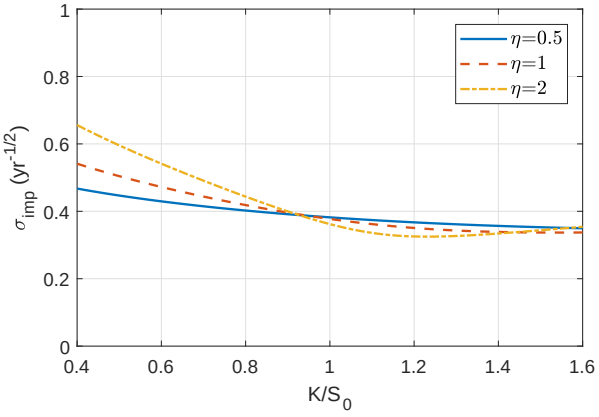

(d) Dependence on η

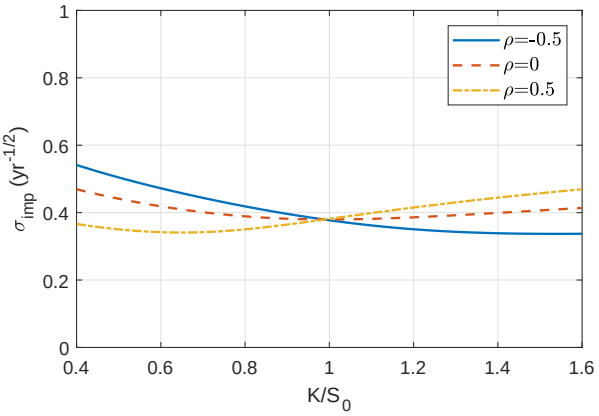

(e) Dependence on ρ

Figure 5.9: Dependence of the implied volatility curve on each of the Heston model parameters. The default parameters used were $S_0 = 1$€, $T = 42$ days and $r = 0$. Furthermore, on all plots, except when the dependence on a parameter is represented, the parameters used were $\kappa = 10$, $\overline{\nu} = 0.25$, $\nu_0 = 0.04$, $\eta = 1$ and $\rho = -0.5$.

The parameters κ, $\overline{\nu}$ and ν_0 are inherently related to one another and their influence can only be understood if all are considered at the same time. The parameter $\overline{\nu}$ is the mean value of the variance (*not* the volatility! $\nu(t) = \sigma^2(t)$), ν_0 denotes the initial variance, and κ is the mean-reversion rate, which controls how fast the variance tends to its mean value.

If the parameter κ is very large, we expect the variance process to converge very fast to its mean value, $\overline{\nu}$. This means that the variance process $\nu(t)$ is not able to change significantly, as it is stuck at $\overline{\nu}$, remaining roughly constant. For this reason, options priced with such parameters would have an almost constant *volatility*, and their implied volatility curve would tend to a horizontal line at the square root of $\overline{\nu}$ (i.e. the mean volatility).

On the other hand, if κ is small, the parameter $\overline{\nu}$ will barely have any influence at all on the implied volatility curve, and the variance process is able to change almost without restrain. This means that the parameter ν_0 will have a large impact on the behavior of the variance process. A large ν_0 enables the variance process to reach higher values so that the implied volatility of options priced with these parameters is higher. A small ν_0 would have the opposite effect, decreasing the implied volatility.

If we now have a moderate value for κ, both parameters $\overline{\nu}$ and ν_0 are expected to have some impact on the implied volatility curve.

By examining Figures 5.9(b) and 5.9(c), with $\kappa = 10$ (which is not too large nor too small), we see that the implied volatility curves increase/decrease as we increase/decrease each of the parameters, which is precisely what we expect. If we now look at Figure 5.9(a), we can confirm that a large value for κ (orange dot-dashed line) will produce an almost constant implied volatility curve around the square root of $\overline{\nu}$ ($\sqrt{\overline{\nu}} = \sqrt{0.25} = 0.5$). For small values of κ (blue full line), the influence of the parameter ν_0 becomes more apparent - notice that the curve is pulled downwards since ν_0 is lower than $\overline{\nu}$ -, and we no longer see the horizontal implied volatility curve from before, which is also expected.

The parameters η and ρ in the Heston model control the volatility of the variance process and the correlation of this process with the stock price process, respectively. They are very much related to the parameters ν and ρ of the Static SABR process, respectively, and their impact on the implied volatility curve is the same. For this reason, they will not be discussed again here.

The Heston model was calibrated to the data provided using the closed form solutions described before. The calibrated parameters were then input into a Monte Carlo pricer and the simulated implied volatilities were obtained. These results are shown in Figure 5.10.

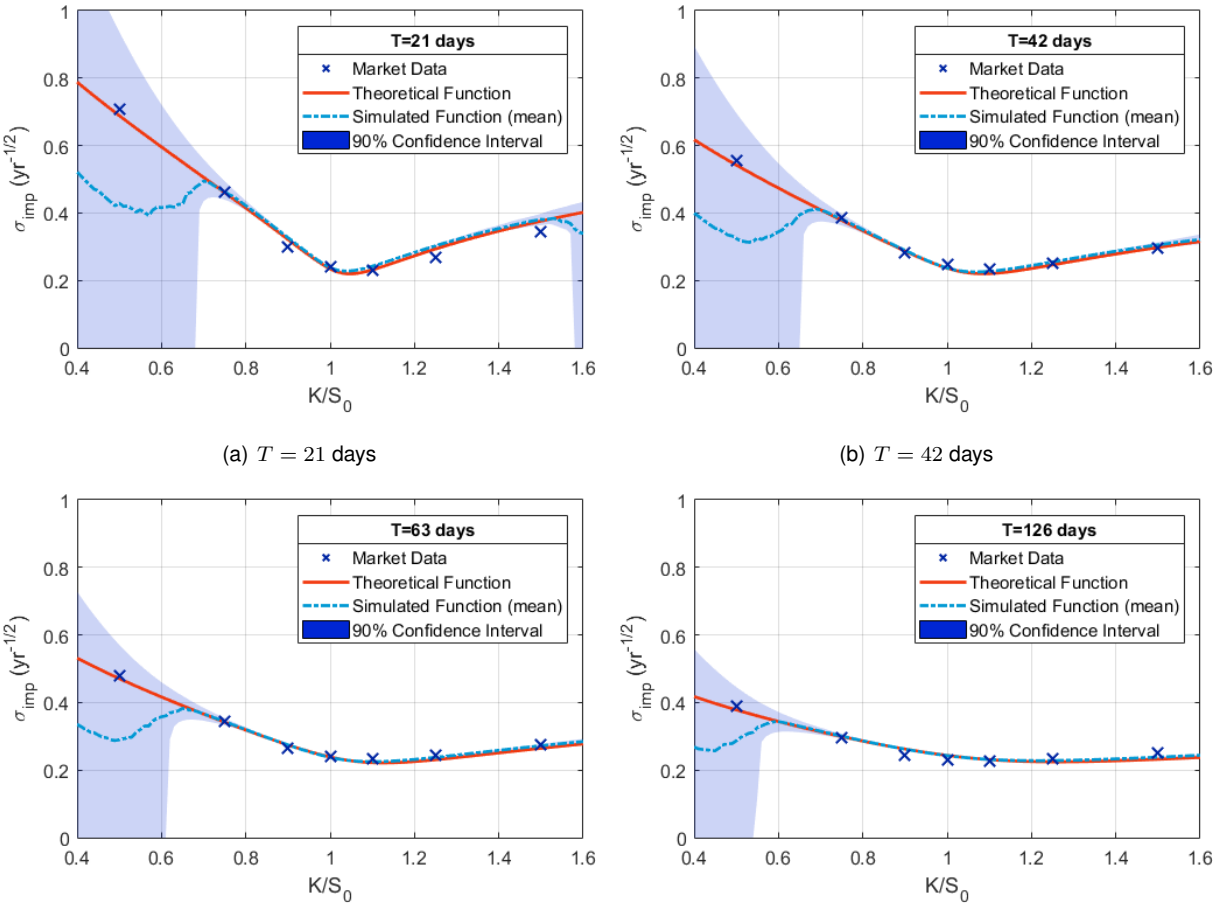

(a) $T = 21$ days

(b) $T = 42$ days

(c) $T = 63$ days

(d) $T = 126$ days

Figure 5.10: Implied volatility functions (red lines) fitted simultaneously to the implied volatility data (crosses) for different maturities under the Heston model, plotted with their respective Monte Carlo simulated functions (light-blue dot-dashed lines) along with their 95% confidence bands (blue region).

The values of the calibrated parameters are shown in Table 5.9.

κ	$\overline{\nu}$	ν_0	ρ	η	Cost
53.4355	0.0653	0.1046	-0.4086	6.2554	0.0025

Table 5.9: Fitted parameters for all maturities (fitted simultaneously) under the Heston model.

We now study the results obtained. Examining the plots in Figure 5.10 we see that the theoretical curves fit the data surprisingly well throughout all the maturities. This is especially surprising when we note that the adjustment is made for the entire data set, with all the different maturities, unlike the Static SABR model, which was only fitted for single maturities.

Observing the simulated curves and their respective confidence bands we again see that they fit the closed-form solutions extremely well in the region around S_0, indicating that the simulations agree with the predictions of the closed form solutions. The large confidence bands described before for the high strikes and early maturities and for the low strikes can also be found here. Because their cause is the same, they will not be described again.

Considering now the cost function value for the fitted parameters (Cost$= 0.0025$), shown in Table 5.9, and comparing it to the sum of the costs of each of the independent fits in the Static SABR model ($\Sigma_{\text{Costs}} = 0.0004 + 0.0002 + 0.0001 + 0.0001 = 0.0008$), in Table 5.7, we note that the cost of the former is higher than that of the latter. This is unsurprising, as the adjustments with the Static SABR were done independently of one another, and a better fit is therefore possible.

Comparing now the cost of the Heston model with that of the constant volatility assumption for dependent fits (Cost$= 0.1248$), shown in Table 5.4, we see that our results improve by approximately 98% here. The improvement is astonishing and completely justifies why the Heston model is so widely preferred over the constant volatility simplification.

Both the simulated and theoretical implied volatility curves shown in the plots of Figure 5.10 for different maturities can be thought of as slices of implied volatility surfaces (one simulated, another theoretical). Similarly to what we did for the Dupire model, we again represent these surfaces and their respective contour plots in Figures 5.11 and 5.12.

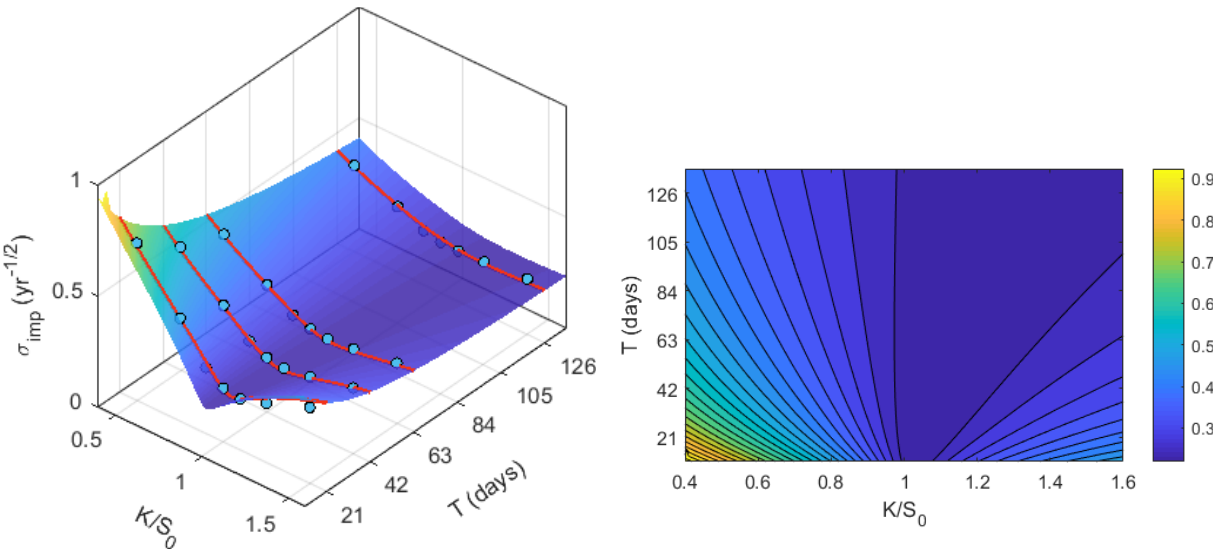

(a) σ_{imp} surface

(b) σ_{imp} contour plot

Figure 5.11: Implied volatility surface (left) and corresponding contour plot (right) of the function fitted simmultaneously to the implied volatility data for different maturities under the Heston model, plotted against the original market data (blue circles) and the fitted functions shown in Figure 5.10 (red lines).

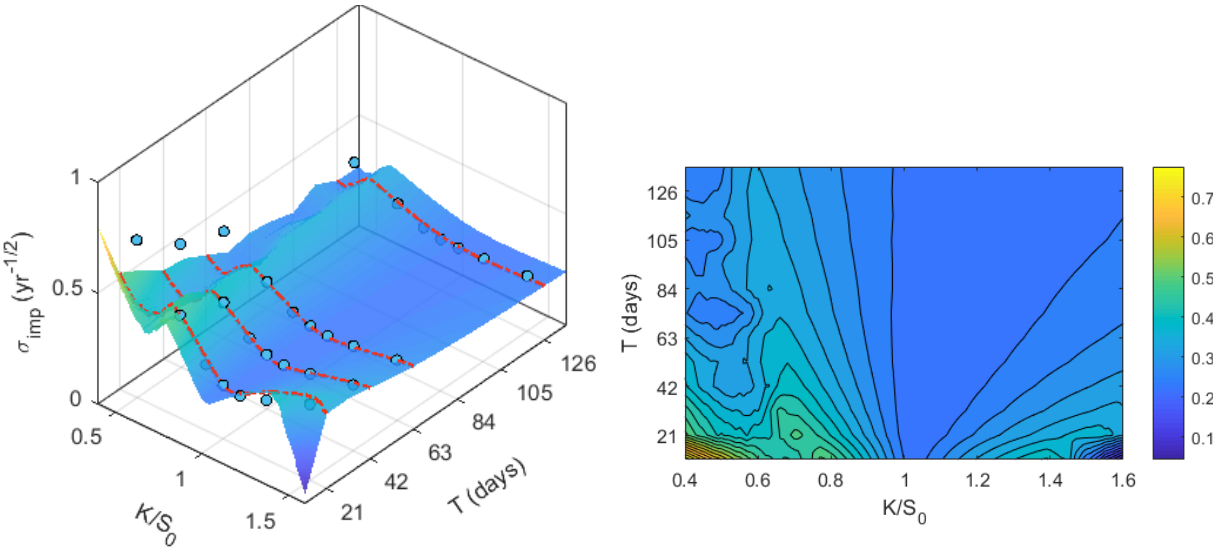

(a) σ_{imp} surface

(b) σ_{imp} contour plot

Figure 5.12: Implied volatility surface (left) and corresponding contour plot (right) of the function simulated using the Monte Carlo procedure with the fitted parameters shown in Table 5.9, under the Heston model, plotted against the original market data (blue circles) and the simulated functions shown in Figure 5.10 (red dot-dashed lines).

The surfaces and contour plots shown in Figures 5.11 and 5.12 should, ideally, replicate the surface and contour plot shown in Figure 5.3, since these last correspond to the real (*interpolated*) implied volatility surface. The simulated theoretical surface mimics the real function very well, which is expected, since the fits adjusted greatly to the data. As for the simulated surface, we can see the expected noisy region for the low strikes. The region around S_0 is very well fitted though, as we can see from the comparison of the contour plots.

T(days)	K(€)	$\sigma_{imp,\mathrm{mdl}}$(yr$^{-1/2}$)	$\mathrm{Error}_\sigma(\%)$	C_{mdl}(€)	$\mathrm{Error}_C(\%)$
	0.50	0.6886	3	5.000×10^{-1}	0
	0.75	0.4604	1	2.506×10^{-1}	0
	0.90	0.3216	8	1.056×10^{-1}	1
21	1.00	0.2346	3	2.702×10^{-2}	3
	1.10	0.2316	0	2.429×10^{-3}	0
	1.25	0.2935	9	1.243×10^{-4}	133
	1.50	0.3759	10	2.958×10^{-6}	415
	0.50	0.5422	2	5.000×10^{-1}	0
	0.75	0.3781	2	2.516×10^{-1}	0
	0.90	0.2873	2	1.112×10^{-1}	0
42	1.00	0.2366	4	3.852×10^{-2}	4
	1.10	0.2205	6	7.021×10^{-3}	18
	1.25	0.2463	2	5.203×10^{-4}	16
	1.50	0.2979	0	1.661×10^{-5}	5
	0.50	0.4709	2	5.001×10^{-1}	0
	0.75	0.3420	1	2.528×10^{-1}	0
	0.90	0.2748	3	1.166×10^{-1}	1
63	1.00	0.2392	0	4.768×10^{-2}	0
	1.10	0.2224	5	1.265×10^{-2}	11
	1.25	0.2310	5	1.312×10^{-3}	27
	1.50	0.2649	4	4.968×10^{-5}	35
	0.50	0.3784	2	5.003×10^{-1}	0
	0.75	0.2993	1	2.573×10^{-1}	0
	0.90	0.2626	7	1.312×10^{-1}	3
126	1.00	0.2439	6	6.870×10^{-2}	6
	1.10	0.2314	2	2.973×10^{-2}	4
	1.25	0.2248	4	6.453×10^{-3}	15
	1.50	0.2324	8	4.446×10^{-4}	48

Table 5.10: Comparison between fitted results and original data under the Heston model.

5.5 Dynamic SABR Model

We now consider the Dynamic SABR Model, for which the stock price and volatility processes were assumed to follow

$$dS(t) = rS(t)dt + e^{-r(T-t)(1-\beta)}\sigma(t)(S(t))^{\beta}dW_1(t), \tag{5.9}$$

$$d\sigma(t) = \nu(t)\sigma(t)dW_2(t), \tag{5.10}$$

with the volatility of the volatility process, $\nu(t)$, and the correlation between $W_1(t)$ and $W_2(t)$, $\rho(t)$, being two functions of time.

To model these functions we chose

$$\rho(t) = \rho_0 e^{-at}, \tag{5.11}$$

$$\nu(t) = \nu_0 e^{-bt}, \tag{5.12}$$

with $\rho_0 \in [-1, 1]$, $\nu_0 > 0$, $a > 0$ and $b > 0$.

The parameters used in the Dynamic SABR model are similar to those used in the Static SABR model and an easy connection can be made between them. Their influence on the implied volatility curve will therefore be the same and, for this reason, they will not be considered again here.

We fitted the Dynamic SABR model to the implied volatility data for all maturities. The fitted theoretical curves (obtained with the closed-form solution in eq.(3.77)) and their simulated counterparts are shown in Figure 5.13.

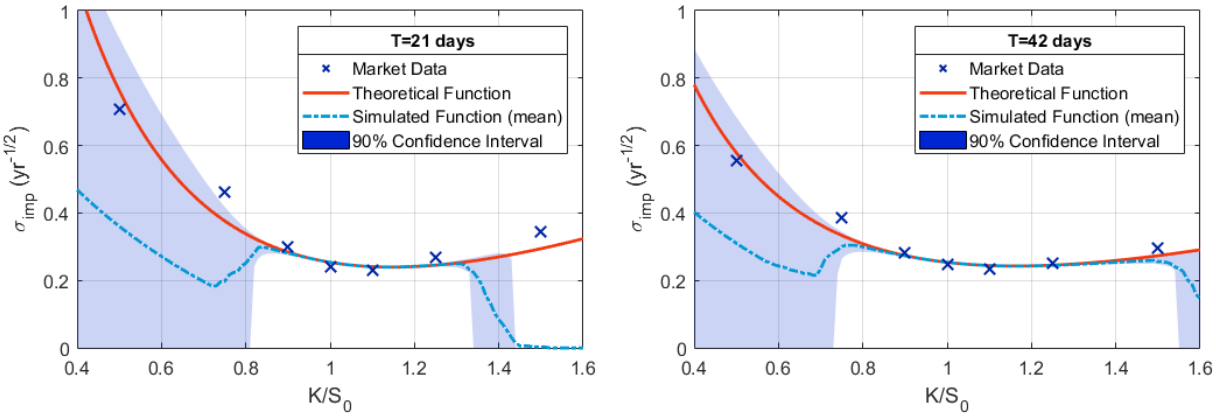

(a) $T = 21$ days

(b) $T = 42$ days

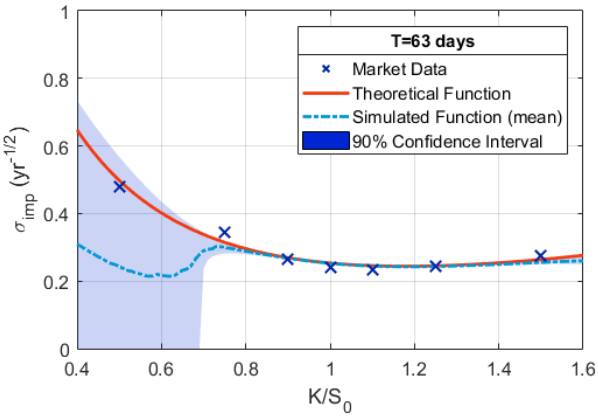

(c) $T = 63$ days

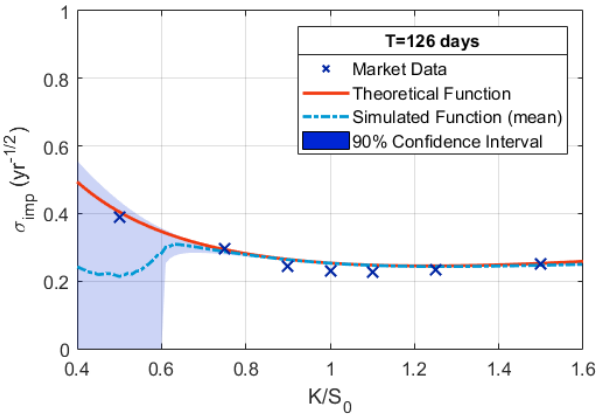

(d) $T = 126$ days

Figure 5.13: Implied volatility functions (red lines) fitted simultaneously to the implied volatility data (crosses) for different maturities under the dynamic SABR model, plotted with their respective Monte Carlo simulated functions (light-blue dot-dashed lines) along with their 95% confidence bands (blue region).

The calibrated parameters obtained from the fit are shown in Table 5.11.

α	β	ρ_0	a	ν_0	b	Cost
0.2540	0.6348	-0.4166	0	1.8673	41.6943	0.0108

Table 5.11: Fitted parameters for all maturities (fitted simultaneously) under the dynamic SABR model.

We now consider the adjustments above. Observing the theoretical curves in Figure 5.13 we can see that they fit the market data relatively well, especially for the later maturities, though for the earlier maturities the fit doesn't appear to be so good.

Considering now the simulated curves, we again see that they accurately follow the theoretical curve for the regions around S_0, behaving very badly for the low strike regions and for high strikes with low maturities. This has been observed before in all models and is therefore expected.

If we now compare the cost function of the Dynamic SABR model (Cost$= 0.0108$), shown in Table 5.11, with the sum of the costs of the independent fits for the Static SABR ($\Sigma_{\text{Costs}} = 0.0004 +$

$0.0002 + 0.0001 + 0.0001 = 0.0008$), in Table 5.7, the former is much greater than that of the latter. This is unsurprising, since the Static SABR fits only a small amount of data for a single maturity and Dynamic SABR attempts to model a whole surface.

Comparing the cost resulting from the Heston model (Cost$= 0.0025$) with that from Dynamic SABR, we see that even though both models fit the same data on a range of different maturities, Heston outperforms the Dynamic SABR quite significantly. This is further corroborated by the comparison of the theoretical functions in Figures 5.10 and 5.13, from which it is clear that the Heston model's curves seemed to better fit the data.

Finally comparing cost of the Dynamic SABR model with the constant volatility assumption for dependent fits (Cost$= 0.1248$), shown in Table 5.4, the results improve by approximately 91%, compared to the 98% here improvement seen with the Heston model. Despite performing worse than Heston, the improvement against the constant volatility model is still striking, though unsurprising.

As we did for the Heston model, we now present the theoretical and simulated implied volatility surfaces of which the plots in Figure 5.13 are slices. These surfaces and their respective contour plots are shown in Figures 5.14 and 5.15.

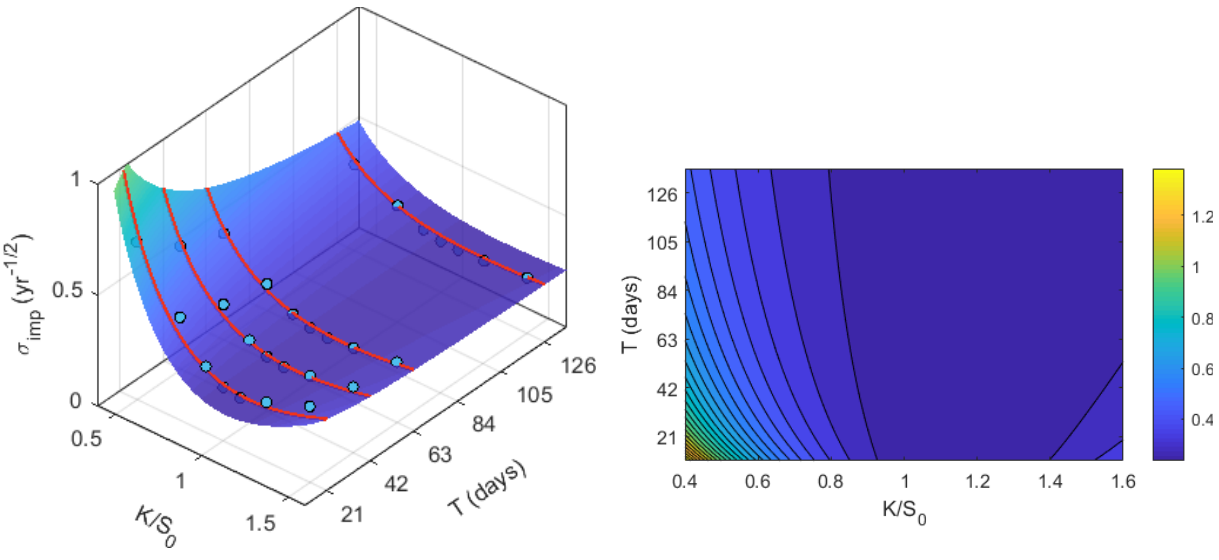

(a) σ_{imp} surface

(b) σ_{imp} contour plot

Figure 5.14: Implied volatility surface (left) and corresponding contour plot (right) of the function fitted simmultaneously to the implied volatility data for different maturities under the dynamic SABR model, plotted against the original market data (blue circles) and the fitted functions shown in Figure 5.13 (red lines).

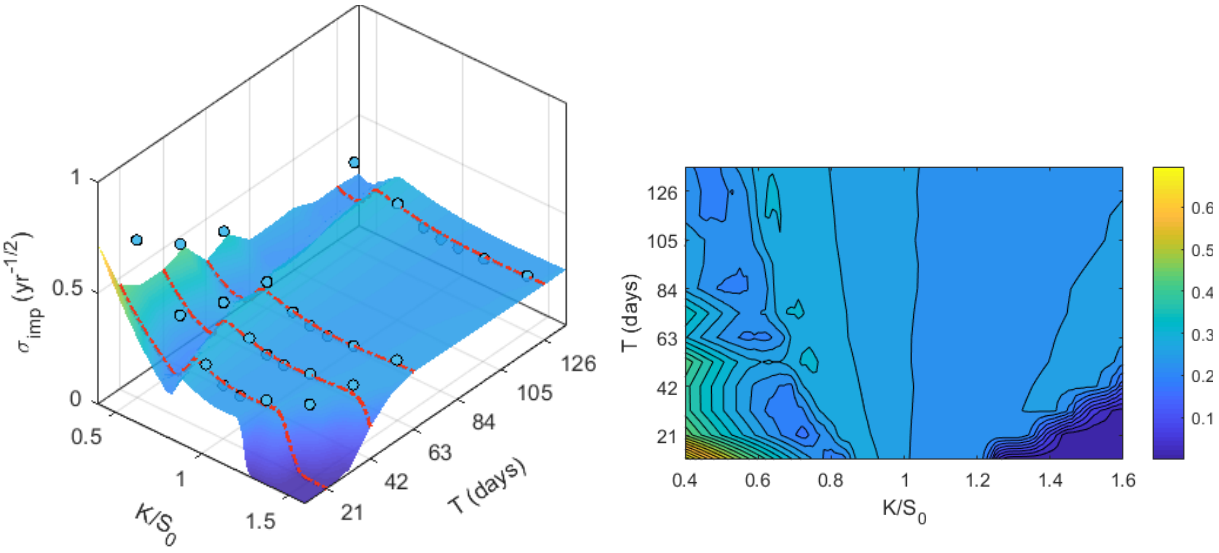

(a) σ_{imp} surface

(b) σ_{imp} contour plot

Figure 5.15: Implied volatility surface (left) and corresponding contour plot (right) of the function simulated using the Monte Carlo procedure with the fitted parameters shown in Table 5.11, under the dynamic SABR model, plotted against the original market data (blue circles) and the simulated functions shown in Figure 5.13 (red dot-dashed lines).

As stated before, ideally the plots in these two Figures would perfectly mimic the surface shown in Figure 5.3. This obviously doesn't occur. The theoretical surface plot in Figure 5.14 seems to be flatter than the actual surface in the regions around S_0 (notice the wider contours in this region) whereas it increases quite abruptly for low strikes. As for the simulated surface in Figure 5.15, the surface is heavily modified by noise, which is expected from the adjustments shown before.

T(days)	K(€)	$\sigma_{imp,\mathrm{mdl}}(\mathrm{yr}^{-1/2})$	$\mathrm{Error}_\sigma(\%)$	C_{mdl}(€)	$\mathrm{Error}_C(\%)$
21	0.50	0.7625	8	5.000×10^{-1}	0
	0.75	0.3765	19	2.501×10^{-1}	0
	0.90	0.2843	5	1.037×10^{-1}	1
	1.00	0.2540	5	2.924×10^{-2}	5
	1.10	0.2410	4	2.858×10^{-3}	18
	1.25	0.2454	9	1.760×10^{-5}	67
	1.50	0.2944	14	1.857×10^{-8}	97
42	0.50	0.5788	4	5.001×10^{-1}	0
	0.75	0.3337	14	2.507×10^{-1}	0
	0.90	0.2740	3	1.099×10^{-1}	1
	1.00	0.2538	3	4.131×10^{-2}	3
	1.10	0.2445	4	9.490×10^{-3}	11
	1.25	0.2455	3	5.072×10^{-4}	18
	1.50	0.2736	8	4.721×10^{-6}	70
63	0.50	0.4980	4	5.001×10^{-1}	0
	0.75	0.3150	9	2.518×10^{-1}	0
	0.90	0.2695	1	1.158×10^{-1}	0
	1.00	0.2537	6	5.057×10^{-2}	6
	1.10	0.2460	6	1.619×10^{-2}	14
	1.25	0.2455	1	1.868×10^{-3}	4
	1.50	0.2642	4	4.810×10^{-5}	37
126	0.50	0.4050	4	5.005×10^{-1}	0
	0.75	0.2935	1	2.568×10^{-1}	0
	0.90	0.2645	8	1.317×10^{-1}	4
	1.00	0.2537	11	7.147×10^{-2}	11
	1.10	0.2477	9	3.382×10^{-2}	18
	1.25	0.2452	5	9.051×10^{-3}	20
	1.50	0.2528	0	8.775×10^{-4}	2

Table 5.12: Comparison between fitted results and original data under the dynamic SABR model.

5.6 Mishaps Found in Implementation

During the implementation of all the models, some problems were found. They were mostly solved and the models were able to perform as expected, as we saw in the previous section. For future reference, and to prevent others from repeating the same mistakes, we now summarize not only the problems observed but also their causes and how we were able to solve them or at least reduce their impact.

5.6.1 Dupire Model

While implementing the Dupire model we noticed that the local volatility surface produced by the model was heavily dependent on the chosen interpolation method. Moreover, we found that it was particularly sensitive to the intervals ΔK and ΔT chosen in the interpolation. If chosen to be too large, the gradients wouldn't be able to capture the surface curvature and the local volatility surface would look unrealistic. If chosen to be too small, because we used Delaunay's triangulation method as interpolation, which creates triangular planes between three points, the second derivative would be (wrongly) zero if K, $K + \Delta K$ and $K - \Delta K$ were all evaluated inside the same triangle, which is bound to be true for the majority of points if ΔK is small enough. Thus, the intervals ΔK and ΔT have to be chosen very carefully.

As an example, in Figure 5.16 we present how different choices for these intervals affects the local volatility surface.

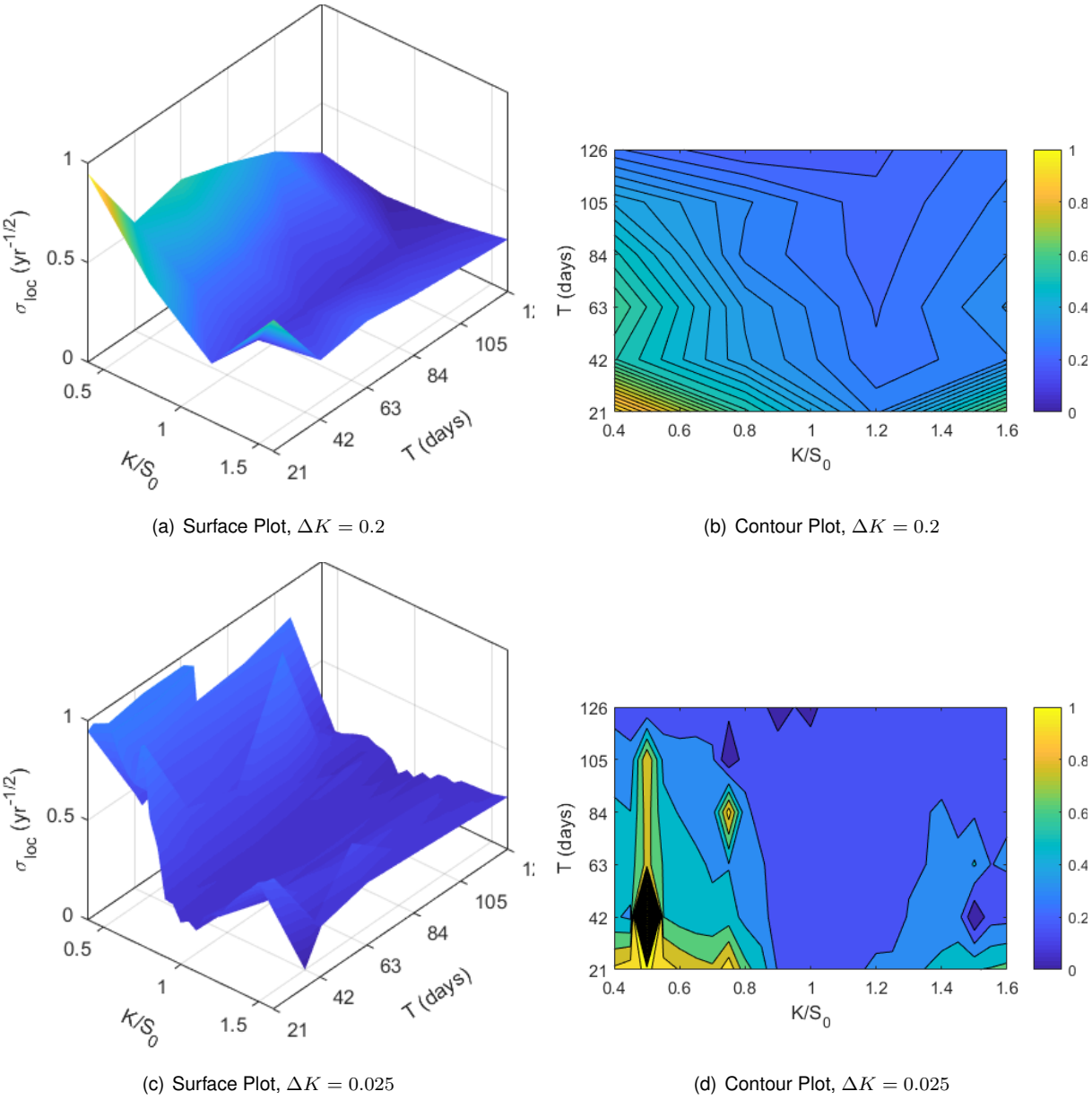

(a) Surface Plot, $\Delta K = 0.2$

(b) Contour Plot, $\Delta K = 0.2$

(c) Surface Plot, $\Delta K = 0.025$

(d) Contour Plot, $\Delta K = 0.025$

Figure 5.16: Influence of ΔK on the local volatility surface.

There exist two possible alternatives to solve this problem. On the one hand, we could significantly increase the number of data points. This would ensure that the size of the planar triangles from Delaunay's triangulation is small enough for the numerical derivatives to produce realistic results. The problem is that more data isn't always available, and this alternative may not be possible. The other possible path, which was the one implemented, is to test several values for the intervals and observe which of them produces the most realistic gradients and the most realistic local volatility surface. This alternative has the caveat that the choice for the intervals is very subjective and that we lose a great deal of robustness because an interval that is appropriate for a given data set is expected to perform poorly on other data sets.

5.6.2 Heston Model

In the Heston model, we need to evaluate some integrals to find the closed-form solutions of call prices. These integrals are evaluated between 0 and ∞, and, because they are not analytically solvable, they have to be calculated numerically. We thus obviously need to define some upper limits for the integrals, since numerical integration until ∞ is impossible. Cui *et al.* [Cui et al., 2017] showed that usually these integrals only have to be evaluated until ≈ 100, because the integrands decrease fast enough that they become negligible after this point. During our implementation, this threshold proved to be insufficient when we evaluated the integrals for the earlier maturities with strikes far below and far above S_0. For such regions, some erratic oscillating behavior was found, which we represent in Figure 5.17. This behavior was not described by Cui *et al.* because they didn't study the implied volatility curve for such high/low strikes.

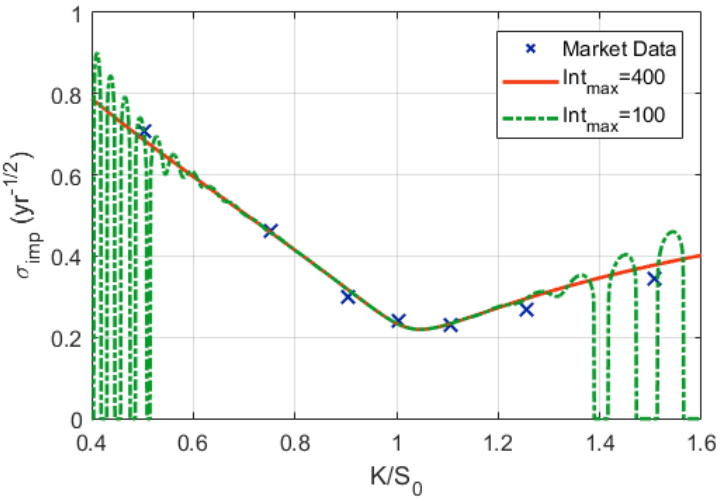

Figure 5.17: Comparison between the theoretical curves obtained with different upper integration limits, namely using the values 100 (green dot-dashed line) and 400 (red full line) as limits.

This problem was solved simply by increasing the upper integration limits to 400, for which the oscillating behavior wasn't found.

5.6.3 SABR Model

One problem related to the SABR models is the fact that stock prices might become negative, which is clearly absurd. This event is very rare and was usually only found in one of the simulated paths out of $100\,000$. The reason why this problem only occurred for the SABR models and wasn't observed in Heston is due to the fact that the volatility process in the former is not mean reverting. This detail enables the volatility process to evolve without restrain. If the volatility process becomes extremely large, the jumps in the stock price process become equally extremely large. In the limit, it is perfectly possible that one of these jumps decreases the stock price process past zero. For the Heston model this problem is

not observed because the volatility process (we used the variance process, but they are equivalent) is mean-reverting, so that the volatility doesn't evolve unrestrained.

This negative price shortcoming is more problematic in the SABR model because, in the stock price process, one of the terms is a stock price with an exponent β. If $\beta \neq 0$ and $\beta \neq 1$ and $S(t) < 0$, the resulting $S(t + \Delta t)$ will become imaginary, and the whole pricing procedure fails.

To solve this problem we simply cut the negative stock price paths to zero, preventing them from becoming negative.

5.6.4 Other Problems

During the implementation we also found that, in the Monte Carlo siimulations, updating the volatility process before the stock price produced results that didn't match the theoretical predictions in both the Heston and SABR models.

In other words, if we used

$$S(t + \Delta t) = \sigma(t + \Delta t).(\ldots) + \ldots, \tag{5.13}$$

instead of the correct

$$S(t + \Delta t) = \sigma(t).(\ldots) + \ldots, \tag{5.14}$$

the simulations deviate significantly from the theoretical predictions. This is expected because the whole correlation mechanism, relating the two stochastic processes through the variable ρ, falls apart when we use the first formula.

Though this might seem trivial, some care must be taken when implementing the Monte Carlo pricer to use the updating equations in the correct order.

5.7 Barrier Options

The Monte Carlo algorithms developed to price the European options in the previous sections under each of the models can be easily adapted to price Barrier options. We are only required to check at each time step if the stock price process crossed the barrier level or not and, at the maturity, only keep the processes that did. This discretization poses a problem when pricing Barrier options, because these contracts assume a continuous time frame. This has been discussed in subsection 4.1.1. Furthermore, as we discussed in subsection 4.1.2, the problem we observed before with the low number of simulated paths contributing to the prices of options with very high strikes and an early maturities is further aggravated with this Exotic option contract.

Despite these expected shortcomings, we priced several Barrier options with different barrier levels and using all the different models described before. In these simulations we assumed a single maturity of 21 days and the calibrated parameters for each of the models, shown earlier in this chapter. The results of these simulations are shown in Figure 5.18.

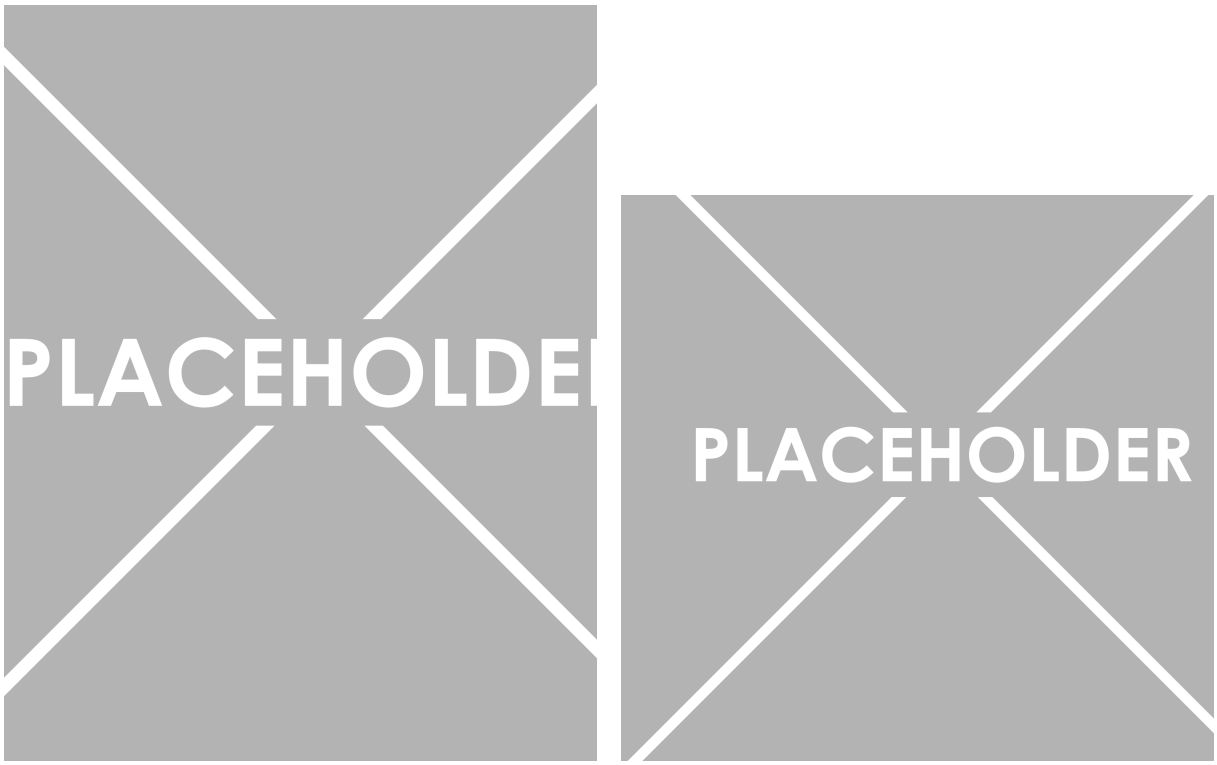

(a) bla bla bla bla

(b) bla bla bla bla

Figure 5.18: Bla bla bla bla

in the tables show only one maturity and show the simulation implied vols, deleting the option prices (or showing in a different table)

create a cost function for the simulated volatility functions besides the already existing cost for the theoretical values, in order to compare dupire's model

plot the decaying functions of rho and nu on the dynamic sabr model

check with Claude if BNPP data assumes a 0 interest rate or not

ask prof Dilao why we use the forward gradient wrt time in the dupire interpolation gradient

put implied volatility applied to barrier options

keep dupire's results table or not. they are the results for simulations not theoretical predictions

why is the coupled constant implied volatility the average of the independent fits of the constant implied vols?

dynamic sabr exponential functions for rho should match the data for the individual fits

mention the implied vol sensitivity to option price but changing maturity.

how is extrapolation done in dupires model

explain why static sabr only works for one maturity

why does rho/nu decrease with maturity in static sabr

why does implied volatility surface become flatter with maturity

check notation:

$\sigma_{i,\mathrm{mkt}}$ vs $\sigma_{imp,\mathrm{mkt}}$;

put units in fitted parameters

put proof of lower bounds for the option prices

in the plots of the chapters background and implementation, use dashed and dot-dashed lines

save files as .png

change labels from "simulated function" to something else

check number of decimal places in the parameters tables (in particular for the cost function value)

explain how the lower bound volatility sensitivity plot was obtained

explain what C means in the lower bound volatility sensitivity plot

redo fokker-planck proof

redo heston proof

in heston proof, show ito's lemma for two dimensions

change the 3d surface captions of the blue circles to something else

put 95 percent confidence bands

in plot of implied vol vs. option price, put C mkt in axis label

explain better the difference between independent and dependent constant volatility plots

replace the word -noise- in monte carlo with -bad estimatio-

mention that for prices far above the lower bound, the implied volatility is very insensitive to the price, so that even a very small error on the implied volatility will produce an extremely large error in the price

mention why we don't have a big table for dupire

mention the relative errors in the captions

reduce decimal places of values in appendix

Chapter 6

Conclusions

Implement importance sampling - this has been done for Heston (and can easily be adapted to SABR) in Stilger [2015]

Implement antithetic paths

we tried several algorithms but CMA and multi-start were better

use mean-reverting sabr

we could study the greeks

we could use low-discrepancy sequences in the monte carlo random number generation.

We could consider other funtions for rho and nu in the dynamic sabr...

comment that we are fitting data for an index (Nikkei) and that some models might be more appropriate for other types of data

Bibliography

H. Albrecher, P. Mayer, W. Schoutens, and J. Tistaert. The little heston trap, 2006.

I. Amidror. Scattered data interpolation methods for electronic imaging systems: A survey. 11:157–176, 04 2002.

Bank for International Settlements. Semiannual otc derivatives statistics. `http://stats.bis.org/statx/srs/table/d5.1`. (Accessed: 2018-05-20).

F. Black and M. Scholes. The pricing of options and corporate liabilities. *Journal of political economy*, 81(3):637–654, 1973.

K. Chourdakis. Financial engineering: A brief introduction using the matlab system, 2008.

R. Crisóstomo. An analysis of the heston stochastic volatility model: Implementation and calibration using matlab. 2015.

Y. Cui et al. Full and fast calibration of the heston stochastic volatility model. *European Journal of Operational Research*, 263(2):625 – 638, 2017.

C. de Graaf. Finite difference methods in derivatives pricing under stochastic volatility models.

S. del Baño Rollin et al. On the density of log-spot in the heston volatility model. *Stochastic Processes and their Applications*, 120(10):2037 – 2063, 2010.

J. Dewynne, S. Ehrlichman, and P. Wilmott. A simple volatility surface parametrization, 1998.

R. Dilão and D. Muraro. A parallel multi-objective optimization algorithm for the calibration of mathematical models. *Swarm and Evolutionary Computation*, 8:13 – 25, 2013.

R. Dilão, J. A. de Matos, and B. Ferreira. On the value of european options on a stock paying a discrete dividend. *Journal of Modelling in Management*, 4(3):235–248, 2009.

D. Duffie, J. Pan, and K. Singleton. Transform analysis and asset pricing for affine jump-diffusions. *Econometrica*, 68(6):1343–1376, 2000.

B. Dupire. Pricing with a smile. *Risk Magazine*, pages 18–20, 1994.

J. Fernández et al. Static and dynamic sabr stochastic volatility models: Calibration and option pricing using gpus. *Mathematics and Computers in Simulation*, 94:55 – 75, 2013.

Financial Times. OTC derivatives shrink to lowest level since financial crisis. https://www.ft.com/content/dbc08ae2-1247-11e6-91da-096d89bd2173, May 2016.

J. Gatheral. *The Volatility Surface: A Practitioner's Guide*. Wiley Finance. Wiley, 2006.

P. Glasserman. *Monte Carlo Methods in Financial Engineering*. Springer, 2004.

P. Hagan et al. Managing smile risk. 1:84–108, 01 2002.

N. Hansen. CMA-ES Source Code - MATLAB and Octave - Code for Reading. http://www.lri.fr/~hansen/purecmaes.m, a. (Accessed: 2018-05-28).

N. Hansen. The cma evolution strategy: A tutorial. b.

N. Hansen. The cma evolution strategy: a comparing review. In *Towards a new evolutionary computation*, pages 75–102. Springer, 2006.

D. Heath, R. Jarrow, and A. Morton. Bond pricing and the term structure of interest rates: A new methodology for contingent claims valuation. *Econometrica*, 60(1):77–105, 1992.

S. Heston. A closed-form solution for options with stochastic volatility with applications to bond and currency options. 6:327–43, 02 1993.

J. Hull. *Options, Futures, and Other Derivatives*. Boston: Prentice Hall, 2012.

J. Hull and A. White. The pricing of options on assets with stochastic volatilities. *The Journal of Finance*, 42(2):281–300, 1987.

Investopedia. American option. https://www.investopedia.com/terms/a/americanoption.asp, a. (Accessed: 2018-05-29).

Investopedia. European option. https://www.investopedia.com/terms/e/europeanoption.asp, b. (Accessed: 2018-05-29).

Investopedia. Exotic option. https://www.investopedia.com/terms/e/exoticoption.asp, c. (Accessed: 2018-05-29).

C. Kahl and P. Jäckel. Not-so-complex logarithms in the heston model.

P. H. Labordère. A general asymptotic implied volatility for stochastic volatility models. May 2005.

F. Longstaff and E. Schwartz. Valuing american options by simulation: a simple least-squares approach. *The review of financial studies*, 14(1):113–147, 2001.

T. Mikosch. *Elementary Stochastic Calculus with Finance in View*. Advanced Series on Statistical Science and Applied Probability. 1998.

G. N. Milstein. Approximate integration of stochastic differential equations. *Theory of Probability and Its Applications*, 19(3):557–562, 1975.

J. Obloj. Fine-tune your smile: Correction to hagan et al. Mar 2008.

Y. Osajima. The asymptotic expansion formula of implied volatility for dynamic sabr model and fx hybrid model. 2007.

F. Rouah. *The Heston Model and its Extensions in Matlab and C#*. Wiley Finance. Wiley, 2013.

W. Schoutens et al. A perfect calibration! now what?

S&P Dow Jones Indices. Dow Jones Industrial Average Index (DJIA). `https://us.spindices.com/indices/equity/dow-jones-industrial-average`. (Accessed: 2018-06-13).

E. M. Stein and J. C. Stein. Stock price distributions with stochastic volatility: An analytic approach. *Review of Financial Studies*, 4:727–752, 1991.

P. Stilger. *Numerical and Empirical Studies of Option Pricing*. PhD thesis, Alliance Manchester Business School, 2015.

N. Taleb. *Dynamic Hedging: Managing Vanilla and Exotic Options*. Wiley, 1997.

G. Vlaming. Pricing options with the sabr model. Master's thesis, 2011.

P. Wilmott. *Paul Wilmott on Quantitative Finance*. The Wiley Finance Series. Wiley, 2006.

P. Wilmott. *Paul Wilmott Introduces Quantitative Finance*. The Wiley Finance Series. Wiley, 2013.

Appendix A

Option Market Data

Here, we present the data kindly provided by *BNP Paribas* for European options. For confidentiality reasons, the strike prices were normalized by the initial stock price i.e. $K \to K/S_0$ so that the original strike prices are inaccessible. Suffice it to say that the underlying asset of the options here represented is a *stock index*, i.e. a weighted average of the prices of some selected stocks (e.g. PSI-20 (Portugal)).

The data provided pertains to the options' implied volatilities. We can easily obtain their prices from these values using eq.(3.4). The converted prices of call European options are shown below.

The number of days here denoted correspond to trading days (i.e. days where exchanges are open and trading occurs) so that one month corresponds to 21 days and one year to 252.

T (days)	K (€)	σ_{imp} (yr$^{-1/2}$)	C (€)
	0.50	0.7082	0.500013
	0.75	0.4632	0.250648
	0.90	0.2989	0.104393
21	1.00	0.2425	0.027923
	1.10	0.2314	0.002421
	1.25	0.2699	0.000053
	1.50	0.3433	0.000001
	0.50	0.5556	0.500050
	0.75	0.3876	0.251865
	0.90	0.2824	0.110693
42	1.00	0.2461	0.040063
	1.10	0.2354	0.008525
	1.25	0.2525	0.000621
	1.50	0.2968	0.000016

T (days)	K (€)	σ_{imp} (yr$^{-1/2}$)	C (€)
	0.50	0.4789	0.500093
	0.75	0.3452	0.252957
	0.90	0.2658	0.115328
63	1.00	0.2401	0.047872
	1.10	0.2330	0.014215
	1.25	0.2438	0.001799
	1.50	0.2749	0.000077
	0.50	0.3878	0.500353
	0.75	0.2954	0.256942
	0.90	0.2444	0.127156
126	1.00	0.2295	0.064670
	1.10	0.2269	0.028619
	1.25	0.2340	0.007569
	1.50	0.2521	0.000858

Table A.1: Data provided by *BNP Paribas* to be used in model calibration and validation.

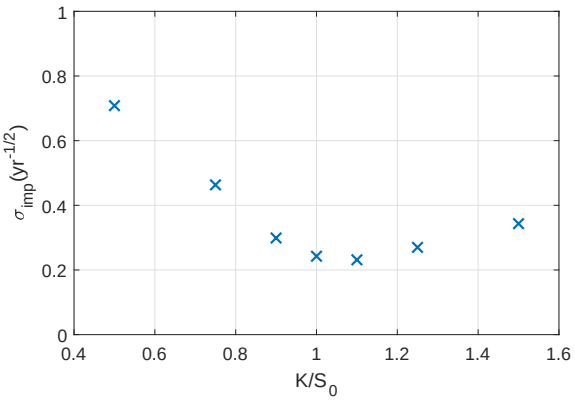

(a) Implied Volatility, T=21 days

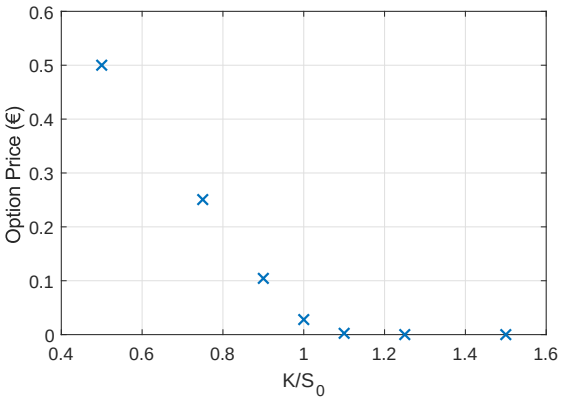

(b) European Call Price, T=21 days

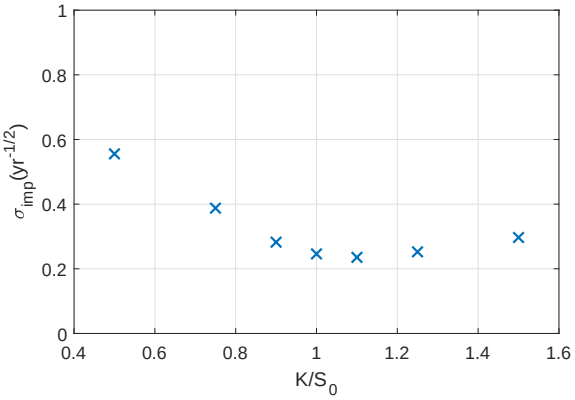

(c) Implied Volatility, T=42 days

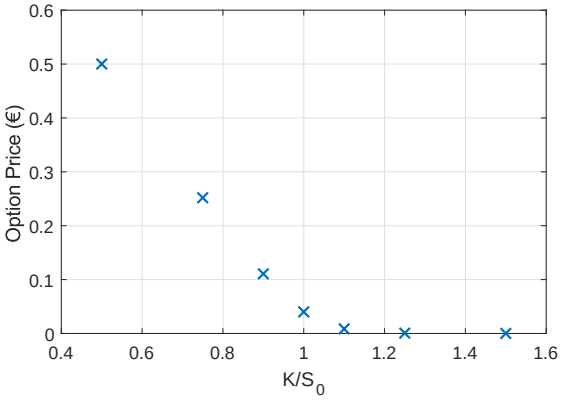

(d) European Call Price, T=42 days

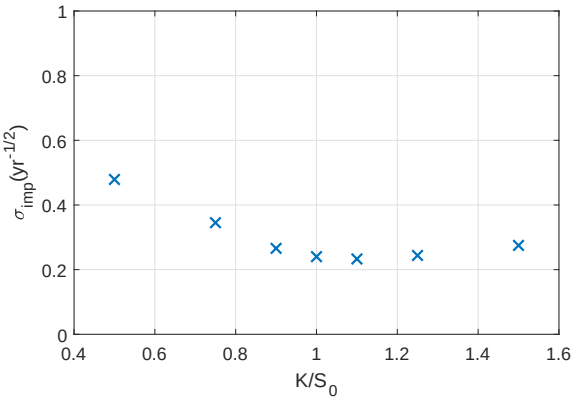

(e) Implied Volatility, T=63 days

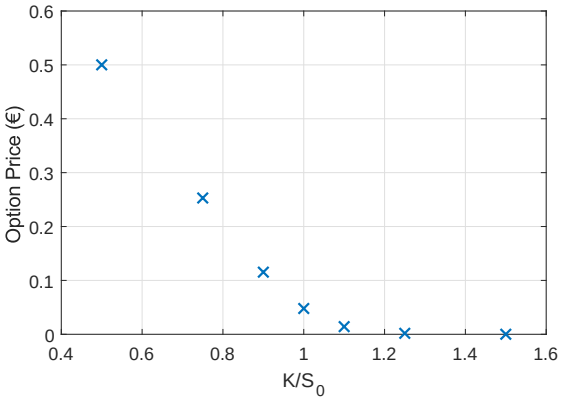

(f) European Call Price, T=63 days

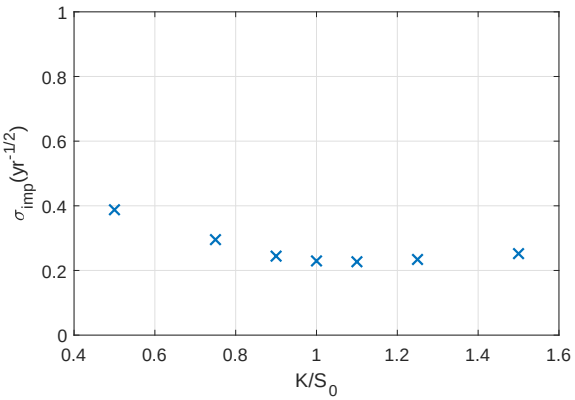

(g) Implied Volatility, T=126 days

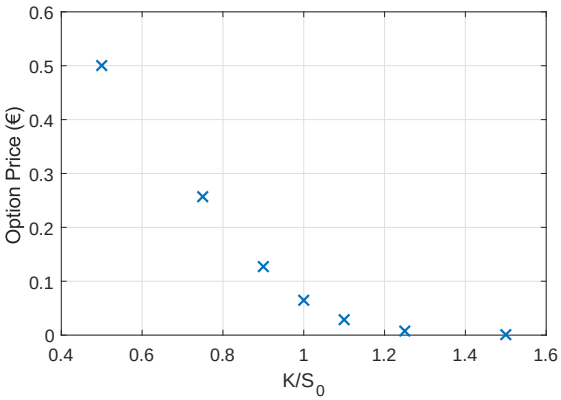

(h) European Call Price, T=126 days

Figure A.1: Scatter plots of the implied volatilities and European call prices provided

Appendix B

CMA-ES Algorithm Formulas

Here we present the formulas required for the calculation of the mean vector, $\mathbf{m}$, and the covariance matrix, $\mathbf{C}$, to be used, at each iteration of the CMA-ES optimization algorithm, on the multivariate normal distribution

$$N(\mathbf{x};\mathbf{m},\mathbf{C}) = \frac{1}{\sqrt{(2\pi)^D|\mathrm{det}\mathbf{C}|}}\exp\left(-\frac{1}{2}(\mathbf{x}-\mathbf{m})^T\mathbf{C}^{-1}(\mathbf{x}-\mathbf{m})\right). \tag{B.1}$$

We will directly follow the steps shown in [Dilão and Muraro, 2013]. For a more in depth explanation of the algorithm, refer to the cited article.

B.1 The Optimization Algorithm

B.1.1 Initialization

We initialize the algorithm by setting the first mean vector, $\mathbf{m}^{(0)}$, to some initial guess, θ_0, and the covariance matrix to the unit matrix, $\mathbf{C}^{(0)} = \mathbf{I}$.

B.1.2 Sampling

We sample λ points, $\mathbf{y}_i^{(1)},\ i = 1,\ldots,\lambda$, from a multivariate normal distribution $N(\mathbf{x};\mathbf{0},\mathbf{C}^{(0)})$, generating the first candidate solutions

$$\mathbf{x}_i^{(1)} = \mathbf{m}^{(0)} + \sigma^{(0)}\mathbf{y}_i^{(1)}, \quad i = 1,\ldots,\lambda, \tag{B.2}$$

where $\sigma^{(0)} = 1$.

B.1.3 Classification

The candidate solutions are ordered based on their cost function, such that we denote $\mathbf{x}_{i:\lambda}^{(1)}$ as the i-th best classified point from the set $\mathbf{x}_1^{(1)},\ldots,\mathbf{x}_\lambda^{(1)}$. In other words, $\mathrm{Cost}(\mathbf{x}_{1:\lambda}^{(1)}) \leq \mathrm{Cost}(\mathbf{x}_{2:\lambda}^{(1)}) \leq \ldots \leq \mathrm{Cost}(\mathbf{x}_{\lambda:\lambda}^{(1)})$.

B.1.4 Selection

From the ordered set $\mathbf{x}_{i:\lambda}^{(1)}$ we choose the first μ data points (with the lowest cost) and discard the others. We then define the weights ω_i as

$$\omega_i = \frac{(\log(\mu + 1/2) - \log(i))}{\sum_{i=1}^{\mu}(\log(\mu + 1/2) - \log(i))}, \qquad i = 1, \ldots, \mu. \tag{B.3}$$

As an alternative we could also use $\omega_i = 1/\mu$.

B.1.5 Adaptation

We are finally able to calculate the new mean vector and covariance matrix using

$$\left\langle \mathbf{y}^{(k)} \right\rangle_w = \sum_{i=1}^{\mu} \omega_i \mathbf{y}_{i:\lambda}^{(k)}, \tag{B.4}$$

$$\mathbf{m}^{(k)} = \mathbf{m}^{(k-1)} + \sigma^{(k-1)} \left\langle \mathbf{y}^{(k)} \right\rangle_w = \sum_{i=1}^{\mu} \omega_i \mathbf{x}_{i:\lambda}^{(k)}, \tag{B.5}$$

$$\mathbf{p}_\sigma^{(k)} = (1 - c_\sigma)\mathbf{p}_\sigma^{(k-1)} + \sqrt{c_\sigma(2 - c_\sigma)\mu_{\text{eff}}} \left(\mathbf{C}^{(k-1)}\right)^{-1/2} \left\langle \mathbf{y}^{(k)} \right\rangle_w, \tag{B.6}$$

$$\sigma^{(k)} = \sigma^{(k-1)} \exp\left(\frac{c_\sigma}{d_\sigma}\left(\frac{\|\mathbf{p}_\sigma^{(k)}\|}{E^*} - 1\right)\right), \tag{B.7}$$

$$\mathbf{p}_c^{(k)} = (1 - c_c)\mathbf{p}_c^{(k-1)} + h_\sigma^{(k)} \sqrt{c_c(2 - c_c)\mu_{\text{eff}}} \left\langle \mathbf{y}^{(k)} \right\rangle_w, \tag{B.8}$$

$$\mathbf{C}^{(k)} = (1 - c_1 - c_\mu)\,\mathbf{C}^{(k-1)} + c_1 \left(\mathbf{p}_c^{(k)} \left(\mathbf{p}_c^{(k)}\right)^T + \delta\left(h_\sigma^{(k)}\right)\mathbf{C}^{(k-1)}\right) + c_\mu \sum_{i=1}^{\mu} \omega_i \mathbf{y}_{i:\lambda}^{(k)} \left(\mathbf{y}_{i:\lambda}^{(k)}\right)^T, \tag{B.9}$$

where we define

$$\mu_{\text{eff}} = \left(\sum_{i=1}^{\mu} \omega_i^2\right)^{-1}, \tag{B.10}$$

$$c_c = \frac{4 + \mu_{\text{eff}}/D}{D + 4 + 2\mu_{\text{eff}}/D}, \tag{B.11}$$

$$c_\sigma = \frac{\mu_{\text{eff}} + 2}{D + \mu_{\text{eff}} + 5}, \tag{B.12}$$

$$d_\sigma = 1 + 2\max\left(0,\ \sqrt{\frac{\mu_{\text{eff}} - 1}{D + 1}} - 1\right) + c_\sigma, \tag{B.13}$$

$$c_1 = \frac{2}{(D + 1.3)^2 + \mu_{\text{eff}}}, \tag{B.14}$$

$$c_\mu = \min\left(1 - c_1,\ 2\frac{\mu_{\text{eff}} - 2 + 1/\mu_{\text{eff}}}{(D + 2)^2 + \mu_{\text{eff}}}\right), \tag{B.15}$$

$$E^* = \frac{\sqrt{2}\Gamma\left(\frac{D+1}{2}\right)}{\Gamma\left(\frac{D}{2}\right)}, \tag{B.16}$$

$$h_\sigma^{(k)} = \begin{cases} 1, & \text{if} \frac{\|\mathbf{p}_\sigma^{(k)}\|}{\sqrt{1-(1-c_\sigma)^{2(k+1)}}} < \left(1.4 + \frac{2}{D+1}\right) E^* \\ 0, & \text{otherwise} \end{cases}, \tag{B.17}$$

$$\delta\left(h_\sigma^{(k)}\right) = \left(1 - h_\sigma^{(k)}\right) c_c \left(2 - c_c\right), \tag{B.18}$$

$$\left(\mathbf{C}^{(k)}\right)^{-1/2} = \mathbf{B}\left(\mathbf{D}^{(k)}\right)^{-1}\mathbf{B}^T, \tag{B.19}$$

with D corresponding to the number of parameters of the model (i.e. the dimensions of the sample space) and we define $\mathbf{p}_\sigma^{(0)} = \mathbf{p}_c^{(0)} = 0$.

This steps are iterated until the termination criterion is met.